HANDBOOK OF PLASMA PHYSICS

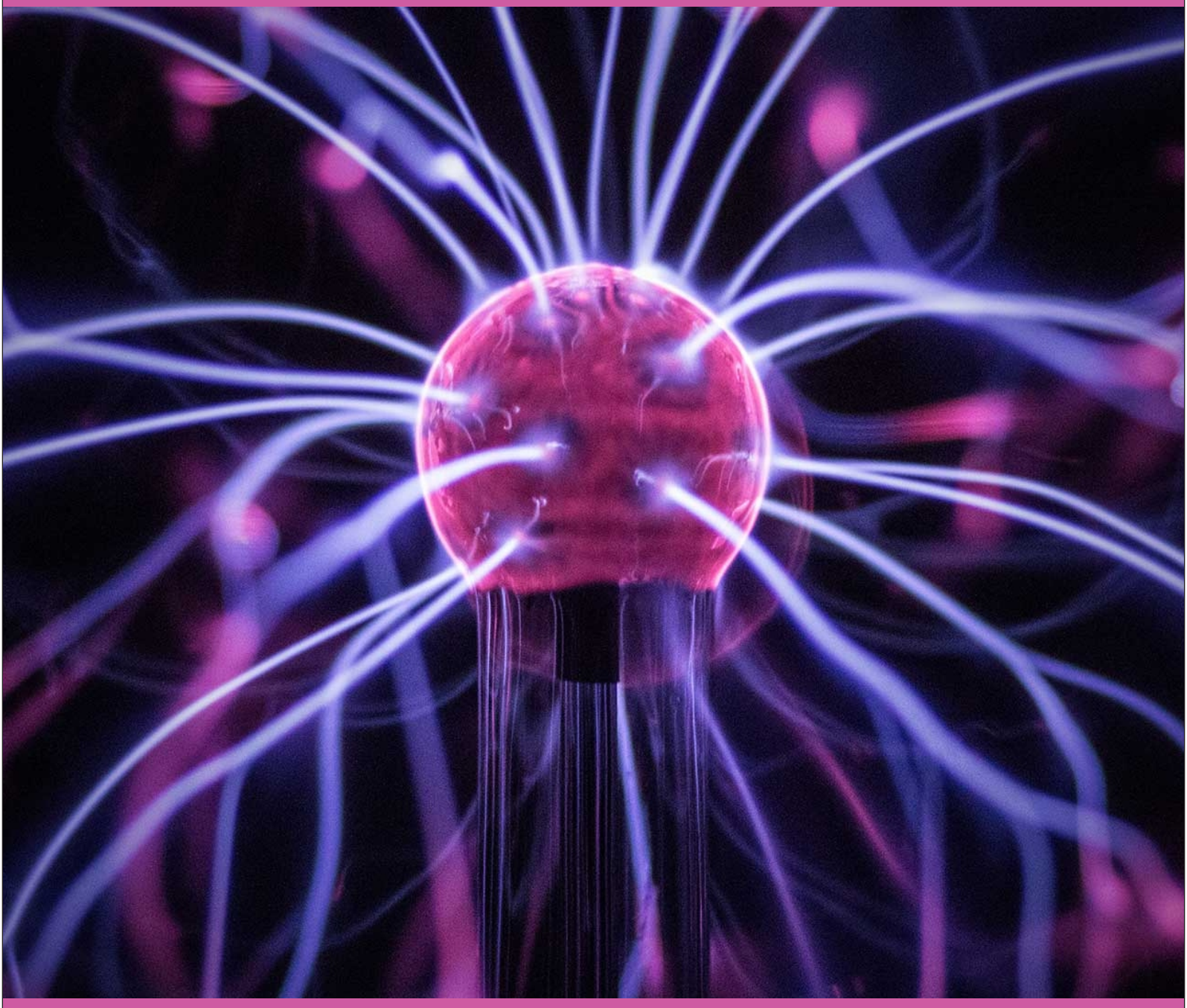

R. P. S. Mangal
Dr. Nishant Kumar

Handbook of Plasma Physics

R. P. S. Mangal
Dr. Nishant Kumar

Handbook of Plasma Physics

R. P. S. Mangal
Dr. Nishant Kumar

Dominant
Publishers & Distributors Pvt Ltd
New Delhi, INDIA

Knowledge is Our Business

HANDBOOK OF PLASMA PHYSICS
By R. P. S. Mangal, Dr. Nishant Kumar

This edition published by Dominant Publishers And Distributors (P) Ltd
4378/4-B, Murarilal Street, Ansari Road, Daryaganj,
New Delhi-110002.

ISBN: 978-81-78886-54-1

Edition: 2022 (Revised)

Dominant
Publishers & Distributors Pvt Ltd

Registered Office: 4378/4-B, Murari Lal Street, Ansari Road,
Daryaganj, New Delhi - 110002.
Ph. +91-11-23281685, 41043100, Fax: +91-11-23270680

Production Office: "Dominant House", G - 316, Sector - 63, Noida,
National Capital Region - 201301.
Ph. 0120-4270027, 4273334

e-mail: dominantbooks@gmail.com
info@dominantbooks.com

w w w . d o m i n a n t b o o k s . c o m

CONTENTS

CHAPTER 1
THE ROOTS OF PLASMA PHYSICS

Dr.Nishant Kumar, Assistant Professor
Department of Science, Maharishi University of Information Technology, Uttar Pradesh, India
Email Id- nishant.kumar@muit.in

ABSTRACT:

Unexpectedly, physics' field of plasma research has existed for a long time despite just receiving its formal name in 1928. The history of electricity is closely tied to the origins of plasma physics. When William Gilbert first defined tribo-electricity, modern electricity was conceived about 1600. One generation later, Otto von Guericke found the corona discharge at sharp-pointed points and created the vacuum pump, revolving sulphur sphere, and electricity. The Leyden jar, a high-voltage capacitor, was created separately in 1746 by Pieter van Musschenbroek and Ewald Georg von Kleist over the course of another century. The phrase "gas discharge" originated from the sound that such a Leyden jar made when it ignited the air, which resembled a gunshot. In the era of enlightenment, nature was studied via organized experiments. Georg Christoph Lichtenberg a well-known scientist. The Lichtenberg figures on the surface of 1.1's electrophor, the greatest high-voltage generator of its time with a capacity of more than 200,000 V, established the electrophor's connection to lightning discharges.

KEYWORDS:

Discharge, Fusion, Magnetic Field, Plasma, Solar Energy.

INTRODUCTION

When high-current electric batteries were made accessible, Vasily V. Petrov (1761-1834) and Humphrey Davy (1778-1829) independently dissected the electric arc in 1803. When the contact between two carbon electrode tips is opened while a powerful current is flowing, such an electric arc occurs. Michael Faraday's portrait may be seen found electric glow discharges in rarefied gases and conducted thorough research over the next 4 years. William Crookes (1832-1919), Johann Wilhelm Hittorf (1824-1914), and Julius Plücker (1801-1868) conducted studies with such low-pressure discharges to enhance their exploration of this topic. This study of gas discharges led to the discovery of a number of things, including cathode rays in 1869 by Hittorf, X-rays in 1895 by Wilhelm Conrad Röntgen (1845-1923), and the electron in 1897 by Joseph John Thomson (1856-1940). In 1891, Nikola Tesla (1856–1943) began examining electric discharges produced by high-frequency electric fields. It was discovered during this archaic period of plasma physics that gas discharges included the migration of positive ions and electrons, which corresponds to the electric current flowing in a gas[1], [2].

It took until the 20th century to find the collective phenomena in gas discharges that constitute the modern idea of a plasma and to properly explain them using mathematical models. The research on gas-filled diodes conducted in the 1920s by Irving Langmuir and his colleagues and Walter Schottky (1886-1976) investigations on gas discharges with cold and hot cathodes laid the groundwork for the systematic study of the plasma state and the formulation of general laws. Many organisations began conducting systematic research of the plasma state in the 1930s. The novels by Max Steenbeck (1904–1981) and Alfred Hans von

Engel (1897–1990) and by Rudolf Seeliger (1886-1965) were early classics and were expanded upon in the review paper on the processes in low-pressure discharges by Mari Johan Druyvesteyn (1901-1995) and Frans Michel Penning (1894-1953).

Today's plasma physics is supported by radio science, which studies the propagation of electromagnetic waves in the ionosphere, as a second pillar. Sydney Chapman (1888-1970) [11], Edward V. Appleton (1892-1965) a Nobel Prize winner in 1947, John Ashworth Ratcliffe (1902-1987) and K. Edwards all worked at the Cavendish Laboratory in Cambridge and contributed to the field's inception. G. Budden (1915–2005]. Karl Rawer (1913-2003) [14] and others established the skill of forecasting the circumstances for short-wave radio communications. The study of controlled nuclear fusion has shaped the discipline of hot-plasma physics since the mid-1950s. Scientific issues including plasma instabilities and the containment of hot plasmas by magnetic fields have gained importance. Igor V. Kurchatov (1903–1963) and Lyman Spitzer (1914–1997) established the principles of magnetically confined systems plasmas for fusion. Improvements in this area also helped solar and magnetospheric physics with related issues. With the advent of powerful lasers, the idea of inertial confinement was also applied to the problem of controlled nuclear fusion. There are too many researchers to include here who contributed to the development of this discipline. Fusion research is still being driven by the need to find a solution to the energy crisis of the twenty-first century[3], [4].

Our planet's plasma environment

We begin our grand tour of the solar system's natural plasmas. A steady-state solar wind, nuclear reactions in the Sun's centre, plasma eruptions from the Sun's surface, interactions between the solar wind and the Earth's magnetosphere, and the creation of an ionosphere are just a few of the plasma processes that regulate the physics of the Sun-Earth system[5], [6].

The Stars' Energy Source

The Sun, which delivers the temperature radiation necessary to maintain the Earth's habitability, is the most significant plasma object in our solar system. The Sun has been extensively researched, and we know a lot about its inner workings since it is the closest star to us. The Sun and other stars are prime examples of steady-state fusion reactors that create energy by fusing protons with heavier atoms and radiating it into space. According to the primary nuclear reaction chain, the proton-proton cycle converts hydrogen into helium in stars with a mass of roughly one solar.

The Dynamic Sun

Galileo Galilei (1564-1642) had already discovered black spots on the Sun in 1616. These areas represent the foot points of powerful magnetic fields, as we now know. Where a magnetic flux tube filled with plasma rises above the sun surface and creates so-called coronal loops, magnetic dipolar structures may be seen on a smaller scale. The faint X-ray light emission from coronal loops as seen by the Transition Region and Coronal Explorer (TRACE) satellite. The NASA Small Explorer programme includes the Stanford-Lockheed Institute of Space Research project TRACE. A dynamo system that derives its shape and energy from the differential revolution of the Sun generates the magnetic fields[7], [8]. As a star, our Sun is active. Huge magnetic structures called solar prominences, which are packed with plasma and distinct from the solar surface, are seen in the sun. Prominences show how a

plasma and magnetic field may coexist and can endure for many days. In solar flares, active coronal loops are destroyed by the explosive ejection of particles and radiation depicts a flare's development using the Sweet-Parker model. An interplanetary field is somewhat coupled to the dipolar field of a coronal loop. Reconnecting the field lines may liberate the magnetic energy that has been trapped in the extended field lines. The contracting field lines accelerate the plasma that is confined within the magnetic field.

DISCUSSION

Coronal mass ejections (CMEs), which unleash an average of 1.6 1012 kg of plasma travelling at a speed of (200-2700) km s1, are the most explosive occurrences on the Sun. With an average of one incident per day at solar minimum and 5-6 occurrences at solar maximum, the frequency of CME events changes according to the 11-year sunspot cycle. The SOHO satellite's Large Angle Spectrometric Coronograph (LASCO) was used to make the observation. The middle disc blocks the sun's direct light. The white circle represents the sun's diameter. This CME event did not result in the propagation of the plasma bubble towards Earth. The Solar TErres- trialRElations Observatory (STEREO) is a brand-new pair of satellites that NASA launched in 2006 to monitor plasma formations that may be travelling towards the Earth in three dimensions. Such plasma bubbles have the potential to cause magnetic storms, which may damage communication satellites and cause enormous induced currents to disrupt power line systems. CMEs and the accompanying high-energy particles present a serious risk to astronauts. The auroral zone, which typically has a southern limit in Europe, extended as a result of the CME that struck Earth on October 30, 2003[9], [10].

The Solar Wind

Plasma from the solar wind fills the area between the Sun and Earth. The Norwegian scientist Kristian Birkeland (1867–1917) initially theorised about this flux of charged particles from the Sun in 1908. Birkeland also understood that the positive ions and negative electrons in this solar wind must be present. The pressure of the solar radiation on the molecules in the comet tail, according to Ludwig Biermann's deduction from 1951, is by much inadequate to explain why comet tails always point away from the Sun. In order to divert the comet tail, a solar corpuscle flow with speeds on the order of 106 m s1 was required.

The "frozen" state of the solar magnetic field is a result of "magneto-hydrodynamics," a revolutionary theory introduced by Hannes Alfven (1908-1995), according to Eugene Parker [20]. Despite the solar wind's mass flowing radially outward, solar rotation causes the particle flow's footpoints to move azimuthally, turning a radial beam into an Archimedian spiral Konstantin Gringauz (1918–1993), who created the hemispherical retarding–potential ion detectors on board the Soviet moon missions Luna 1 and Luna 2, both of which were launched in 1959 provided experimental proof of the solar wind's existence.

Plasma streams with origins on the Sun that are present for more than a single day, sometimes for weeks or even months, are referred to be quasistationary solar wind. The slow solar wind, which has velocities below 450 km s-1 and originates in the coronal streamer belt at low heliospheric latitudes, and the fast solar wind, which has velocities between 700 and 800 km s-1 and originates from coronal holes at high heliospheric latitudes, have different plasma properties. The ULYSSES4 spacecraft discovered these two forms of solar wind during its first journey across the Sun which coincided with the solar cycle's 11-year low.

The magnetosphere and ionosphere of the planet

Spectacular plasma events in nature are caused by the solar wind's interaction with the Earth. The magnetic field of the Earth shields it from the solar wind's influx of energetic particles. Some of these particles have the potential to move along magnetic field lines and strike the upper atmosphere at polar latitudes, where they result in the Northern Lights, which resemble a curtain. Fridtjof Nansen (1861–1930), a Norwegian arctic explorer, had previously been captivated by these events. Nansen often used coloured woodcut illustrations of the aurora to accompany his publications. The Northern Lights may be seen in bands around the magnetic North and South poles that create an auroral oval when seen from space.

The bow shock separates the magnetosphere from the approaching solar wind. The solar wind's impending moment flow significantly distorts the Earth's dipolar field, creating a lengthy magnetotail on the night side. Another Norwegian scientist, Kristian Birkeland, who investigated the correlation between auroral activity and variations in the Earth's magnetic field, had previously seen the resemblance between the aurora borealis and a gas discharge.

New discoveries were made possible by active space research, which started in the International Geophysical Year of 1957. James van Allen (1914–2006) [25] created two toroidal bands of energetic particles between 700 and 10,000 km in height visible in 1958–1959 during the Pioneer IV and Explorer I&III rocket flights. The van Allen radiation belts are the name given to this inner belt and a second outer ring between 13,000 and 65,000 km in height. Protons with an energy of 100 MeV and electrons with an energy of hundreds of keV make up the inner belt. It is thought that protons are created when neutrons from cosmic rays striking the upper atmosphere decay in a process known as beta decay. Most of the energetic electrons in the outer belt come from Protons, beta particles, O+ ions, and energy between 0.1 and 10 MeV. The ionosphere is the region of the upper atmosphere where ionizing atoms and molecules receive solar UV energy. lists the names of the several areas of the neutral and ionized atmosphere of the Earth. An growing atom density is encountered by the entering UV photons as they travel from space into the atmosphere.

Gas Emissions

Now let's talk about cold plasmas created by humans using electric discharges. This is the field of applied plasma science, which also includes fluorescent lights, flash photography tubes, plasma TVs, high-power arc lamps for data projectors or street lighting, and many industrial applications like silicon wafer etching or silicon deposition on substrates for the production of solar cells and computer displays. Direct current (dc), alternating current (ac), or radio frequency (rf) voltage is supplied to each one of them, causing an electric gas breakdown that maintains the discharge.

Illumination

One of the classic fields for plasma use is lighting. Street illumination is provided by electric arcs in high-pressure lamps, while household and business lighting is provided by low-pressure discharges in fluorescent tubes based on their effectiveness, which is expressed in lumens per watt of electric input power. A lumen is a measurement unit used to describe the visible light flux (v into the complete solid angle 4), which is weighted by the relative sensitivity (V) () of the human eye. The highest potential effectiveness of a monochromatic source at the maximum of V () at 555 nm would be 683 lumens per watt. The colour

rendering index (CRI), which may be as high as 100 for accurate representation of coloured objects, is a crucial factor in household lighting. Plasma-based illumination uses radiation efficiently since it is within the human eye's spectral sensitivity range. Although the sun's broad spectrum provides light and heat to keep our habitat in good condition, it is currently not a good idea to imitate the sun's spectrum with incandescent lighting due to both economic and environmental reasons. Many nations have started to phase out the manufacture of all-purpose incandescent bulbs while this material is being written. Instead, high-tech incandescent lights employ a halogen cycle to reduce the amount of tungsten that evaporation blackens the glass and reduce heating power consumption thanks to an interior coating that reflects the infrared portion of the spectrum back to the filament. The efficiency is almost two times higher than that of regular bulbs.The fact that around 80% of the electric power of a low-pressure discharge in mercury vapour may be translated into ultraviolet light, which can subsequently be converted to visible light by fluorescent materials, is used by the majority of energy-efficient plasma-based light sources. Early fluorescent tubes produced the yellow and red portions of the spectrum using the mercury spectral lines at 435 nm and 546 nm in conjunction with the fluorescence of a halophosphor coating on the inner tube wall.

The CRI should be more than 80 for workplace lighting. Customers prefer values above 90 for home applications. Emerging technology known as light-emitting diodes has recently caught up to fluorescent lights in terms of effectiveness and colour rendering and may even surpass them in certain applications. This is accurate for computer screen backlighting and perhaps true for household usage. Previously, effectiveness for street lighting was more important than colour rendering. Modern urban lighting is starting to gain from increased effectiveness and better colour rendering as upgraded metal halide lamps replace high-pressure mercury lights. For high-power stadium lighting with more than 1 kW per luminaire, plasma lights are the only option available right now. The effectiveness and less carbon footprint of a lighting system based on mercury lamps are advantages from an environmental standpoint, whereas mercury poisoning is a disadvantage. Alternative mercury-free plasma light sources have already been encouraged by the prohibition on mercury in plasma lamps for automobile headlights and they may soon replace high-pressure lamps for street lighting.

Plasma Screens

Technical discharges up to this point have continued to be huge objects, ranging in size from a few centimeters to a meter. Plasmas with very tiny sizes of under a millimetre have most recently grown in significance. Plasma plays are one such example. Based on micro-discharges of submillimeter dimensions, they are used. The three fundamental colors of light—red, green, and blueare created using the same basic principle: a plasma discharge creates UV radiation, which in turn excites a phosphor, which emits the correct spectrum. The plasma display follows a similar set of procedures to a fluorescent tube discharge in this regard. In contrast to fluorescent tubes, which use mercury as their UV light source, plasma displays use a combination of neon and xenon as their filling gas, with the latter providing the UV light.

The discharge cell, which typically has dimensions of 0.5 mm, is made of a sandwich of transparent conducting electrodes that are printed in rows and columns to create a display matrix on a front glass and back glass substrate. By delivering a voltage pulse between the address electrode and bus electrode, the cells may be addressed. A sustain electrode with a lower voltage keeps the discharge going after it has discharged. The discharge electrodes are

encased in a dielectric layer rather of being in direct contact with the plasma. As a result, the discharge current is a dis- placement current that only runs briefly and produces a brief discharge flash. The brightness of the pixel is determined by the number of successive flashes. This discharge's cathode is composed of a thin layer of magnesium oxide. One ion impinging on this substance produces more than 30 secondary electrons, which sustain the discharge. This allows the discharge cell to function at a relatively low discharge voltage (95 V) while yet being quite effective. Glass barrier ribs are used to divide adjacent cells. A pixel is made up of three adjacent cells with distinct colours.

Diffuse Plasmas

We have so far covered the basic workings of a gas discharge as well as their technological application. Let's briefly go off topic to a subject where study is driven by the complexity of plasma systems. Stars and planets are created from the dust in outer space the sombrero galaxy M104's edge-on view reveals the enormous quantity of dust present in the galaxy, while the Whirlpool galaxy M51's face view reveals the dispersion of spiral arms. Newborn stars are created in proto-stellar discs as a result of the collapse of a dust cloud, which is often sparked by a supernova or the powerful stellar winds from neighboring star clusters.Since the 1990s, the study of dusty plasmas has expanded quickly. Phase transitions, wave phenomena, dust charge, and interaction forces have all been examined. Dusty laboratory masses demonstrated novel physics, such as the creation of spherical Yukawa balls or two- and three-dimensional plasma crystal. The extreme transparency of the dust clouds and the slow motion of the dust particles, which can be seen with quick video cameras, are what make this area of research so attractive. The ability to simultaneously observe the many-particle system at the "atomic level" and study plasma processes is very uncommon.

Regulated Nuclear Fusion

The heated plasmas of the stars are where our journey through plasma science eventually ends. But for now, we're interested in finding a way to use heated plasmas contained within fusion reactors to recreate the conditions seen inside stars. The rising global energy demand in the 21st century and beyond may be met through research into controlled nuclear fusion. Nuclear energy research was carried out under the cover of covert programmes in the post-World War II cold war period. At Princeton University in the United States, astronomer Lyman Spitzer (1914–1997) started constructing a stellarator apparatus. At the University of California's Livermore laboratory, Richard F. Post (1918–) began assembling a mirror machine. Igor Tamm (1895–1971) and Andrei Sakharov (1921–1989) were responsible for popularising the tokamak idea in the Soviet Union. Igor V. Kurchatov (1903–1960) unilaterally divulged to Western scientists the Soviet Union's work on controlled nuclear fusion in 1956. The 2nd Atoms for Peace Conference in 1958, where scientists from all over the world were permitted to share their findings, quickly paved the way for the peaceful use of nuclear fusion energy and laid the groundwork for "one of the most closely collaborative scientific endeavours ever undertaken" All of these initiatives have the same objective of using the energy generated by the fusion of deuterium and tritium nuclei to power a power plant.

Only at such kinetic energies of the fusion partners that defeat the Coulomb repulsion between the like-charged nuclei can a considerable yield of fusion events be anticipated. The fusion cross sections as a function of the particle energy in the center-of-mass system. The

tabulated data from are used in the illustration. The energy range for the fusion processes is between 10 and 100 keV. At the same energy, it is also discovered that the cross section for the D-T reaction is much bigger than that for the D-D or 3He-D reactions. This is the rationale for the use of D-T mixes in all current fusion reaction ignition investigations[11], [12].

A Particle Accelerator Does Not a Fusion Reactor

Why can't a particle accelerator be used as a fusion reactor right away? Obviously, accelerating ions to is not a significant technological challenge today. Assume that a beam of tritium ions with the right amount of energy is fired into a solid deuterium ice target, which may be a cube with a 1 cm edge length and deuterium atoms within. The ratio of the blocked area to the cube's cross section, or p, determines the likelihood of striking one of these target atoms. However, this indicates that only 99.97% of the bullets have generated a fusion reaction. Let's make the further assumption that the tritium beam represents a 1A electric current, which is rather significant at 100 keV energy. The cube is then struck by tritium ions per second at a rate of dNT/dt I/e (e is the elementary charge). A decent fusion power of 4.6 kW per cubic centimeter is obtained by multiplying this hit rate by the reaction likelihood, the fusion energy of 17 MeV, and the reaction probability. Will this ion beam, however, be able to break through a solid deuterium ice cube? Regrettably, no. The exchange of ions made of tritium with the electrons

CONCLUSION

Dust that is electrically charged may be found in Saturn's rings in our solar system. The interaction of the dust as a whole may be seen while the specifics of dust charging in the ring system are still being studied. Unexpected radial features (spokes) were discovered in the B-ring during the passage of the Voyager 2 spacecraft in 1981; they look black in backscattered light. Voyager 2 saw the same structures as brilliant features in forward scattered light after passing Saturn. This is a blatant indication that the spokes are made of dust with a diameter of a few microns. These spokes, which are normally 10,000 km long and 2000 km broad, do not move with the ring particles according to Kepler's laws. According to one of the existing theories, the dust is electrostatically levitated above the ring plane. A brief, concentrated plasma might be produced by an early transient event, such as a meteorite impact or a high-energy auroral electron beam, charging the rocks in the main ring with a negative potential. Dust particles on the boulder's surface pick up an additional electron and are driven away from the surface. They then emerge from the thick plasma cloud and are discovered in the constant background plasma environment. The Cassini probe, which is orbiting Saturn, is now doing a thorough analysis of the spokes.

REFERENCES:

[1] D. A. Uzdensky and S. Rightley, “Plasma physics of extreme astrophysical environments,” *Reports on Progress in Physics*. 2014.

[2] P. Gibbon, “Introduction to plasma physics,” in *CAS-CERN Accelerator School: Plasma Wake Acceleration 2014, Proceedings*, 2014.

[3] N. J. Kramer, R. J. Anthony, M. Mamunuru, E. S. Aydil, and U. R. Kortshagen, “Plasma-induced crystallization of silicon nanoparticles,” *J. Phys. D. Appl. Phys.*, 2014.

[4] W. Zou, F. Li, M. Liu, and B. Lv, "Existence of solutions for a nonlocal problem arising in plasma physics," *J. Differ. Equ.*, 2014.

[5] C. Charles, "Grand challenges in low-temperature plasma physics," *Front. Phys.*, 2014.

[6] W. J. Miloch, "Plasma Physics and Numerical Simulations," *W.J.Miloch@Fys.Uio.No*, 2014.

[7] B. M. Glinskiy, I. M. Kulikov, A. V. Snytnikov, A. A. Romanenko, I. G. Chernykh, and V. A. Vshivkov, "Co-design of parallel numerical methods for plasma physics and astrophysics," *Supercomput. Front. Innov.*, 2014.

[8] J. Willert, W. T. Taitano, and D. Knoll, "Leveraging Anderson Acceleration for improved convergence of iterative solutions to transport systems," *J. Comput. Phys.*, 2014.

[9] B. Pongrác, H. H. Kim, N. Negishi, and Z. Machala, "Influence of water conductivity on particular electrospray modes with dc corona discharge - Optical visualization approach," *European Physical Journal D*. 2014.

[10] S. L. Prunty, "A primer on the theory of Thomson scattering for high-temperature fusion plasmas," *Physica Scripta*. 2014.

[11] H. Xie, J. Zhu, and Z. Ma, "Darwin model in plasma physics revisited," *Phys. Scr.*, 2014.

[12] R. A. Treumann and W. Baumjohann, "Superdiffusion revisited in view of collisionless reconnection," *Ann. Geophys.*, 2014.

CHAPTER 2
DEFINITION OF THE PLASMA STATE

Dr.Nishant Kumar, Assistant Professor, Department of Science
Maharishi University of Information Technology, Uttar Pradesh, India
Email Id- nishant.kumar@muit.in

ABSTRACT:

When referring to plasmas, we will continue to use the same nomenclature, but in the plasma state, we have a mixing of two separate gases, light electrons and heavy ions. As a result, we must differentiate between the electron and ion gases using their respective densities, ne and ni. Additionally, plasmas often exist in a non-equilibrium state with distinct electron and ion temperatures, Te and Ti. Gas discharges are where these two-temperature plasmas are commonly encountered. On the other hand, a nice example of an isothermal plasma with Te,Ti is the solar plasma (in the interior and photosphere).There are several atom ionisation processes that may take place in the environment that plasmas inhabit. These include collisional ionisation caused by powerful electrons or photoionization caused by high ultraviolet light. Due to the abundant availability of energetic electrons in gas discharges, impact ionisation is the predominant mechanism electrons. Space plasmas with low electron and atom concentrations but potentially high UV photon densities are where photoionization occursthese processes and their reciprocal processes may be expressed in terms of simple reaction equations

KEYWORDS:

Electrons, Gas, Ions, Magnetic Field, Plasma.

INTRODUCTION

Positive ions and electrons combine gaseous to form the plasma state. The plasma in the Sun is totally ionized. Fluorescent lights, which have a lot of neutral atoms, are partly ionized. We will talk about the characteristics of the plasma state in this section, which arise from the presence of a large number of charged particles that interact with one another via electric forces. We'll show in particular how the plasma state may respond in a group setting. As a result, the plasma medium is greater than the sum of its parts[1], [2].

States of Matter

Let's review the characteristics of a neutral gas before delving further into the definitions of the plasma state. The numerical density n—abbreviated as n—of particles in a given volume defines a gas m^3 is the unit of n. The temperature T of the gas affects how the particles move when they are in thermodynamic equilibrium. The pressure in an ideal gas is given by the product of number density and temperature, where kB is the Boltzmann constant.

In addition to these volume processes, surfaces, such as the walls of discharges or embedded microparticles, may effectively recombine electrons and ions. Each of these volume processes, such as photoionization and two-body recombination or impact ionisation and three-body recombination, is counterbalanced by its equivalent reciprocal process in thermodynamic equilibrium. Plasmas created by impact ionisation often exist at high temperatures because neutral atoms' ionisation energies range from 3 to 25 eV. Short wavelength light, often in the UV area, is necessary for photoionized plasmas. In hot and

diluted plasmas, there are also situations when collisional ionisation is effective yet there aren't enough electrons for three-body recombination. Once a stable state is attained, two-body recombination balances impact ionisation. One such plasma that is not in thermodynamic equilibrium is the solar corona. As a last point, it is important to note that certain plasmas are controlled by non-local processes rather than local equilibria. For instance, the emission process at the Sun's surface and heating processes (such as shocks) that occur throughout the propagation of the solar wind from the Sun to Earth dictate the majority of the solar wind's characteristics at the Earth's orbit. The production of a negative glow by electrons that have acquired their energy in a separate location will be shown in Chapter 11 of the book.

The Boltzmann Distribution

Before delving further into the thermodynamic equilibrium of a plasma, it is important to keep in mind several fundamental ideas from classical statistical mechanics. The Boltzmann factor governs the relative population of various energy states there[3], [4].

Plasma Collective Behavior

What distinguishes a plasma from a neutral gas? Only after a collision, or when two gas atoms "feel" the short-range van der Waals force, which decays with the inter-particle distance as r 6, can particles in a neutral gas interact. Most of the gas atoms typically follow a straight route apart from other atoms. In a plasma, this is entirely different. Being a long-range force, the Coulomb force that characterizes electrostatic interaction decays only slowly as r 2. This implies that a huge number of particles interact with each plasma particle.

As a result, plasmas exhibit a multitude of particles responding simultaneously to an external stimulus. Plasmas exhibit collective behavior in this sense, which implies that the macroscopic reaction to an external stimulus is the coordinated action of many plasma particles. Examples of collective behavior include wave processes or the mutual shielding of plasma particles.

Debye Shielding

The capacity of a plasma to efficiently diminish electric fields is its most crucial characteristic. By adding a point-like additional charge Q to an indefinitely vast homogenous plasma that initially contains equal concentrations of electrons and singly charged positive ions ne0 ni0, we may examine this shielding effect. Let's suppose that the coordinate system's origin is where this additional charge Q is positioned. This causes a net space charge to develop close to Q, which tends to make Q's electric field weaker.The particle energy affects how the trajectory bends. The trajectory gets stiffer as the energy of the electrons (ions) increases, i.e., as the temperature of the electron (ion) gas increases.

As a result, a cold species of particle will be excellent at dissipating the excess charge, and we may assume that the perturbed area has a limited dimension whereas the perturbation has a larger range for hotter electrons (ions).Obviously, the thermal mobility of the plasma electrons and ions controls the shielding process, which is not static. Therefore, the Boltzmann factor is used to provide a straightforward statistical explanation. We count the quantity of electrons and ions present at an elevated electric potential in the region of Q to provide a quantitative description. For an objectionable potential [5], [6].

Plasma frequency and response time

The combined activity of many particles determined the reaction to an external electric disturbance. Debye shielding is therefore an illustration of the group behaviour of a plasma. The temporal scale is the second component of collective behaviour.The electrons then achieve a protected equilibrium. It will take a lot longer for the heavier ions to get to their equilibrium locations. The electron energy is not much altered from its thermal value when the potential perturbation is minimal, e kBT. As a result, the mean electron velocity continues to be near to the thermal velocity ve (kBTe/me)1/2 (for a more detailed explanation, see Sect. 4.1). The electron must be able to travel the usual distance.Due to its new location in order for the new equilibrium to be established. This period of time may be calculated as De/ve. The electron plasma frequency is the reciprocal of this reaction time we shall show that a change in thermodynamic equilibrium may cause oscillations in the plasma that are rather near to the electron plasma frequency. These waves or oscillations represent the electron gas's typical collective modes.

DISCUSSION

Plasmas may be found in a vast parameter space that spans twenty-five orders of magnitude in electron density and seven orders of magnitude in temperature. The electron temperature is shown by the temperature scale. Astrophysical circumstances, a few technological plasmas, and the controlled nuclear fusion regime are noted as typical instances.

Strong-Coupling Limit

The condition that there be a large number of electrons within the electron Debye sphere is the typical definition of a weakly linked or perfect plasma. This guarantees both the accuracy of the statistical derivation of a Debye length and the collective nature of Debye shielding. For this reason, we refer to the plasma parameter Quantum Effects as being the number of electrons within the electron Debye sphere. When the electrons' interparticle distance equals their thermal de Broglie wavelength, quantum processes start to take place. The most likely speed of a Maxwell distribution in this situation is vTe (2kBTe/me)1/2. The Pauli exclusion principle becomes crucial in this restricted scenario, necessitating the use of Fermi-Dirac statistics. Degenerate plasmas are what are known as cold, dense plasmas, and they are often seen in dead stars like White Dwarfs. Notably, the exclusion principle prevents the eventual collapse of such a burnt-out star[7], [8].

The second borderline for the degeneracy of the electron gas, B ne1/3, is similarly shown as a dashed line. The slope in this log n-log T figure is 3/2. Keep in mind that a metal's electrons constitute a highly linked degenerate system. The dot-dashed line indicates the temperature at which relativistic effects for the electrons become significant (T > 109 K). Non-relativistic models may all be used to analyse the designated areas of typical plasmas. This makes the plasma models in the next Chapters simpler.There are two types of plasmas: magnetised and unmagnetized. Because the travel of electrons and ions is controlled by electric fields and collisions and the Earth's magnetic field is too weak to affect the trajectories, the plasma in a fluorescent tube is not magnetic. Examples of naturally magnetised plasmas include the ionosphere, magnetosphere, solar wind, interstellar medium, and solar surface. The magnetic field there has a significant impact on how the particles move.

The mobility of individual charged particles under certain electric and magnetic fields is the main topic of this Chapter. The hunt for magnetic confinement of plasmas is particularly significant. Complex particle motion is caused by magnetic field lines' inhomogeneity, curvature, or fluctuation over time. The impact of particle currents on the electric and magnetic fields is disregarded by the single particle motion model. The model is still lacking in this area. However, the reader will learn about the fundamental characteristics of a plasma that is exposed to electromagnetic fields through studying particle motion.

The ions (or electrons) are said to be magnetised when they are capable of performing full gyroorbits. When gyroorbits are uninterrupted by collisions, this is the situation. The ion (electron) collision frequency must be less than the ion (electron) cyclotron frequency for this to occur. Typically, electrons rather than ions may better satisfy this criterion. The ions in a gas discharge plasma in the presence of the Earth's magnetic field may be treated as unmagnetized; a more thorough explanation of the interaction of gyromotion and collisions is given. This may have nothing to do with the frequency of collisions and is instead a result of the gyroradius's size, which is bigger than the discharge tube's diameter.

The Magnetic Field of the Earth

The magnetic field is shaped as a dipole field in the area immediately around the Earth. A magnetic dipole with a magnetic moment of M 7.3 1022A m2 may serve as a representation of the source of this field. The magnetic poles diverge from the geographic poles as a result of this dipole's tilt from the axis of rotation. Electric currents flowing through the Earth's core produce the magnetic field there. Confinement of Non-neutral Plasmas The basic configuration of the Earth magnetic field under the influence of the solar wind was demonstrated to be altered. The only kind of charged particles seen in a non-neutral plasma are typically positive ions. A typical Penning-Malmberg type magnetic trap appropriate for catching ions or electrons is seen. These traps use B > 1 T strong magnetic fields. This device's tests have been reviewed. By causing the ions to spin around the magnetic field line, the axial magnetic field B creates magnetic confinement. The positively-biased outside cylinders' electric fields, which push the ions away from the centre, provide the axial confinement. An area of positive space charge may be seen in the ion cloud. From cylindrical geometry and Poisson's equation, 3.2The Approximation for Drift. For the scenario of inhomogeneous and curved magnetic fields, approximative solutions are explored non this section. Despite the fact that the effects of inhomogeneity and curvature are linked by Maxwell's equations, we shall analyse each element separately.

A Guiding Center's Concept

As we've seen, an external force may be thought of as a net drift motion that is overlaid on a rotating particle's gyromotion. This concept will be used to describe motion in inhomogeneous magnetic fields. In order to do this, we presume that the genuine particle orbit may be divided into two parts: a circular orbit around a local guiding centre, and a drift motion of the guiding centre. We determine a net force for the drift motion, which is the average over one gyro-period. As with gravitational drift, this net force is then transformed into an equivalent electric field, and the drift velocity is calculated. A tiny magnetic field gradient is necessary for this approximation. This may be shown by the condition that the magnitude of the magnetic field at the guiding centre must not be significantly different from the change in the magnetic field over one gyroradius.

Drift in Curvature

We now go on to step two, where we evaluate curved field lines with constant Rc curvature. At the same time, we ignore the magnetic field's gradient, which was covered in the sentence before. The curvature causes a centrifugal force Fc to act on the particle as it moves down the field line, causing the curvature drift.

The Toroid Drift

A definition of the curvature drift expression As long as we do not understand how to link the radius of curvature of a field line to the gradient of the magnitude of B, seems to be substantially different from the gradient drift. We suppose that currents flowing beyond the considered volume are what cause the field lines of interest to form. These might be dynamo currents in the Earth's core that produce the magnetic field or currents in magnetic field coils that confine plasma. We may assume that the magnetic field is ir-rotational since the current area and the field region are not connected.

The Mirror Effect

A magnetic mirror field's confinement quality may be determined using the magnetic moment's adiabatic invariance. The magnetic dipole field of the Earth serves as a natural magnetic mirror. One may detect the rise in field line density and, therefore, magnetic flux density while following a field line from the equator to the pole (see Fig. 3.10a). Therefore, between the mirrors at the North and South poles, charged particles may get trapped. In the lab, magnetic mirrors may also be created, for example, between a group of coils that make a circular magnetic field. when the coils' separation The high density of field lines at the coil site and the lesser density in the midplane indicate that the magnetic field is inhomogeneous throughout the axis of the system when is greater than their radius. We shall now talk about the confinement of a charged particle travelling along the system's central field line. The particle's velocities at any place are vz along the axis and v = (v2 + v2)1/2, which is the gyro-speed. The magnetic field is B B0 and the particle has beginning velocities of v0 and vz0 in the mirror's symmetry plane. Around the mirror coils, the magnetic field B Bm is at its strongest. Energy conservation and the magnetic moment's adiabatic invariance regulate the particle's motion, respectively.

The Flux Invariant and the Longitudinal

There are precisely three adiabatic invariants that may be defined in terms of the three degrees of freedom of motion. The magnetic moment, which corresponds to the regular gyro-motion, is the first, trapped particles in a magnetic mirror bounce back and forth between the reflection sites on a slower time scale. An energetic proton is there held captive by the Earth's dipole field. We link the second adiabatic invariant J, also known as the longitudinal invariant, J = vdl, to this secondary periodic moment. Between the reflection spots, the integral is calculated. Compared to the magnetic moment, which is rather stable, the invariant J is more delicate.

The toroidal drift of this bouncing trajectory in the curved dipole field which results in a circular motion in the equatorial plane, is connected to the third periodic motion, which is linked with an even longer time scale. The third flux invariant, or the total magnetic flux encompassed by the drifting bounce-trajectory, is connected to this slow periodic drift motion. Even more brittle than J, is seldom ever used to computations.

Magnetic Confinement via Toroids

Because of continual particle scattering into the loss-cone area of velocity space caused by Coulomb collisions the issue of magnetic confinement in mirror fields is unsatisfactory. These particles constitute an intolerably enormous loss that leaves the mirror at both ends and prohibits a prolonged period of confinement. By bending the straight field lines into a torus, which eliminates the end losses, it advises avoiding these losses. These stellarators and tokamaks2 are ring-shaped confinement systems. The inhomogeneity and curvature of the magnetic field are the price for avoiding end losses. The toroidal magnetic field in tokamaks and stellarators is produced by external field coils, as for a straightforward torus. The fundamental principles of plasma confinement will be covered in this section using the single particle model.

The Tokamak Theory

By twisting the toroidal field lines such that after a few rotations around the torus' main axis, a field line on the outside of the torus goes to the interior of the torus, the net outward drift of the particles in a simple magnetized torus may be compensated. By superimposing a poloidal magnetic field B, it is possible to rotate the magnetic field in this manner. Such a poloidal field is produced in a tokamak by forcing a toroidal current into the plasma ring, which acts as the one-turn secondary of an enormous transformer. Although tokamaks have been used successfully to show energy gain through fusion reactions their operation is limited to about ten seconds due to the need to ramp-up the magnetic field in the transformer to drive the toroidal current by induction, which is ultimately limited by the saturation of the transformer's iron core. In theory, it is possible to produce a mode of quasi-steady state operation by using another method to drive the toroidal current, such as the radiation pressure of powerful radio waves or microwaves[9], [10].

The Stellarator Principle

The rotational transform in a stellarator is created by outside currents. Because it enables steady-state operation, this makes the stellarator appealing. In a traditional stellarator, pairs of conductors that are coiled in a helix around the torus produce the poloidal field. Such a configuration for the Wendelstein 7-A stellarator. The cross-section of the plasma is elliptical, with abrupt bends and rotations of the main axis. Modern stellarator theories use non-planar field coils that generate magnetic fields that are both toroidal and poloidal. The stellara- tor Wendelstein 7-X, which is now being built in Greifswald, Germany, is the most recent improvement depicts a schematic of how the superconducting modular coils are organised. The cryostat and vacuum vessel have been left out.

Collisions

The notion of atomic cross sections, which describe the collisions between charged plasma particles and atoms in gas discharges, is first introduced in this section. Later, we talk about charged particle Coulomb collisions, which are crucial for completely ionized hot plasmas.

Cross Section

The cross section of an alleged atomic sphere, a geometrical measure, may be used to represent the likelihood that an electron would collide with an atom. When the de Broglie wavelength of the electron is short in comparison to the size of the atom, quantum mechanics

may also explain how such a classical image of tiny particles striking a target works. The collision of two pool balls with radii r1 and r2 may often be used to represent collisions between atoms or between an ion and an atom. The projectile is assumed to be point-like in the cross-section idea, and the target is given the cross section that is really effective. As a result, the total of the collision radii serves as the definition of a collision between billiard balls[11], [12].

CONCLUSION

There are many non-deterministic or stochastic processes involved in the description of the hot gas of electrons and ions producing a plasma that call for a statistical description. The gas atoms of the parent gas or other charged particles may collide with the plasma components, which move at a broad range of velocities. It is no longer possible to explain the behavior of the plasma as a whole in terms of the predictable mobility of individual particles in predetermined fields. Instead, since there are so many particles, there are more uncertainties, which require us to characterize the plasma using average values. For instance, the average motion is influenced by macroscopic factors like temperature and density gradients, which produce electric currents or particle fluxes. In order to characterize typical transport patterns in gas discharges, this Section talks about the stochastic motion of particles and introduces basic statistical notions. Examples of common applications are presented in gas discharges, ion thrusters made for spacecraft, or the heat balance for nuclear fusion to demonstrate the ideas.

REFERENCES:

[1] T. Von Woedtke, H. R. Metelmann, and K. D. Weltmann, “Clinical Plasma Medicine: State and Perspectives of in Vivo Application of Cold Atmospheric Plasma,” *Contrib. to Plasma Phys.*, 2014.

[2] *et al.*, “RF Radiation Behavior of Rare Gas in Plasma State,” *IOSR J. Electron. Commun. Eng.*, 2014.

[3] M. Pernemalm and J. Lehtiö, “Mass spectrometry-based plasma proteomics: State of the art and future outlook,” *Expert Review of Proteomics*. 2014.

[4] D. Paraskevas, K. Vanmeensel, J. Vleugels, W. Dewulf, Y. Deng, and J. R. Duflou, “Spark plasma sintering as a solid-state recycling technique: The case of aluminum alloy scrap consolidation,” *Materials (Basel).*, 2014.

[5] C. Z. Wu *et al.*, “Accurate method to estimate insulin resistance from multiple regression models using data of metabolic syndrome and oral glucose tolerance test,” *J. Diabetes Investig.*, 2014.

[6] S. M. Vinko, O. Ciricosta, and J. S. Wark, “Density functional theory calculations of continuum lowering in strongly coupled plasmas,” *Nat. Commun.*, 2014.

[7] A. J. Cerfon and M. O’Neil, “Exact axisymmetric Taylor states for shaped plasmas,” *Phys. Plasmas*, 2014.

[8] C. Luschnig and G. Vert, “The dynamics of plant plasma membrane proteins: PINs and beyond,” *Development (Cambridge)*. 2014.

[9] Shailja Singh*et al.*, “The bright future of dentistry with cold plasma – Review,” *IOSR J. Dent. Med. Sci.*, 2014.

[10] H. Yoshida-Komiya, K. Takano, K. Fujimori, and S. I. Niwa, "Plasma levels of leptin in reproductive-aged women with mild depressive and anxious states," *Psychiatry Clin. Neurosci.*, 2014.

[11] A. Shahzad, A. Aslam, and M. G. He, "Equilibrium molecular dynamics simulation of shear viscosity of two-dimensional complex (dusty) plasmas," *Radiat. Eff. Defects Solids*, 2014.

[12] A. A. Ivanov *et al.*, "Arc plasma generator of atomic driver for steady-state negative ion source," *Review of Scientific Instruments*. 2014.

CHAPTER 3
MOBILITY AND DRIFT VELOCITY

Dr.Vikas Kumar Shukla, Assistant Professor
Department of Science, Maharishi University of Information Technology, Uttar Pradesh, India
Email Id- vikash.shukla@muit.in

ABSTRACT:

The applied electric field and collisions with the atoms of the background gas control the mobility of the electrons and ions in a gas discharge with a low degree of ionization. Most electron collisions take place in elastic media. We shall thus exclude ionizing collisions when calculating the frictional forces. The parent gas's positive ions and atoms have identical masses, which greatly facilitates the effective exchange of momentum between the heavier particles. In addition to elastic scattering, the process of charge exchange—in which a fast-moving ion picks up an electron and leaves a sluggish ion behind—also plays a significant role. This technique is analogous to a head-on collision in a game of pool in terms of momentum balance depicts a cartoon depicting electron motion on a gaseous backdrop. The momentum transfer is minimal when a light electron collides with a heavy atom.

KEYWORDS:

Collisions, Density,Electric, Electrons, Field, Plasma.

INTRODUCTION

Instead, the momentum of the incoming electrons is randomly redirected. There are many parabolic portions throughout the trajectory. We are limited to analyzing the average velocity of an ensemble of electrons because we lack a diagnostic to track the paths of individual electrons.

Dispersion

Electric field forces and density gradients control the average electron and ion mobility in a gas discharge. Diffusion is the name for the latter kind of net motion. What does microscopic diffusion entail? Let's take a look at a scenario where a heated electron plasma initially exhibits a negative x-direction density gradient.We presume that the gas atoms are at rest since the thermal speed of an electron is substantially greater than that of a gas atom. The density gradient makes it obvious that more electrons will flow to the right over time than to the left. As a result, there is a net downward motion. However, collisions with the gas atoms impede this electron mobility. The diffusion coefficient D describes this interaction of thermal motion of the electrons and friction with the neutral gas. Once again, we can only explain the average velocity in terms of the Fick's law relationship between the density gradient and the consequent particle flow.

In neutral gases, where particle motion is governed by collisions with other particles of the same species, such relationships were first discovered. In such case, diffusion is caused by more collisions with nearby particles of the same sort coming from the left than coming from the right, which results in an overall net force that is directed downward[1], [2].

Ambi-polar Diffusion

Since diffusion does not imply that the electrons clash with other electrons, the scenario for plasma electrons is quite different. For plasmas that are weakly linked, this impact may be disregarded. Instead, as stated above, the inhomogeneous density distribution and their thermal motion alone define the net motion. Since the electron temperature and density gradient act as the driving forces, electron diffusion is analogous to drift motion in this regard. Ions are subject to the same considerations.

Diffusion coefficient and mobility have been shown by Einstein to be linked to gas temperature. The above-mentioned reasons that temperature drives and electron-neutral collisions restrict electron transport in a neutral gas backdrop with a density gradient are quantified by this connection. The plasma responds by creating a space charge electric field E because the diffusion of electrons and ions results in various particle flow values, which would result in uneven densities of electrons and ions. In order for the plasma to stay macroscopically neutral, this field lowers the electron diffusion and speeds up the ion diffusion until they both reach a similar value. When electrons and ions are lost at the same rate, the end state is referred to as ambi-polar diffusion, and E is referred to as the ambi-polar electric field.The schematic representation of the electron and ion density profiles in a plasma under the effect of ambipolar diffusion. For the sake of clarity, the differences between the two profiles are exaggerated. Because electrons tend to exit the system quicker than ions, the plasma centre is predicted to contain an excess of ions, which creates a positive plasma potential. As a result, the outer plasma zone has a tiny electron excess. The corresponding space charge field E, which slows down electrons while accelerating ions, is shown[3], [4].

Diffusion in Cylindrical Geometry

The development of a plasma density profile in a homogeneous cylindrical glass tube of length L a, where an is the tube radius, serves as a common illustration of a diffusion issue. This condition occurs in the positive column, a region of quasineutral plasma in gas discharge physics, when plasma formation and radial ambipolar diffusion are in balance, leading to recombination at the wall. The extended equation of continuity with an ionisation source term serves as the governing equation for the steady-state issue.Here, we have set ne ni n while ignoring the little difference between ne and ni that generates the ambipolar field. Furthermore, it is believed that the temperature of electrons is constant everywhere. This supports assigning each electron a constant ionisation frequency. As a result, the ratio of electron density to ionisation frequency may be used to calculate the number of ionisation processes per volume and second[5], [6].

Magnetic field motion when collisions are present

We saw an ion in crossed electric and magnetic fields conducts an E B drift at a right angle to the electric field, even in the absence of collisions. The next section will demonstrate how collisions are necessary for current flow across the magnetic field. When we assume that a collision results in the complete transfer of momentum, as in charge-exchange collisions, we may examine the trajectory of an ion in crossed electric and magnetic fields under the influence of collisions in great detail. As a result of the perpendicular components of the electric field being bigger than the parallel electric fields, the trajectory lines basically become equipotentials.

In conclusion, the appropriate model to analyse the change from unmagnetized to magnetised ions is the motion of the ions in crossed electric and magnetic fields under the action of collisions. The ion Hall parameter ci/vm, ii B, which controls the degree of Hall motion, is a crucial parameter. The ions are unmagnetized and collisions take precedence over gyromotion when the Hall parameter is minimal. The ions get magnetised as it becomes big. The electrons are described using the same language. The plasma is said to be magnetised when both the electrons and the ions are affected. The example below demonstrates the intriguing new features of a plasma with magnetised electrons but unmagnetized ions.

DISCUSSION

Small spacecraft ion thrusters nowadays make advantage of the plasma Hall effect discussed in the section above. Such a gadget was used for the ESA's Earth-to-Moon mission SMART-1 and is discussed in the study and references therein. Fig. 4.17 illustrates the device's operating principle. The metallic anode within the annular gap where the plasma is formed is used to introduce the xenon propellant gas. Ceramic materials are used to insulate the plasma gap's walls. The magnetic circuit of this device, which consists of magnets and ferromagnetic discs (hatched regions), is its most crucial component since it creates a concentrated transverse magnetic field close to the plasma channel's exit. A high voltage is applied between an electron gun and the anode to perform a dc discharge[7], [8].

Electronic weapon serves as a neutralizer for the departing ion beam and provides primary electrons for the discharge process. In the discharge gap of Br 160 mT, the transverse magnetic field ensures that the electron Hall parameter ce/vm, e increases to a very high value. As a result, the electrons are essentially contained in a ring and move preferentially in the E B direction, as shown by the symbols and. When we suppose that the discharge voltage of 300 V lowers over a distance of 7.5 mm, which corresponds well with the thickness of the magnetized zone, we may explain the speed of these electrons. When compared to the ionization energy of xenon, which is 12.1 eV, the mean electron speed equates to an energy of 17.7 eV. Under these circumstances, the number of ionization processes per volume and second, reaches high values, resulting in 90–95 percent ionization of the propellant gas.

Because the cross-field mobility of the electrons resulting from electron-neutral collisions is too low to accurately reflect the real electron current, the axial motion of electrons, which makes up a portion of the discharge current, is still not entirely understood. It was hypothesized that micro-instabilities, the focus of current research, are what cause an unusual collision frequency. Although the effective electron Hall parameter will decrease due to the anomalous collision frequency, the electron cross-field resistivity will still be sufficiently enough to cause almost the whole discharge voltage drop to occur across the magnetised plasma layer.

The magnetic field in the discharge gap essentially has no impact on the ion mobility. The argument that the ion-neutral collision frequency is higher than the ion cyclotron frequency is not applicable in this case since it only holds true for prolonged plasma areas that are significantly bigger than the gyro-orbit. Instead, we see that the plasma gap's anodic region's xenon ion is virtually at wall temperature. The ion performs a brief segment of a gyroorbit with a radius of rL E(Bci)1 204 m as soon as it exits the gap and reaches the magnetised area, thanks to the strong electric field Ez 4 104 V m1. The ion orbit is almost straight since this radius is significantly bigger than the thickness of the magnetised zone, and the ion absorbs

all of the potential energy from the potential drop before leaving the thruster with 300 eV of energy. By taking measurements of the spatially resolved laser induced fluorescence on Xe+ ions, it has been confirmed that the acceleration to such an exhaust velocity of about 2 104 m s1 over the magnetized plasma area.

Because a beam of charged particles represents a space charge called ji/v, which repels other ions, it cannot simply be blasted into surrounding space. In Sections 9.2 and 9.4.4, these basic issues relating to space-charge constrained flow will be covered. Therefore, a supply of electrons closes to a thruster's exhaust neutralizes the ion space charge. These electrons are delivered by the electron cannon into the Hall thruster. In conclusion, the Hall ion thruster is an example of a plasma where different Hall parameters result in the localization of the potential drop in the magnetised region and subsequent acceleration of ions in the axial electric field, on the one hand, and the E B motion of the electrons for efficient ion-ization, on the other[9], [10].

Plasma Heat Balance

We will talk about the heat balance in several plasma systems in this section. The heating of electrons in a low-pressure gas discharge provides the clearest illustration of how the electron temperature may differ significantly from the temperature of heavier particles. The remaining two examples discuss the prerequisites for achieving controlled nuclear fusion in inertial confinement fusion and magnetic confinement fusion experiments.

Gas discharge using electron heating

We were only concerned with the average mobility of the electron (or ion) gas up until this point, which produced the diffusive flux and the electric current. The random mobility of electrons is now being studied, in particular the energy gains and loss processes and the consequent electron temperature. Electrons in the electric field acquire kinetic energy at a rate between two elastic collisions. The electron temperature is proportional to the energy gained between two collisions, which is proportional to E mfp, the sum of the electric field and the mean free path, as we had anticipated. However, contrary to what one may have assumed from the proportionality factor is just the square root of that equation and not the atom-electron mass ratio. Along with raising the temperature, we also had to take the square root of temperature into consideration to account for the drop-in growth rate and rise in loss rate. In gas discharge physics, the basic law Te f (E/p), where the gas pressure p stands in for the atom density, is known as the proportionality TeEmfp. In conclusion, the energy gain E mfp between two collisions does not only determine the electron temperature. Instead, only a tiny portion of the energy is lost in the impact, which is mostly responsible for changing the momentum vector's direction. Consequently, the electron's kinetic energy increases throughout a series of free flights in between two collisions. When the rate of energy gains as predicted matches the rate of energy loss, a steady state is obtained. This demonstrates that the ineffective cooling mechanism is the reason of the elevated electron temperature depicts a typical scenario for a flow equilibrium that is controlled by a loss rate that relies on the amount of a quantity that has been attained. Bernoulli's law, which states that the speed of outflow is given by v = (2gh)1/2 and the water level h is defined by the water level h when a bath tub is filled with a constant water current Iin.Up until the outflow rate equals the input rate, the water level increases to the filling height h. The electron temperature increases until gain-loss equilibrium is established according to the same theory[11], [12].

Fusion Reaction Ignition Using the Lawson Criteria

Nuclear fusion reactions must create more energy per unit of time than is lost via radiation processes and the loss of energetic particles to the walls in order for them to reach a stable state. Otherwise, the temperature of the plasma would drop and the fusion event would stop. All deuterium and tritium atoms will be entirely ionized in a hot plasma with T > 10 keV. In dilute plasmas utilized in magnetic fusion experiments, Bremsstrahlung, which results from electron-ion Coulomb collisions, is the major radiation source.

Bremsstrahlung

In X-ray tubes, bremsstrahlung occurs when electrons with an energy of 20–100 keV strike a solid target, such as a copper or tungsten anode. The powerful electric field of the atomic nucleus deflects these energetic electrons, which may go far into the atom's electron shells. The acceleration of the deflection causes the electrons to radiate. Operating the plasma in the so-called high-confinement mode (H-mode) allowed for lengthy energy confinement durations. The purpose of this introduction does not extend to an explanation of H-mode physics has extra information on this topic for those who are interested.

Fusion via Inertial Confinement

The Lawson criterion's principles may be used in two distinct situations. The plasma density in magnetic confinement fusion is modest (1020 m^3) and the energy confinement duration is lengthy. The opposite idea is used in inertial confinement fusion (ICF), which has a quick confinement period and a high plasma density. The goal is to burn a considerable portion of a tiny pellet's D-T content before the plasma has greatly grown. Reviews and a tutorial have both discussed contemporary ICF principles in detail.

Time of Inertial Confinement

A homogeneous sphere of hot plasma's confinement time may be calculated as follows: Assume for the moment that a vacuum surrounds the high-pressure plasma of radius R. Then, a rarefaction wave from the spherical Implosion will move at the speed of sound (cs). When a spherical target is exposed to strong laser light with a power density of 10^{14}–10^{15} W m2, the energy is absorbed on the surface, creating a plasma with a temperature of (2–3) keV and a few hundred megabars of pressure. A low-Z material, such as beryllium, or plastic foam make up the outermost layer (ablator). A D-T ice layer with a thickness of around 80 m is deposited within. D-T gas, which has a mass density of 0.3 mg/cm^3 and a pressure of 30 bar at room temperature, is used to fill the volume. The idea is to keep the primary fuel close by dense and relatively cold while heating and compressing the central gas filling to fusion temperature of around 5 keV. The underlying idea is that the centre hot area will self-ignite.

The motion of the particles in the single-particle model was generated from fixed external electric and magnetic fields. This method is highly helpful in gaining a preliminary understanding of the complexity of plasma motion, which causes a variety of particle drifts. This model's main flaw is that it ignores how these drifts reflect the electric currents that modify the fields. This problem is addressed in the current Chapter on fluid models.

A plasma model's self-consistency is a crucial component. Only in such models can phenomena like solar prominences be explained when a magnetic field seems to be locked in the highly conductive plasma. Hannes Alfvén (1908–1955), a Swedish scientist and Nobel

laureate, had seen this interaction between the magnetic field and plasma and had predicted the existence of a new class of magneto-hydrodynamic waves that have since been given the name Alfvén waves.

Model of Two Fluids

Newton's equation cannot be solved individually for each of the countless particles. Therefore, rather than following individual molecules, we will look for a description that is akin to hydrodynamics, which studies the motion of fluid components. In particular, a self-consistent description for the plasma motion and the electromagnetic fields will be employed to make the plasma model realistic.

Maxwell's Equations

A correct integration of Maxwell's equations with particle currents and space charges serves as the foundation for the fluid model. The electric field E and the magnetic field B are used in the form that Maxwell's equations are presented in. The terms magnetic induction, magnetic field, and magnetic flux density will all be used interchangeably when referring to B. E and B are the natural field quantities since they may be seen in the equation of motion. Here, j is the particle current density and is the overall charge density. These two numbers capture how the plasma mobility affects the fields. Recalling briefly the physical components of the collection of Maxwell's equations.

The Poisson equation, which connects the electric field with the space charge, is the basis of the connection. For issues with electrostatics in plasmas, this will serve as our mainstay. We often also make use of the electric potential, which is connected to the electric field by the equation E. Faraday's induction law is presented in differential form in equation (5.2). The integral version of the induction law, Uinddm/dt, which says that the voltage induced in the loop is the (negative) change in the magnetic flux through this loop, is obtained by integrating the electric field around a loop of area A that surrounds a magnetic flux m = A B dA. A change in area A, a change in the magnetic flux density B, and a change in the angle between the magnetic field direction and the area normal, which is included in the dot product B dA, may all affect the induced voltage.

It has been shown experimentally that there are no magnetic monopoles in everyday stuff due to the disappearance of the divergence of the magnetic flux density B. According to Ampere's equation the displacement current E/t and the conduction current j determine how the magnetic flux density B curls. We will use the integral version of Ampere's equation, B • ds = 0 I, to get the stationary magnetic field of a straight wire. We now need to talk about why we don't utilise the dielectric displacement D or the magnetic field strength H. An significant finding of the single particle model was that a rotating particle possesses a magnetic moment that is perpendicular to the direction of B. A plasma is a diamagnetic medium as a result. Furthermore, when changing the magnetic flux density, the magnetic moment is either a conserved quantity or scales as 1/B when the particle energy is set. As a result, we cannot anticipate the usual proportionality of ferromagnetic materials. Therefore, adding H would not aid in the simplification of our models.

Additionally, we had observed that a plasma's electric polarization only manifests itself in time-varying fields. Any static polarization charges can only be found at the plasma surface, but the associated electric field will be insulated within the plasma. D is thus not a number

that can be used to represent static circumstances.On the other hand, while discussing plasma waves, we shall specifically refer to a plasma as a dielectric medium. We may divide the plasma particles into pairs of electrons and ions that produce local oscillating dipoles when we use the simplified model for electron waves in a low-temperature plasma, where an ion is virtually at rest and the electron responds to the oscillating electric field.

A Fluid Description's Concept

Between plasma fluid models and hydrodynamics, there is a key distinction. The liquid's molecules are tightly linked in hydrodynamics. This indicates that the molecules are constantly crashing into one another. By diffusion, a pair of particles will only gradually move away.

CONCLUSION

As a result, it makes sense to divide the liquid into macroscopic fluid components since these components have numerous molecules that stick together for a long period. These fluid components follow the flow pattern's streamlines as they travel. However, the electrons and ions do not interact with their close neighbors in a perfect plasma. Therefore, Coulomb collisions are few. Instead, the average electric and magnetic fields that are created by several other particles act as forces that the electrons and ions must obey. As a result, the plasma may be divided into tiny cells, but this does not guarantee that the particles will remain there for a long period. After a transit period, the electrons and ions usually depart a cell of size while particles from other cells enter this volume. In order to keep track of gains and losses in the total number of particles, total momentum, or total heat content in each cell, we may utilize these cells as a form of bank account. We shall show that although this method provides us with a hydrodynamic description, the comparison to actual liquids has its limits. Depending on the circumstance, we may haphazardly choose a description with fixed cells in a resting frame of reference or switch to a moving frame of reference that tracks the plasma's mean flow velocity.

REFERENCES:

[1] V. Lisovskiy *et al.*, “Electron transport parameters in NF3,” *J. Phys. D. Appl. Phys.*, 2014.

[2] A. Chandra, A. Bhatt, and A. Chandra, “Ionic mobility, drift velocity, and dielectric studies on Ag+ ion conducting glassy electrolytes,” *Chinese J. Phys.*, 2014.

[3] A. V. Chudinov *et al.*, “Study of electrospray ion mobility dependence on the ion bunch drift velocity in the radio frequency quadrupole,” *J. Anal. Chem.*, 2014.

[4] R. E. Troncoso and Á. S. Núñez, “Brownian motion of massive skyrmions in magnetic thin films,” *Ann. Phys. (N. Y).*, 2014.

[5] R. Shi and Y. T. Wang, “One-dimensional steady transport by molecular dynamics simulation: Non-Boltzmann position distribution and non-arrhenius dynamical behavior,” *Commun. Theor. Phys.*, 2014.

[6] O. Bénichou, P. Illien, G. Oshanin, A. Sarracino, and R. Voituriez, “Microscopic theory for negative differential mobility in crowded environments,” *Phys. Rev. Lett.*, 2014.

[7] K. J. Gillig and C.-H. Chen, "Increasing the Performance of Portable Ion Mobility Analyzers: Development of the Periodic Focusing Differential Mobility Analyzer (PFDMA)," *Mass Spectrom.*, 2014.

[8] A. Kanevce, D. H. Levi, and D. Kuciauskas, "The role of drift, diffusion, and recombination in time-resolved photoluminescence of CdTe solar cells determined through numerical simulation," *Prog. Photovoltaics Res. Appl.*, 2014.

[9] S. Rakheja, Y. Wu, H. Wang, T. Palacios, P. Avouris, and D. A. Antoniadis, "An Ambipolar Virtual-Source-Based Charge-Current Compact Model for Nanoscale Graphene Transistors," *IEEE Trans. Nanotechnol.*, 2014.

[10] A. Ilgaz, S. Gökden, R. Tülek, A. Teke, S. Özçelik, and E. Özbay, "Temperature dependent hot electron transport in slightly lattice mismatched AlInN/AlN/GaN heterostructures," *J. Optoelectron. Adv. Mater.*, 2014.

[11] D. A. Prokopovich, M. Ruat, D. Boardman, and M. I. Reinhard, "Investigation of Polarisation in CdTe using TCT," *J. Instrum.*, 2014.

[12] V. M. Rozenbaum, I. V. Shapochkina, and T. E. Korochkova, "Adiabatic Brownian ratchets with the inclusion of inertia," *JETP Lett.*, 2014.

CHAPTER 4
THE PINCH EFFECT

Dr.Vikas Kumar Shukla, Assistant Professor
Department of Science, Maharishi University of Information Technology, Uttar Pradesh, India
Email Id- vikash.shukla@muit.in

ABSTRACT:

The idea of a pinch discharge is a highly effective way to create a hot plasma without worrying about lengthy confinement durations. A plasma may be magnetically contained and heated to millions of degrees using strong pulsed currents, ranging from 10 kA to several MA. The Z-Pinch and the -Pinch are two distinct geometries that make use of the pinch effect. The names in cylindrical coordinates indicate the direction of current flow. The plasma in the Z-pinch comes into touch with metallic electrodes, which might lead to plasma contamination. There are no electrodes on the -pinch. Instead, the surface current I of the plasma cylinder is induced by the current I in an external coil with just one winding. In the gap, both currents produce the axial magnetic field Bz. Both times, the magnetic pressure at the plasma surface causes the plasma to be compressed into a small cylinder.

KEYWORDS:

Frequency, Interferometer, Magnetic, Plasma, Wave.

INTRODUCTION

The balance of kinetic pressure in the center and magnetic pressure at its surface, may be used to define the equilibrium of a Z-pinch. Alfven's Compression Wave In order to be thorough, it should be noted at the conclusion that there is a second kind of Alfvén wave that propagates against the direction of the magnetic field and includes compression of the magnetic field when gas pressure influences When the phase velocity is omitted, it changes back to, but this time the analogy to a sound wave, is valid. Since there are two degrees of freedom in this scenario, which correspond to the two directions perpendicular to the magnetic field, the magnetic pressure acts as the gas pressure. The compressional Alfvén wave transforms into a magneto-sonic wave when the kinetic pressure cannot be ignored the magneto-sonic wave's propagation speed is given [1], [2].

The Parker Spiral

High conductivity is a property of the solar wind. As a result, the magnetic field is imbedded in the growing plasma's mass flow. The Parker spiral, so called in honour of Eugene Parker who originally defined this structure via MHD is an Archimedian spiral that is created by the rotation of the Sun. We shall now talk about how this will affect the interplanetary magnetic field. The solar wind would simply increase in flux tubes created by radial magnetic field lines if the Sun didn't spin. In this spherical shape, flux conservation would lead the mass density to drop.

Br is what the magnetic flux conservation would result in. Because the construction of an Archimedian spiral is only a translation to a rotating coordinate system, which has no effect on the number of field lines crossing a spherical shell of radius r, this condition is true even in the presence of solar rotation. There will be an azimuthal component B in the solar equatorial plane in addition to the radial magnetic field component Br. We were only concerned with

the evolution of the magnetic field components through a single flux tube, which is one branch of the Parker spiral, up until this point. It is not unexpected that the Parker spiral contains two or four sectors of alternating polarity under calm circumstances because the Sun cannot be a magnetic monopole with outward field lines of the same polarity. These sectors are stable for many solar rotation times. The sector structure is intricate and characterized by a significant number of transient disturbances during solar maximum circumstances.

Different factors have sparked interest in wave propagation in plasmas. One of them was the ionosphere's ability to reflect electromagnetic radiation Oliver Heaviside (1850–1925) and Arthur Edwin Kennelly (1861–1939) independently proposed in 1902 that the Earth's atmosphere at high altitude must contain an electrically conducting layer that reflects radio waves like a mirror in response to Guglielmo Marconi's (1874–1937) experiments on long-distance radio in 1901. Carl Friedrich Gauss (1777–1855) proposed the theory that electric currents in the upper atmosphere may be connected to variations in the Earth's magnetic field many years earlier, in 1839. The vertical sounding experiments conducted in the United States by Gregory Breit (1899-1981) and Merle Antony Tuve (1901-1982) as well as in Great Britain by Edward V. Appleton (1892-1965) which established the existence of a conducting atmospheric layer, now known as the ionosphere, in the altitude regime of (100-500) km, marked the beginning of the quantitative investigation of the ionosphere with radio waves. of the same time, Irving Langmuir of the General Electric Laboratories discovered what are now known as Langmuir oscillations, which are high-frequency variations in gas discharges The categorization of the basic wave types in a plasma, which illuminates the many processes that give rise to wave phenomena, is of interest to us at the book's introductory level. At the same time, we'll talk about how different wave types may be used to plasma diagnostics. There are many contemporary textbooks that provide an in-depth discussion of plasma waves.

The Wave Equation and Maxwell's Equations

This Section examines the plasma's interactions with electromagnetic waves using a novel theory in which the plasma is seen as a dielectric medium. The dielectric constant of the plasma medium, which is used for this, includes the linear response of the plasma particles to the wave field influences the plasma waves' polarisation and rate of propagation. The Maxwell equations serve as the beginning point for this model's development[3], [4].

Dielectric or conducting media

We may interpret the current density differently since we assumed a linear relationship between the alternating current and the electric field. The wriggling motion of electrons and ions may be seen of as a polarisation current when the plasma is viewed as a dielectric media. This polarisation current can be paired with the vacuum displacement current 0(E/t). Only at the upper limit of extremely high frequencies. The considerably heavier ions will be stationary while the electrons will fluctuate around their mean location. As a result, we are free to think of the plasma as a collection of dipoles generated by couples of ions at rest and an electron circulating around them. A characteristic of such a media is the dielectric displacement.

I serve as the unit tensor here. The electric field vector E and the electric current vector j may no longer be parallel to one another as a result. Additionally, the plasma is a lossy dielectric medium due to particle collisions, therefore is often a complicated function. There are two main perspectives on the plasma medium, to sum them. When there are only minor losses, the

plasma mostly exhibits dielectric behaviour, and this behaviour is captured by the dielectric function (or tensor), in which the real component predominates over the imaginary part. When collisions happen often, the plasma mostly functions as a conductor and is represented by the complex conductivity, where the imaginary component reflects phase changes brought on by inertial factors. Following, we'll focus mostly on scenarios when the plasma waves are just somewhat dampened. Thus, the majority of the dielectric tensor's components are actual quantities. We shall thus favour the dielectric description of a plasma.

DISCUSSION

We have assumed up to this point that friction with the neutral gas has no impact on the velocity of the electron in the wave field. When the wave frequency (such as that of a laser beam) is much greater than the collision frequency, this approximation is unquestionably accurate. This hypothesis is backed by Newton's equation in Fourier notation, which demonstrates that the resultant electron velocity may be divided into a real and imaginary response component with respect to the electric field. The in-phase response, which results from the collisions of electrons, mimics the function of a resistor. The imaginary portion of the response corresponds to a current that lags the voltage by 90. The system's electron inertia, which acts like an inductance, is what causes the lag[5], [6].

We may apply a quick method to write down the dispersion relation with collisions by noticing that when we rewrite in terms of an effective mass m, it becomes equal with the collisionless limit displays the resultant complicated dispersion relation k. While the imaginary component of the wavenumber explains the damping of the wave amplitude, the real part of the wavenumber provides the development of the spatial phase. Keep in mind that at plasma frequency, the imaginary and real parts of k intersect. The collisionality makes the plasma a resistive material for wave frequencies below the plasma frequency. This explains why, despite the electron plasma frequency being significantly greater, we can generate a plasma at radio frequency (for example, at 13.56 MHz). The correct wave energy dissipation caused by the collisionality results in the heating of the electron gas via the Joule effect. On the other hand, when > 2pe, collisional damping is hardly noticeable. In light of this, it is still possible to determine the refractive index of a weakly collisional plasma if the wave frequency is significantly higher than the cut-off frequency[7], [8].

Laser and Microwave Interferometry

Because the unmagnetized plasma is an isotropic media, a dielectric constant rather than a tensor is used to characteriseits dielectric characteristics. Therefore, we may determine the electron density by measuring the refractive index, such as using an interferometer. The refractive index N for a collisionless plasma is less than unity, zero at the frequency of the electron plasma, and imaginary at lower frequencies. When the wave frequency is lower than the electron plasma frequency, an electromagnetic wave is therefore reflected at the surface of a plasma. This explains why a small coating of silver on a glass mirror may reflect visible light but becomes transparent in the UV range thanks to the free electrons of the silver atoms in the conduction band. A weakly collisional plasma would permit wave penetration with an exponential decay exp(kIx) given by the imaginary component of k, as was previously explained. We may investigate a plasma with a density gradient and a wave with a set frequency instead of taking into account a specific plasma with a constant density for different wave frequencies. The cut-off density nco is thus defined as the location at which

the local plasma frequency, which at that location corresponds to the electron density, coincides with the wave frequency. Similarly, we may take into account a non-stationary plasma that is turned on at time t 0 and eventually approaches the cut-off density. Therefore, the cut-off density may be associated with an inhomogeneous plasma, its temporal development, or both. As a result, the simplest approach of diagnosing plasma density is to determine whether the plasma permits wave transmission or not.

Mach-Zehnder Interferometer

But using an interferometer to measure the refractive index is a more tasteful approach. Depending on the plasma density, this may be accomplished using coherent radiation sources in the microwave, infrared, or visual range. A Mach-Zehnder interferometer is a standard setup for interferometry using microwaves or lasers. The basis for interferometry is the phase difference between the reference wave, which travels the same distance in air, and the wave that enters the plasma. In practise, this is done by dividing the wave into two identical branches and merging them together on a detector where the waves interfere. The geometric length L and the refractive index R are multiplied to create the optical path through the plasma. The phase shift is no longer proportional to the wavelength's inverse, as may first imply, but rather becomes proportional to the wavelength as the cut-off density falls with. This means that long-wavelength lasers or microwaves are required for density measurements at low electron densities. The geometric optics approximation, on the other hand, restricts the maximum wavelength and necessitates that the plasma dimensions be big relative to the wavelength. The attainable sensitivity of interferometers is constrained by this conflict[9], [10].

The plasma density during the present pulse is much greater than the cut-off density. The interferometer signal exits the cut-off zone 600 seconds after the present pulse ends and begins to fluctuate around a mean value. The phase shift of one interferometer fringe is equal to two units. A quarter fringe resolution is obtained by reading the interferometer signal's peaks, minima, and zero crossings. These result in the data points in Fig. 6.6b, which are shown on a logarithmic scale to illustrate the exponential decrease of plasma density in the discharge's afterglow. The precise formula (6.48) was used to examine the data points close to the cut-off in this evaluation.

Michelson interferometer that is folded

There are two techniques to increase an interferometer's sensitivity: First off, a new kind of interferometer should be employed, such the Michelson kind, which already has a beam that has passed twice through it. By folding the beam into a z-shape, which creates a six-fold passage, the sensitivity may be increased even further, albeit at the sacrifice of spatial resolution. The transmission band of quartz windows is still in the range of the laser wavelength (3.39 m). Special materials would be needed for windows and optical components with a longer wavelength. Second, reading accuracy is only 45 when counting interferometer fringes. As a result, a more accurate method should be used to measure the real phase angle. This may be done via quadrature detection, which involves making two separate interferograms with sine and cosine waves in the reference branch. Technically, this is accomplished by dividing the two interferometer signals using orthogonal polarizers and employing a circularly polarized wave in the reference beam that is produced by a /8 plate that is crossed twice.

Interferometer for Second-Harmonic Waves

The second-harmonic interferometer is a unique kind of two-wavelength interferometer that was developed by Hopf and colleagues. Currently, this method is used, for instance, in the diagnostics of the Alcator C-mode tokamak. Because the reference beam and probe follow the same route in second-harmonic interferometry, the interferometer is less sensitive to mechanical vibrations than it is in traditional interferometers with a distinct reference branch. The probe beam is the original signal from aNd: YAG laser operating at a wavelength of 1064 nm.

Although it likewise travels through the plasma, the frequency-doubled wave at 532 nm does so with a distinct phase shift. The probe wave is still powerful behind the plasma and may have its frequency increased by using a second crystal. Then a filter stops the basic wave. On the detector, interference fringes are produced by both 532 nm waves. When we disregard the various refractive indices of air at the two wavelengths, we can see that the contribution from the air gap cancels. By a ratio of 1.5, the second-harmonic interferometer is more sensitive than a typical interferometer that operates at the fundamental frequency.

Microwave Cavities with Plasma

It is also possible to detune the resonance frequency of cylindrical microwave cavities using the refractive index of a plasma. Due to the resonance frequency's high sensitivity to changes in electron density, this is especially helpful at low electron densities. Fig. 6.9a depicts a typical setup for this approach. The TM0m0 cavity modes, which have an electric field aligned with the cylinder's z-axis, are suitable for detecting the resonance. (For more on microwave cavities and wave-guides, see, for instance, [74])

As a result, the top and bottom of the cylinder are perpendicular to the z-axis and the electric field is uniform along the z-axis. The TM0m0 modes' eigenfrequencies are therefore unaffected by the resonator height. The eigenfrequency of the cavity is determined by the radial boundary condition at the cylinder radius, Ez(R).

The eigenfunctions have the following structure when the cavity is filled with a homogenous dielectric material of dielectric constant. The frequency of the empty cavity determines the cut-off density in this approximation. The cavity's Q-factor may be increased to a very high value, Q010 > 5000. A density resolution of n nco/Q results from this. Fundamental resonance f1 1.15 GHz and cut-off density nco 1.6 1016 m3 are found in an empty cavity with R 100 mm. As a result, densities as low as 1 1014 m3 may be determined with accuracy. For example, the impact of electron depletion in a dusty plasma was studied using cavity detuning [109]. The cavity approach may also be used to discharge tubes with a radius of a R that only partially fill the cavity [Fig. 6.9b]. Consequently, a factor of about a/R is added to the reduction in sensitivity to plasma density.

Bohm-Gross Waves

The aforementioned Langmuir oscillations become dispersive when we think of a heated electron gas, where pressure forces are comparable in strength to electric forces. The following may be used to obtain the dispersion relation: Since the electrostatic waves are one-dimensional, we begin by incorporating the pressure per particle into Newton's equation in one spatial dimension.

Ion-Acoustic Waves

There is a second electrostatic wave in a plasma containing heated electrons when we let the ions to participate in the wave motion. This is feasible at wave frequencies that are significantly lower than the frequency of the electron plasma. It should be noted that low-frequency electrostatic modes are unaffected by the plasma cut-off, which was a characteristic of the transverse electromagnetic mode. When considering low-frequency modes, inertial forces may be disregarded since the motion of the electron is only affected by pressure forces. Alternatively, we may think of the ions as a fluid that is controlled by the interaction of the electric field force, ion inertia, and ion pressure. It is advisable to account for various ion and electron equilibrium densities. Because of quas-ineutrality, a two-component plasma of electrons and positive ions has ne0 ni0; nevertheless, we'll look at a more general example in which the existence of a third negative species results in the difference in densities. These might either be negatively charged dust particles or negative ions.

When we see that the numerator rather than, as we would require for the electron pressure, this interpretation is plainly incorrect. The ion mass density creates the same issue in the denominator. Therefore, the model of the ion-acoustic wave's mechanism has to be updated. By thinking of the electrons as a fluid with the opposite charge that protects the electric repulsion between the ions rather than a gas that imposes pressure, the seeming contradiction may be explained. The interaction between the ions is thus nearing their bare repulsion when the phase velocity rises when the electron density is decreased. The rise in phase velocity with increasing ratio n/ne, indicates that this phenomenon is well known from negative ion plasmas. the phase velocity of the ion-acoustic wave in a dusty plasma is larger than it would be in a plasma without dust.

Waves in Magnetized Plasmas

The impact of a magnetic field on the propagation of plasma waves will be covered in this section. We limit the subject to cold plasmas to prevent the entanglement of magnetic field effects and pressure effects. We are then able to apply the single particle model. The beginning is once again, using Newton's law of motion[11], [12].

CONCLUSION

Modern approaches include polarization analysis of coherent radar backscatter or Faraday rotation imaging with numerous satellites while studying the ionosphere plasma. After being shown in the TEXTOR device polarimetry with numerous ray pathways is now a widely used technique that can measure the poloidal component of the magnetic field in fusion devices. Long wavelengths in the far infrared are favored from the perspective of sensitivity. These infrared wavelengths have also been used in the Compact Helical System and a reversed field pinch. The magnetic field in the solar corona may be studied using Faraday rotation, as is common in the example. Here, a radio telescope is used to estimate the rotation measure for several radio sources that are close to the ecliptic as the sun and its corona pass by them at various distances. Because the rotation measure only yields the line-averaged product of the electron density and parallel magnetic field, the amount of the effect is predicted using a model for the density distribution and the coronal magnetic field illustrates the contrast between measurement and anticipation. Radio transmitters on solar-orbiting spacecraft were used in a similar manner.

REFERENCES:

[1] R. Nataraj, P. J. Evans, W. H. Seitz, and Z. M. Li, "Effects of carpal tunnel syndrome on reach-to-pinch performance," *PLoS One*, 2014.

[2] J. H. Villafañe and K. Valdes, "Reliability of pinch strength testing in elderly subjects with unilateral thumb carpometacarpal osteoarthritis," *J. Phys. Ther. Sci.*, 2014.

[3] X. Ye, X. Li, G. Song, and G. Tang, "Effect of recovering damage and improving microstructure in the titanium alloy strip under high-energy electropulses," *Journal of Alloys and Compounds*. 2014.

[4] H. L. H. Barden, I. J. Baguley, M. T. Nott, and C. Chapparo, "Measuring spasticity and fine motor control (Pinch) change in the hand after botulinum toxin-a injection using dynamic computerized hand dynamometry," *Arch. Phys. Med. Rehabil.*, 2014.

[5] P. E. C. Hammer, R. Shiri, A. I. Kryger, L. Kirkeskov, and J. P. Bonde, "Associations of work activities requiring pinch or hand grip or exposure to hand-arm vibration with finger and wrist osteoarthritis: A meta-analysis," *Scandinavian Journal of Work, Environment and Health*. 2014.

[6] S. D. Knecht, W. Lowrie, and U. Shumlak, "Effects of a conducting wall on Z-pinch stability," *IEEE Trans. Plasma Sci.*, 2014.

[7] C. Ma *et al.*, "Research on Flashover Characteristics and the Physical Mechanism of High-Gain GaAs Photoconductive Switches," *IEEE J. Quantum Electron.*, 2014.

[8] L. C. Kuo *et al.*, "In vivo analysis of trapeziometacarpal joint kinematics during pinch tasks," *Biomed Res. Int.*, 2014.

[9] M. A. Bani, M. Arazpour, S. W. Hutchins, F. Layeghi, M. Bahramizadeh, and M. A. Mardani, "A custom-made neoprene thumb carpometacarpal orthosis with thermoplastic stabilization: An orthosis that promotes function and improvement in patients with the first carpometacarpal joint osteoarthritis," *Prosthet. Orthot. Int.*, 2014.

[10] M. M. Mansoor, J. O. Marston, I. U. Vakarelski, and S. T. Thoroddsen, "Water entry without surface seal: Extended cavity formation," *J. Fluid Mech.*, 2014.

[11] T. Maysonnave *et al.*, "Investigation of switch designs for the dynamic load current multiplier scheme on the SPHYNX microsecond linear transformer driver," *IEEE Trans. Plasma Sci.*, 2014.

[12] S. Bouhlal, S. Issanchou, C. Chabanet, and S. Nicklaus, "'Just a pinch of salt'. An experimental comparison of the effect of repeated exposure and flavor-flavor learning with salt or spice on vegetable acceptance in toddlers," *Appetite*, 2014.

CHAPTER 5
THE BASICS OF PLASMA BOUNDARIES

Dr.Vikas Kumar Shukla, Assistant Professor
Department of Science, Maharishi University of Information Technology, Uttar Pradesh, India
Email Id- vikash.shukla@muit.in

ABSTRACT:

We may anticipate that the plasma particles will have established quasi-neutrality beyond a certain location x d from the wall due to the effect of Debye shielding. The area d x 0 in which a sizable departure from quasi-neutrality is permitted is referred to as the space charge sheath, or simply the sheath. The sheath edge is located at location x d. The ion mobility in the sheath is further considered to be collision less. Since electrons have a much higher thermal velocity than ions do, they will collide with initially uncharged walls more frequently than ions do. This results in the accumulation of a net negative surface charge on the wall and a negative wall potential relative to the electric potential inside the quasi-neutral plasma. We'll assume for the time being that the wall is electrically grounded and that the charges aren't escaping via an external circuit. When the wall potential is negative, the amount of electrons that may reach the wall decreases until an equilibrium is established, in which the net charge on the wall achieves an equilibrium value, the floating potential, and the remaining electron flow to the wall equals the ion flux

KEYWORDS:

Current, Electron, Ion, Probe, Voltage.

INTRODUCTION

The boundary layer that a plasma forms to isolate itself from metallic or dielectric surfaces is darker than the main plasma itself. This is the first indication that there aren't enough electrons in the boundary layer to excite neutral atoms and create the glow of an electric discharge. Langmuir was the first to identify these dark areas as being regulated by a net (positive) space charge rather than being electrically neutral. Physical processes distinct from those mentioned for the quas-ineutral region of the plasma control the motion of the particles. A novel sort of many-body interaction that is typical of the collective behavior of a plasma is the interaction of one ion with the electric field from the space charge of all the other ions[1], [2].

Space-Charge Sheath

This straightforward illustration helps us understand why all isolated entities inside a plasma charge up negatively. This holds true for satellites in the Earth's plasma-sphere, small metal wires that Langmuir introduced as probes into the plasma, and dust particles in a plasma. Of fact, the actual situation is more complicated since, as we will show, the ion flow to a negative body is not governed by the ion thermal velocity except for the first instant. Furthermore, we could have overlooked further charging-related operations. These processes, which apply to satellites, include photoemission from solar UV radiation and secondary emission caused by the collision of energetic particles.

For completeness, we also add a presheath, a transition layer between the space charge sheath and the unperturbed plasma that corresponds to the circumstances between them. The electron and ion densities will vary on location, the ion drift velocity will not be zero, and the presheath will be quasineutral. The thickness of this transition area is about equal to one ion mean free path[3], [4].

The Child-Langmuir Law

Here, we take into account a scenario in which the wall is subjected to an external voltage, which determines the potential difference between the wall at (0) and the sheath edge at (d). The situations that result in a high potential barrier for thermal electrons (0) (d) kBTe/e are the ones that we are most interested in. Then comes the Boltzmann factor, which was first developed for the space-charge constrained electron flow in a vacuum diode.The Child-Langmuir law establishes the volt-ampere characteristic of a vacuum diode and the spacing d between the cathode and anode is fixed in a vacuum diode. The voltage drop in a plasma sheath is fixed, and as we'll see later, the ion current is likewise determined by the characteristics of the undisturbed plasma. In order to satisfy the limits imposed by the space-charge constrained flow as stated by the Child-Langmuir equation, the plasma sheath responds by varying the sheath thickness 'd'[5], [6].

The Bohm Standard

The topic of why such a significant breach of quasi-neutrality does not produce a large-amplitude ion acoustic wave, via which the charge disturbance may propagate into the plasma bulk, is raised when a space charge sheath matches up with a plasma. What thus prevents the space charge from transferring into the plasma? Of course, we want the plasma-sheath barrier to be stable. What circumstances likely to cause a neutral plasma to become charge-imbalanced? The steady-state considerations of the preceding Section cannot provide a solution to such a query. Instead, we must make use of more all-encompassing ideas, such as those for mechanical stability.

Analysis of Stability

Think about a point mass's equilibrium in the mechanical potentials shown. In case (a), the point mass achieves a steady equilibrium at the potential well's minimum. When the mass deviates from the minimum, the potential well exerts a restoring force. The point mass's stable "trajectory" is the uninteresting function. In case (b), the mass is perched atop a conceivable hill (consider an inverted pendulum). Any deviation from the ideal location results in a force that pushes the point mass further from its original equilibrium. Because of the instability of the equilibrium, the point mass follows a non-trivial trajectory, x(t). Of course, the stability or instability of the equilibrium depends on the sign of the mechanical potential's second derivative.

DISCUSSION

The pseudo-potential's second derivative, d2/d2, must be negative at equilibrium in order for a plasma to form a space charge sheath, therefore our last goal is to compute it. The point mass sits at its stable minimum position when it is positive, keeping the plasma neutral in this situation. We may simply compute the first derivative of the space-charge function, d f ()/d, rather than the second derivative of the pseudo-potential. Retaining the electron space charge at the sheath edge provided is crucial for this calculation. Therefore, the ion speed at the

sheath edge must be greater than or equal to the Bohm velocity vB, which is unavoidably the same as the ion sound speed. A Mach number may be defined as well and rewrite the Bohm requirement as M 1, which requires a supersonic ion flow[7], [8].

Consequently, the first query, why the space charge layer does not simply develop into a plasma by means of an ion acoustic wave, may be addressed as follows: The presheath's plasma is not at rest. Instead, a mass motion at or faster than ion sound speed enters the sheath. In the frame of reference of the lab, an ion sound wave in this medium would either be stationary or swept back into the sheath. Consequently, for the transmission of information from the sheath into the plasma, the Bohm criteria serves as a sound barrier. The plasma "does not know" that there is a space charge sheath present in this language of information.

The Bohm Criterion

The Bohm criterion's inequality has an unsatisfactory aspect. Why should Mother Nature choose the most cost-effective solutions elsewhere while allowing for a broad range of potential entry speeds into the sheath? The solution ties in with the finding that directed ion motion near the sheath edge necessitates an electric field in the presheath that accelerates the ions to the Bohm speed (or higher). The presheath, on the other hand, ought to be regarded as quasineutral. As a result, the electron and ion densities are almost identical, and the electron Boltzmann factor controls the ion density.

The Langmuir Plane Probe

Small extra electrodes were added to a plasma in 1925 by Mott-Smith and Langmuir who then analysed the plasma's volt-ampere characteristic. These Langmuir probes' straightforward design and adaptability make them popular in plasma physics. The electron density and electron temperature of a plasma may be ascertained using the probe characteristic, as we'll demonstrate below. The basic electric circuit used in a Langmuir probe experiment. In a gas discharge, a tiny plane electrode is introduced.

A current-limiting series resistor Rs is commonly used to power the discharge tube from a high-voltage source. An external voltage is supplied between the probe and a suitable electrode, biassing the probe. This electrode must be properly grounded for lab safety concerns. The power supply must also be able to run in a state where the positive output is grounded and the negative output is the "hot lead". Because the voltage drop in the anode layer is often significantly less than that in the cathode layer (the negative electrode), the anode (positive electrode) was selected in this instance.

A current metre measures the probe current Ip while a voltmeter provides the probe bias voltage Up[9], [10]. A contemporary implementation of the circuit for computer-based probe characteristic recording. The digital-to-analog converter (DAC), which produces a bias voltage of (5... 5) V, is amplified 20 times by a high-voltage operational amplifier. An optically-isolated operational amplifier is used to shield the DAC and the computer from any unwelcome plasma currents. A second optically isolated operational amplifier detects the probe current as the voltage drop (1 V) across a tiny series resistor Rm. The computer then uses an analog-to-digital converter (ADC) to read the current signal. Finally, the probe characteristic may be shown and recorded when the computer adjusts the probe bias for the voltage drop across the series resistor.

A connection between the ground terminal of the high-voltage opamp and the reference electrode, which is linked to the lab's protected ground, closes the probe circuit once again. Make sure the PC is also properly grounded for your own protection. The high voltage symbols serve as a reminder that the probe circuit and the dc discharge must both be adequately insulated and touch-free during operation.

A tiny (2–3) mm in diameter tantalum disc with a thin wire soldered to the back may be used to create a plane probe. The wire is passed via a ceramic tube. The back of the probe is given an isolating coating by a layer of ceramic cement, which also secures it to the ceramic tube. The probe may be expanded for use in space, it is suggested to provide the probe a guard ring that is maintained at probe potential. Only the centre disc is used to measure the probe current. Edge effects that may increase the saturation current with probe bias are lessened by the guard ring. The design of a cylindrical probe is shown.

A hypodermic needle-sized thin-walled stainless-steel tube with a 1 mm diameter may be used in the probe's construction to minimize the perturbation of a (low-density) plasma. The steel tube provides mechanical support and shielding for a ceramic tube that serves as isolation for the probe wire, which, depending on the application, has an exposed length of (5-20 mm) and a thickness of (50-100) m. A typical Ip-Up feature of a plane Langmuir probe. Three regimes may be used to categories the attribute. A steady ion saturation current is drawn from the plasma at high negative bias (region I), where no electrons can reach the probe. An electron saturation current that is continuous is seen at high positive bias (region III). The ion saturation current will be detailed shortly, however the electron saturation current is significantly larger in size.

A portion of the electrons may cross the energy barrier and get to the probe in the intermediate area II, also known as the electron retardation regime. The Boltzmann factor states that the electron current grows exponentially with bias voltage.The attribute has two distinct physical significance points. The probe potential, at which there is no net current flowing in the probe circuit, is the same as the potential of a metal object floating in plasma. This is the probe's floating potential, f. The plasma potential, or the potential inside the surrounding plasma, is determined by the border between electron retardation and electron saturation, and is often defined as zero-reference, or p = 0.

The electron saturation current

The electron saturation current is the electron current at the plasma potential. In contrast to the ion saturation current scenario, this circumstance is unique. After gaining energy in the pre-sheath and entering the sheath as a virtually mono-energetic group with directed velocity, the ions in a dis-charge plasma with a temperature of TiTe. But there is no sheath development at the plasma potential. Instead, the probe is no longer obstructed from being reached by the Maxwellian electrons of the plasma.

All electrons will thus arrive to the probe if they are moving in the direction of the probe. However, each electron will only contribute to the probe current with its perpendicular velocity, if its velocity vector is inclined by an angle from the normal to the probe surface. We may first integrate across the magnitude of the velocities since the Maxwell distribution of the electrons is isotropic. This gives us the representative velocity, which is the mean thermal velocity. To complete the correct angular average.

Advanced Langmuir Probe Methods

Thermal plasmas and the measurement of electron temperature and density are not the only things that may be considered while analyzing a Langmuir probe feature. Rather, the electron distribution function and derivatives of the characteristic have a special connection in a non-Maxwellian plasma.

The Druyvesteyn Approach

The true distribution function in gas discharges may diverge greatly from a Maxwellian. In 1930, Druyvesteyn presented a technique for determining the electron distribution function from the probe characteristic's second derivative, d2 Ip/dUOur earlier considerations allow us to deduce his approach as follows: Let's define the z-direction as the probe surface's normal. Only electrons with a sufficiently enough z-component to get past the potential barrier may reach the probe surface in the event of electron retardation.

A Druyvesteyn Technique Realisation in Practice

Calculating two numerical derivatives is required for the Druyvesteyn method's easy implementation. This would dramatically worsen the noise for data with noise overlay on it. This is the reason why before taking derivatives, many plasma scientists smooth the data. A alternative approach to noise reduction relies on modulation strategies and narrow-band Fourier component identification. The purpose of the second harmonic probe or the two-frequency approach is to create harmonics or combination frequencies by using the probe's curvature as a nonlinear element. Assume that two sine voltages with frequencies of 1 and 2 and tiny amplitudes U1 and U2 are superimposed on the probe voltage Udc. The resultant spectrum components are given by the addition theorems for sines and cosines when the probe current is extended into a Taylor series centred on Udc.In addition to combination frequencies that are proportional to the second derivative of the probe characteristic, the probe current also has Fourier components. Finding the second harmonic at produces the required distribution function when a single modulation voltage is used. The method's disadvantage is that any additional nonlinearities in the electric circuit that apply the modulation voltage or detect the current result in frequency components at 21 and reduce the method's dynamic range. When the applied signal at 1 seep through the narrow-band filter centred at 2-1, this is a common issue.

Double probes

The electric circuit must be closed via a sufficiently big reference electrode, often one of the discharge electrodes, in order to use the Langmuir probe technique as previously explained. In certain circumstances, such as in induced rf discharges or aboard a satellite, it may be prohibited to utilize the satellite body as a reference electrode if such a reference electrode is absent. The double-probe approach, in which two identical Langmuir probes are run in series, was developed for these applications depicts the probe circuit's basic operation. A (battery-operated) floating voltage source Up and a current-measuring device that produces Ip are used to link the probes 1 and 2. As observed both probes are functioning close to the floating potential f. For easier reading, the ratio of the electron saturation current to the ion saturation current was artificially fixed to a certain value. The ion-saturation current is the highest current that can pass through the probe circuit. The other probe is now active in the area of electron retardation.

Motion of Cylindrical and Spherical Probes in Orbit

The effective probe area increases and surpasses the geometrical probe area as a result of the ion mobility in a thick sheath, De a, surrounding a tiny sphere or thin wire of diameter illustrates the problem's geometry. The ion has a velocity of v0 when it is far from the probe. When sheath collisions are few, the conservation of energy and angular momentum, as in celestial mechanics, may be used to explain ion mobility. The Orbital Motion Limit (OML) of probe theory is the term given to this concept as a result. There are orbits with b bc that collide with the probe and add to its current. The crucial impact factor in grazing collisions is bc. The ion current is not affected by orbits with b >bc, although they do supply space charge for shielding. We shall see how every trajectory contributes to the momentum transmission of a tiny spherical dust particle.

As schematically, by substituting W_0, we may determine the form of the ion saturation current of a cylindrical and spherical probe. Similar arguments can be made for the electron saturation current, which results in the same functional dependency for W_0. When the probe is circular (or spherical), the attractive regime no longer produces a steady current. The value of the electron current at the plasma potential is how we define the electron saturation current. The electron current in a cylindrical or spherical probe's attractive zone thus has the following shape: The plasma potential of a cylindrical probe is determined by the point at which the characteristic inclines. Since there is no inflection point for a spherical probe, the plasma potentialwhich is required to read the electron saturation current—can only be approximated by figuring out how far the plasma potential is from the floating potential and then fixing it in the observed curve[11], [12].

A first warning applies to the straightforward OML model that is provided here. The reader will undoubtedly be perplexed by the fact that we did not scale the ion current with the electron temperature using a Bohme criterion for the ion current. The ion OML-factor is instead determined by the ion temperature. This is a byproduct of applying the limit De, which is the thick sheath approximation. The sheath edge is thus at infinity, and the whole volume of interest is a sheath area. In reality, the probe of the order of the ion mean free path is far enough away to have already passed the OML model's limit of validity. The orbital motion during the most recent mean free path is therefore described by the OML model. The OML model also makes sense since the ions would "cool" from Bohme energy to gas (ion) temperature via elastic or charge-exchange collisions with the neutral gas. The typical characteristic of orbital motion is the observed rise in the ion collecting current with applied probe bias. There is one more caution. As soon as the sheath diameter matches the probe length, cylindrical probes of finite length act like spherical probes. The reader should review additional specialized literature for a fuller knowledge of Langmuir probes.

Double Layers

A collision less plasma can only produce the Bohme current, which starts the construction of a space charge sheath, according to what we learned. However, this plasma has a substantially greater electron current capacity. Langmuir had discovered that unexpected potential jumps often arise near to the diameter restrictions of his discharge tubes within the plasma volume. These were what he referred to as double layers (DLs). In both astrophysical and laboratory plasmas, double layers are present. Raadu had noted that the DL functions as an electric load wasting energy at a rate, where I am the entire current through the DL, since

particles are driven by the net potential difference demonstrates internal resistance in this manner. This resistance's nature differs significantly from that of an ohmic resistance, which converts electrical energy into random motion. Instead, a DL is more like an antique television tube, where the moving bright dot on the screen is created by an electron beam. Since the DL operates as a load, the potential difference must be maintained by an external source. In the lab, this is an example of in space, the power source might be a magnetic energy storage system that uses an extended current system to react to changes in current by producing an inductive voltage.

CONCLUSION

The classic illustration of effective ion extraction from plasma is an ion thruster. The ion acceleration within the plasma volume is carried out by Hall thrusters, while alternative models make use of a pair of grids that are in touch with a dc or radio frequency plasma. The NASA Solar Electric Propulsion Technology Application Readiness (NSTAR) program me has created a 30 cm diameter xenon ion thruster for use in planetary missions On the Deep Space 1 (DS1) mission in 1998, the NSTAR engine was successfully used a simplified simulation of the DS1 thruster is shown. A dc discharge occurs between a hollow cathode and a large-area anode to create plasma. A high-low cathode is a reliable source of electrons when used at low gas pressure. Magnets made of permanent materials (not shown) improve plasma confinement. The plasma is in touch with two grids on the exhaust side. The initial electrons are electrostatically contained and the plasma is terminated by the inner screen grid, which has the same voltage as the cathode between the electron source and the anode, which effectively determines the plasma potential.

REFERENCES:

[1] O. Schmitz *et al.*, “Formation of a three-dimensional plasma boundary after decay of the plasma response to resonant magnetic perturbation fields,” *Nucl. Fusion*, 2014.

[2] G. Hommen *et al.*, “Real-time optical plasma boundary reconstruction for plasma position control at the TCV Tokamak,” *Nucl. Fusion*, 2014.

[3] W. J. Sun *et al.*, “The current system associated with the boundary of plasma bubbles,” *Geophys. Res. Lett.*, 2014.

[4] I. T. Chapman *et al.*, “Three-dimensional distortions of the tokamak plasma boundary: Boundary displacements in the presence of resonant magnetic perturbations,” *Nucl. Fusion*, 2014.

[5] R. Ghadiri, Y. Sadeghi, and M. H. Esteki, “Plasma boundary determination in Damavand tokamak by using current filament method,” *Int. J. Mod. Phys. E*, 2014.

[6] G. Sánchez-Arriaga, J. Sanz, A. Debayle, and G. Lehmann, “The behavior of the electron plasma boundary in ultraintense laser-highly overdense plasma interaction,” *Phys. Plasmas*, 2014.

[7] O. J. Kwon, “Effect of the shape of the plasma boundary on the peeling and the ballooning modes,” *J. Korean Phys. Soc.*, 2014.

[8] B. Bahnev, M. D. Bowden, A. Stypczyńska, S. Ptasińska, N. J. Mason, and N. S. J. Braithwaite, “A novel method for the detection of plasma jet boundaries by exploring DNA damage,” *Eur. Phys. J. D*, 2014.

[9] I. T. Chapman *et al.*, "The effect of the plasma position control system on the three-dimensional distortion of the plasma boundary when magnetic perturbations are applied in MAST," *Plasma Phys. Control. Fusion*, 2014.

[10] M. Odstrčil *et al.*, "Plasma tomographic reconstruction from tangentially viewing camera with background subtraction," *Rev. Sci. Instrum.*, 2014.

[11] J. Hwang, K. Rha, J. Seough, and P. H. Yoon, "Electron distributions observed with Langmuir waves in the plasma sheet boundary layer," *Phys. Plasmas*, 2014.

[12] Q. Sun, Y. Li, W. Cui, B. Cheng, J. Li, and H. Dai, "Shock wave-boundary layer interactions control by plasma aerodynamic actuation," *Sci. China Technol. Sci.*, 2014.

CHAPTER 6
LANGMUIR'S STRONG DOUBLE LAYER

Dr.Vikas Kumar Shukla, Assistant Professor
Department of Science, Maharishi University of Information Technology, Uttar Pradesh, India
Email Id- vikash.shukla@muit.in

ABSTRACT:

The geometry of a double layer a positive space charge is responsible for the potential step's negative curvature, whereas a negative space charge is in charge of the electric potential's positive curvature. The system is assumed to be one-dimensional with only x-direction variation. Negatively electrons arrive at the low-potential side with a positive current density. Each of these currents is retained via continuity. The instantaneous velocity of electrons and ions during the transit are determined by energy conservation. However, the free-streaming electrons and ions by themselves are unable to produce this quasi-neutrality. When we demand quasi-neutrality on the high potential side and see that the ions are diluted by acceleration in the sheath, this becomes obvious. The electrons' density must be larger on the low-potential side and quasi-neutrality would be broken there, according to the same logic. As a result, extra populations of trapped particleselectrons on the side with high potential and ions on the side with low potentialmust exist in order to achieve the quasi-neutrality.

KEYWORDS:

Beam, Electron, Plasma, Potential, Wave.

INTRODUCTION

However, because to the high potential step in a sturdy double layer, these imprisoned (thermal) particles are unable to enter the sheath. Because the square of the electric field grows less relative to the values within the DL, we may roughly set at the margins of the strong double layer. In the limit of vanishing starting velocities. We can observe that in a DL, electrons supply the majority of the current. The Langmuir criteria, on the other hand, stipulates that both charge carrier species, which are driven by the same space charge potential, contribute to the creation of this space charge to the same extent. So, via ion depletion on the side with low potential and electron depletion on the side with high potential, we get a symmetrical space charge. The DL's macroscopic neutrality is identical to the requirement that the electric field disappears at x L.The Langmuir criteria has the following physical meaning that may be understood: Keep in mind that mi(2e0/mi)1/2 is the momentum that the ion has acquired while crossing the DL and ji/e is the (constant) ion flux density. Then, according, the electron momentum flow departing at x 0 is equivalent to the ion momentum flux exiting the DL at x= L. This relationship may be thought of as a force balance that keeps the DL at rest. On the other hand, when this requirement is broken, the DL will move at a speed vDL, ensuring that the Langmuir criteria is once again satisfied in the moving frame of reference[1], [2].

Experimental Proof of Double Layers

Coakley and Hershkowitz conducted a thorough comparison of the DL potential structure and the electron distribution function. According, the strong double layer with e/kBTe 14 was created in-between two grids that divide the device's three portions. The DL potential was

determined by the grid voltage difference. Using a Langmuir probe, the electron distribution function was measured. A focused electron beam is created in the current scenario. In light of this, the beam may be seen in the initial derivation of the probe characteristic. Plots of the distribution functions are shown for a series of locations that are spaced apart by around 2 cm. On the low-potential side, the dashed horizontal line designates the energy zero. The plasma potential fluctuation is shown by the solid line. When moving from the low-potential side (left) to the high-potential side (right) of the DL, a group of free electrons is accelerated, as shown by the arrows. On the high-potential side, a second set of trapped electrons is discovered. The dashed line denotes where it is. Take note of how the height of the later peak diminishes when the DL's repulsive potential is approached.

A plasma system's stability may be examined using a variety of techniques. The property that a deflection from the equilibrium position (shown in grey) results in a restoring force Frest, which pushes the pendulum back to its original position, defines stability for a simple mechanical system like the pendulum made up of a massless rod and a bob. Harmonic oscillations result from the interaction of a restoring force that is proportional to the deflection and the inertia of the pendulum bob.The behavior of the inverted pendulum in Fig. 8.1b is quite different. The force that results from a deviation from the unstable equilibrium tends to amplify the original deflection. An initial disturbance will increase exponentially over time since the deflecting force is again proportional to the deflection angle[3], [4].

Analysis of a system's potential energy is another method for determining its stability. When the potential energy for any potential disturbance rises, the system is stable. In light of this, the lowest of potential energy is a stable point. In the event that a nearby point has lower potential energy than the initial location, the equilibrium is unstable. The study of the restoring or deflecting forces enabled a quick quantitative prediction of the motion of the pendulum, but the analysis of the system's energy did not instantly reveal how it enters the lower energy state.Decomposing a tiny initial perturbation into Fourier components, known as modes, exp(it), is a third method of analyzing stability. The system is stable if all of the modes' frequencies are actual. However, a Fourier mode will increase in size over time if it has a complex frequency with a positive imaginary portion. The term "normal mode analysis" refers to this process.

We will examine two distinct groups of instabilities in this Chapter. Homogeneous plasmas, which significantly depart from a Maxwellian distribution function, are described by the first class of instabilities, known as micro-instabilities. Situations when an electron or ion beam travels through a population of plasma particles at rest are typical examples of this class. We will employ a beam-system to explore the impact of limited length on the instability since these systems can be handled by straightforward mathematical techniques. This research is very relevant for laboratory experimentation.Inhomogeneity in real space is a defining characteristic of the second class of macro-instabilities. Here, we are interested in circumstances like a heavy fluid resting on a lighter fluid under the impact of gravity, as well as the stability of current-carrying pinch plasmas.

Beam-Plasma Instability

Langmuir made the discovery that oscillations at the electron plasma frequency, often known as Langmuir oscillations, may develop on their own in a plasma that is not in equilibrium [154]. Such a non-equilibrium distribution function may be made up of a beam-like collection

of fast electrons flowing in one direction and background plasma. A cold plasma model may easily explain the plasma bulk when the beam's velocity is higher than the background electrons' thermal velocity. The ions will not participate in the wave motion since we are interested in high-frequency waves close to the electron plasma frequency, and they will instead produce a homogeneous neutralizing background[5], [6].

DISCUSSION

The electron distribution function for the beam-plasma system. The reader may be curious as to why the axes were switched in this instance. The comparison to an atomic system with (non-degenerate) energy levels a, b, and c as illustrated in Fig. 8.2b explains why. The Boltzmann factor n(W) exp W/(kBT) determines the equilibrium population of these levels. When the populations of levels b and c are inverted, that is, when the population in c is greater than that in b, such an atomic system may be employed as a laser.Think about how the rivalry between stimulated emission Bbcnphnc and absorption Bcbnphnb determines the (negative) pace at which the upper laser niveau c is net depopulated.

Spontaneous emission: dt = dt at high photon densities, processes between layers' c and b may be disregarded. The Einstein coefficients are the same for non-degenerate levels and are BcbBbc. When nc>nb, the quantity of photons increases exponentially with time. The laser process is related to the exponential increase in photon density. This comparison demonstrates how a significant departure from thermal equilibrium results in instability expressed in terms of exponentially rising waves.Let's define the overall electron density for the beam-plasma scenario as ne0 and the corresponding electron plasma frequency as pe. We'll suppose b 1 and that the beam population is nb bne0 of the overall electron population.The beam moves at v0. With the beam propagating in the x direction, the issue is thought of as being one-dimensional.

Beam-Plasma Mode Dispersion

First-order perturbation theory was used determine the cold plasma's dielectric function as The permittivity of the vacuum ("1") and the susceptibility of the plasma electrons are added to form the dielectric function. The relationship between the electron conduction current and the vacuum displacement current at a certain time may likewise be used to interpret p the frequency. We can instantly calculate the total dielectric function for the beam-plasma system from this example.Here, the electron densities have been modified by the variables (1 b) and b, with the Doppler-shifted frequency serving as the denominator of b. The reader may see that the susceptibilities of the various plasma elements can be added to get the dielectric constant of a plasma for electrostatic waves. A derivation of the Doppler shift in the beam susceptibility will be provided. Electrostatic (longitudinal) waves are described by the dispersion relation (k), which is defined by the constant 0. We can see from looking at that solving a fourth-order polynomial with real coefficients is technically similar to finding the zeroes of this equation. The basic theorem of algebra states that such polynomials have pairs of real roots or roots that are complex conjugate. As a result, we anticipate that wave dispersion (k) will have four independent branches. If two complex-conjugate roots occur, we are done since one of these complex roots defines instability and will develop exponentially over time[7], [8]. The functional dependency of the dielectric function on the wave frequency. As predicted by the vanishing denominators the dielectric function exhibits (negative) singularities for 0 and kv0. One real root, /pe 1, is mostly unaffected by the beam's

existence. A distinct pattern may be seen in the roots when /pe > 0. There is one root for the weakest beam fraction that is close to 1/pe 1. These two roots are what we refer to as the plasma modes. We refer to the second set of roots, which are symmetric around /pe k V0/pe as beam modes. The spacing between the beam roots widens as b grows, eventually merging the left beam root with the right plasma root. At larger b values, the dielectric function remains negative across the whole range 0 kv0. However, if is assumed to be a complex variable, a pair of conjugate complex roots will exist, with the real component of falling inside this range.

Various branches of the (k) function make up the dispersion relation for the beam-plasma modes. There will be rising waves in accordance with our wave perturbation and allowing for a complex r. The (degenerate) beam mode kv_0 and the plasma modes at pe are uncoupled in the limit. Positive plasma mode for non-vanishing b links to beam mode to form fast space-charge wave with /k > v0. The beam modes form a conjugate pair for kv0/pe 1.3. These waves, also known as slow space-charge waves, spread more slowly than the beam. The one where I > 0 is increasing over time exponentially. Close to the intersection of pe and kv0, the growth rate reaches its greatest value. The slow beam mode and the plasma mode are formed at the triple point when the slow space-charge waves materialize. The beam has no impact on the second plasma mode with negative.

Once again, the electron exhibits inductor behaviour when kv0 is greater than 0, as is the case with the fast space-charge wave. However, the converse scenario is realised for the slow space-charge wave with kv0 = 0. As a result, when they come into contact with the slow wave, beam electrons behave in an unusual way. They behave as if they had a "negative mass" in the wave field. The electron now functions as an electronic capacitor, where the phase shift between the current and voltage is 90 degrees. The idea of a "negative mass" has a physical connotation that is clear to perceive. We shall talk about this impact in terms of the wave's typical kinetic energy. Calculating the density variations in the beam, which are connected to the velocity modulation by the flow's continuity, is necessary for this purpose.Wave growth is caused by the interaction of this negative energy wave with the plasma oscillations, which represent a positive energy wave. The wave potential energy seems to increase despite the kinetic energy loss. In this method, the beam velocity is sacrificed as the wave potential increases over time. We shall use computer simulations to track this progression into the non-linear realm. Returning to the idea of "negative mass," the density clumps for the slow wave are expanding by slowing down the initial beam, while the clumps for the fast wave are filling up by accelerating slower electrons. In the first instance, energy moves from the beam to the wave, while in the second instance, the wave expands. Electrons are accelerated by the wave, which releases energy[9], [10].

Growth in time or space

It was presumpted in the previous paragraph that the wave is defined by an imaginary component i of the wave frequency. This indicates that the wave amplitude increases uniformly throughout. One may also envision an unmodified beam entering a finite plasma in the beam-plasma system. Any little wave-like disruption will expand in space as the beam moves through the plasma. For this situation, we must use the dielectric function from (8.3) to solve the dispersion relation for real frequency and complex wavenumber k. Simple algebraic operations result in the wavenumber's imaginary component, which is given.

Buneman Instability

A current-carrying plasma provides a second, related example of the instability of counter-streaming charged particles. In this plasma, a dc electric field causes the flow of all the plasma electrons relative to the ions. Oscar Buneman (1913–1993) initially described this instability Once again, we ignore collisions and assume that the plasma ions' drift velocity is substantially lower than the electron beam velocity. As a result, we characterise the ion instability in its rest frame. Furthermore, according to the cold beam assumption, the electron beam velocity v0 is much greater than the thermal spread of the electron distribution.

The increased ion mass is explained by the fact that the ion plasma frequency pi determines the ion contribution in this case. When we acknowledge that is a tiny amount with equal electron and ion density, the mathematical structure of the problem is obviously identical to the beam-plasma instability. In contrast to the beam-plasma system, a little disturbance of the flowing electrons is now represented by the ion term. As a result, we may anticipate that the unstable waves will have frequencies that are lower than the frequency of the electron plasma. The Doppler-shifted electron plasma oscillations in the beam pair with these low-frequency ion fluctuations.

Finite System Beam Instability

We are interested in how limited length affects the instabilities of an electron beam in this section. A Pierce diode is a setup like this. Finding the highest stable electron current in the presence of a background of positive ions that balances the mean electron space charge was the initial problem that John R. Pierce attempted to solve.

The stability of finite-size collisionless discharge systems with an electron flow is often studied using the extended Pierce diode, which permits external circuit components. In the late 1980s, interest in this model system resurfaced in relation to nonlinear waves, chaos, or the impact of ion dynamics Computer simulations made access to the chaotic and nonlinear states possible. The system was further employed as a model for plasma system chaos control.

The Pierce Diode's Geometry

The two conducting planes at x 0 and x L make up the Pierce diode. An unmodified electron beam with a velocity of v0 may enter the system via the electrode at x 0. This electrode can be thought of as a transparent grid. A uniform backdrop of immobile neutralising ions fills the diode. The term "Pierce diode" refers to vacuum diodes in which the right electrode (anode), which receives a positive voltage, accelerates electrons that are thermally emitted from the left electrode (cathode). There will be discussion of the electron flow in diodes. The conventional Pierce diode's two electrodes are joined together and maintained at ground potential 0 in contrast to the vacuum diode.

A Free Electron Beam's Dispersion Relation

With the exception of pi 0, which results from the ions' supposed immobility, which may be realized by giving them an infinite ion mass, the dielectric function for an electron beam crossing an immobile ion background is the same as for the Buneman instability (8.21). Following that, the electron beam oscillates.

The Effect of Boundaries

We may infer that standing waves are created as a result of the action of the boundaries. The fact that the waves that propagate forward and backward have different wavelengths makes the problem more complicated. The electric charges on the metallic barriers' surface must also be taken into consideration since they create an electric field within the diode. This is why Pierce used four components to create the oscillating electric wave potential within the diode. This is an implied relationship between the Pierce parameter P and the variable, which includes the wave frequency. Due to the transcendental character of the equation, the solutions for will often be complicated and endlessly many.

The Pierce Modes

The existence diagram for the many modes of the Pierce instability. For P, a stable mode with frequency 0, or a uniform dc current flow of the beam, is discovered. When the imaginary portion of changes from negative to positive, this electron flow becomes unstable. This occurs for P 2 and causes any initial disturbance to expand exponentially but non-oscillatory. In the range of 2P to 3P, a first oscillatory unstable Pierce mode is discovered. As P increases, the mode stabilises once again. At P 3 P, a second oscillatory Pierce mode with an even higher frequency takes over. It becomes unstable for P 3 P, and it disappears once again for P 4 P. With increasing frequency, this pattern keeps repeating.

Discussion of the Pierce Model

For P, the Pierce model provides a uniform, steady electron flow. An imagined fraction of v0/L that is negative establishes the stability. Why does the Pierce system experience damp even when electron motion is collision-free? The electron beam enters the diode unmodulated and exits the diode with some density modulation, therefore there is energy loss for any initial disturbance. As a result, the system is forced to release the kinetic energy of the wave motion. This elimination is effective at damping the initial disturbance for short systems less than half a wavelength. This process degrades as the system becomes longer, which might lead to instability. Consideration of the interaction of the negative energy wave in the beam with the oscillating surface charges on the electrodes might lead to an alternative interpretation of the Pierce instability. This coupling causes instability similar to that of the beam-plasma or the Bune-Man instability, but it needs the system to have at least one complete wavelength to be considered a linear wave-wave coupling.

We now know that P is where the Pierce diode's maximum stable and homogenous solution may be found. The maximum current density that may flow without accumulating space charge is thus established. It is clear how the Child-Langmuir legislationis comparable. The buildup of space charge in the centre of the diode is related to the non-oscillatory mode that enters at P. This could be advantageous or detrimental. The electron beam slows down for negative space charge, which increases the negative space charge. The electron beam is accelerated in response to an initial positive space charge in the diode's centre, and the beam electron density decreases until it is below the ion density, adding net positive charge in space. Both situations result in an expanding, non-oscillatory space charge and are plainly unstable. We must keep in mind that in a typical vacuum diode, the electrons start with at the cathode and depart with at the anode in order to compare the maximum stable current in a Pierce diode with the Child-Langmuir equation of a vacuum diode, consider the injection of beam electrons with into the space between two grounded electrodes[11], [12].

CONCLUSION

The electrons will almost come to rest in the center of the gap at the maximum current because they are slowed down by the electric field created by their own space-charge. It is possible to think of the left half of the gap as a time-reversed Child-Langmuir scenario. Since our derivation of the Child-Langmuir rule was based on kinetic energy, which stays constant under time reversal for a stationary flow, it is not surprising that the same law holds when v is substituted by v. Therefore, running two Child-Langmuir diodes, each of length L/2, back to back is equivalent to injecting a beam into a vacuum gap. The grounded electrodes may be thought of as anodes, while the low potential in the center of the gap acts as a virtual cathode. The development of virtual cathodes in front of thermal emitters will be covered in, as well as the stability of electron flow injected into a gap between grounded electrodes, which was investigated.

Since the Child-Langmuir rule must be stated for a diode of length L/2 in the latter case, an honest comparison of the maximum current in the neutralized. Pierce diode with a non-neutralized electron flow must take this into account. As a result, the maximum currents ratio is changed to molecular Instabilities The macro-instabilities, or plasma instabilities that occur in actual space, are the focus of this section. The displacement of the plasma in relation to a magnetic field is what gives rise to these instabilities. Here, the stability of the system may be assessed using the energy concept. However, the method to identify the wavelength and rate of expansion of the unstable modes will be normal mode analysis.

REFERENCES:

[1] M. S. Benilov and D. M. Thomas, “Asymptotic theory of double layer and shielding of electric field at the edge of illuminated plasma,” *Phys. Plasmas*, 2014.

[2] T. Shirafuji, A. Nakamura, and F. Tochikubo, “Numerical simulation of electric double layer in contact with dielectric barrier discharge: Effects of ion transport parameters in liquid,” *Jpn. J. Appl. Phys.*, 2014.

[3] H. C. Chuang, Y. S. Lin, Y. H. Lin, and C. S. Huang, “The fabrication of a double-layer atom chip with through silicon vias for an ultra-high-vacuum cell,” *J. Micromechanics Microengineering*, 2014.

[4] S. Machida, Y. Miyashita, A. Ieda, M. Nosé, V. Angelopoulos, and J. P. McFadden, “Statistical visualization of the Earth’s magnetotail and the implied mechanism of substorm triggering based on superposed-epoch analysis of THEMIS data,” *Ann. Geophys.*, 2014.

[5] R. Pottelette, M. Berthomier, and J. Pickett, “Radiation in the neighbourhood of a double layer,” *Ann. Geophys.*, 2014.

[6] M. Sivakandan, D. Kapasi, and A. Taori, “The occurrence altitudes of middle atmospheric temperature inversions and mesopause over low-latitude Indian sector,” *Ann. Geophys.*, 2014.

[7] S. M. Khalil and N. M. Mousa, “Dispersion characteristics of plasma-filled cylindrical waveguide,” *J. Theor. Appl. Phys.*, 2014.

[8] A. V. Melnikov *et al.*, “Effect of magnetic configuration on frequency of NBI-driven Alfvén modes in TJ-II,” *Nucl. Fusion*, 2014.

[9] L. Sironi and D. Giannios, "Relativistic pair beams from TeV blazars: A source of reprocessed gev emission rather than intergalactic heating," *Astrophys. J.*, 2014.

[10] S. Bayat, S. Babanejad, S. M. Hasheminejad, and S. M. Vahabi, "Exact numerical solution of the dispersion relation in relativistic backward-wave oscillator and relativistic travelling-wave tube filled with plasma," *Plasma Phys. Control. Fusion*, 2014.

[11] J. Xiao, S. Chen, W. Tian, and K. Chen, "Influence of the beam self-fields on the dispersion characteristics of em waves in a dielectric waveguide filled with plasma," *Plasma Sci. Technol.*, 2014.

[12] S. Saviz, "The effect of beam and plasma parameters on the four modes of plasma-loaded traveling-wave tube with tape helix," *J. Theor. Appl. Phys.*, 2014.

CHAPTER 7
EXPLORING THE PINCH INSTABILITIES

Dr.Vikas Kumar Shukla, Assistant Professor
Department of Science, Maharishi University of Information Technology, Uttar Pradesh, India
Email Id- vikash.shukla@muit.in

ABSTRACT:

The squeeze effect was previously mentioned. The pinch effect is not always a uniform mechanism. The magnetic pressure at the plasma surface will rise if we suppose that the plasma cross section is lowered at some point. The plasma radius is now further reduced by the increasing magnetic pressure, and the plasma column experiences a sausage instability. When the plasma column is curved, the magnetic pressure may also differ from its equilibrium value. The magnetic field line density and magnetic pressure are greater on the inner side of the curved plasma column and lower on the outer side because the magnetic field lines are perpendicular to the local current direction. As a result, the column will become even more displaced and kink due to the imbalance of magnetic pressure. A superimposed longitudinal magnetic field that is frozen in the plasma may stabilize the sausage and kink instability. The tension T of the magnetic field lines tends to straighten the field lines. This results in a net restoring force that balances the azimuthal magnetic field component's magnetic pressure imbalance.

KEYWORDS:

Fluid,Particles, Plasma, Velocity Distribution, Waves.

INTRODUCTION

The horizontal dashed line depicts the boundaries of the undisturbed plasma. The top half-space is filled with plasma. The x-y plane and the magnetic field are perpendicular. When we can ignore ion-neutral collisions, the ions suffer a drift under the influence of gravity with a velocity given. The electrons' (opposing) drift velocity is less by a factor of me/mi and will not be included in this. The force balanceoccurs, may be used to understand the initial homogeneous equilibrium of the boundary. We assume an initial sinusoidal disturbance of the boundary, as shown by the heavy line, to comprehend the instability process. The ions are slightly shifted in the x direction as a result of the g B drift, as seen by the bright line. Due to an overshoot of ions on the leading edge and a deficiency of ions on the following edge, this causes positive surplus-charges to form at the surface. As seen by the box arrows, these surface charges cause the perturbed plasma area to move in an motion. Keep in mind that the E B drift does not cause additional charge separation and is the same for electrons and ions. This secondary drift amplifies the first disturbance as its result. The gravitational Rayleigh-Taylor instability has this as its mechanism[1], [2].

Initially, the Rayleigh-Taylor instability was used to explain the interface between two fluids—a heavier fluid (like water) lying on a lighter fluid (like oil), for example. There, an interface disruption caused by a sinusoidal wave causes water and oil blobs to rise and fall, respectively. The magnetic field is horizontal in the equatorial ionosphere, and the ionosphere plasma, which symbolizes the lighter fluid, rests on the magnetic field. The lowest portions of the ionosphere (E-region) quickly vanish through recombination after sunset.

A strong density differential arises at the base of the F-layer (270 km altitude), which may become Rayleigh-Taylor unstable and cause bubbles of low-density plasma to rise into the high-density F-layer. In a comparison of the density profile during the up-leg and down-leg of the rocket trajectory, the bubbles show up as lower plasma density. While the down-leg passed through undisturbed plasma, the upleg crossed the bubble area. During the DEOS rocket programme, this finding was attained.

Generally speaking, Rayleigh-Taylor-like instabilities may occur in magnetized plasmas. The internal kinetic pressure of the plasma particles in this situation may replace gravity. The plasma surface begins to experience periodic perturbations. The number of grooves in the plasma column is indicated by the azimuthal mode number, m. This design is similar to the fluted columns seen in ancient Greece, which explains why it is called flute instability[3], [4].

The description of the plasma state was improved. The interaction between the particles and the alteration of the fields caused by the existence and mobility of charged particles were overlooked in the single-particle model, which focused on the motion of individual particles in normal magnetic field configurations.

We have taken into account the typical behavior of particles occupying a tiny amount of space in the fluid model. Only some portions of the shifted Maxwell distribution, such as the mean flow velocity or gas temperature, were preserved in this approximation; nonetheless, when combined with Maxwell's equations, the model was made to be self-consistent.

Since pressure effects are now taken into account, the fluid model is superior than the single-particle model. The combined macroscopic motion of plasma and magnetic field lines might be described using this fluid model and its formulation in terms of MHD equations. A beam-plasma system was initially used to cope with non-Maxwellian velocity distributions. This system produces self-excited electrostatic waves close to the electron plasma frequency.

The idea of pressure falls short when applied to the thermal effects of high-temperature plasmas. Instead, many particle groups within the distribution function interact with a wave in quite different ways. The kinetic description of a plasma with an arbitrary velocity distribution using the Vlasov equation will be briefly introduced in this Chapter. This is the third level of improvement in the sketched description of the plasma state.

The focus in this context is on velocity-space phenomena like the wave collision less Landau damping. We will look at the connection between single-particle motion and kinetic theory for space-charge-limited electron flow in diodes as a second example.

Finally, a short discussion of particle simulation as a tool for kinetic plasma description will take place.There are more methods of plasma description, such as considering the plasma as a dielectric, in addition to this hierarchy of models, which may be ordered according to plasma temperature and collisionality. We have shown that several sorts of waves, including light waves, plasma oscillations, ion sound waves, and Alfven waves, may exist in plasmas. We may mix the concept, depending on what has to be clarified any one of the three levels of plasma description of a dielectric. We shall examine the meaning of the terms "cold plasma" and "warm plasma" specifically in the context of kinetic theory[5], [6].

The Vlasov Model

A full description of a plasma must take into account both the particle species' velocities and fluid characteristics, such as self-consistent fields and fluid features. Kinetic theory develops such a notion. The probability distribution in real space and velocity space will be used in this section instead of the actual particle locations. This may be done in terms of the Vlasov model, which was first proposed in 1938 by Anatoly Vlasov (1908-1975), for collision less plasmas.

Vlasov Equation Heuristic Derivation

We learned about the idea of substituting particle paths in the fluid model with a statistical representation of the average attributes of the plasma particles contained inside tiny fluid components. There, we defined the mass density m(r, t) and flow velocity u(r, t), which are linked by the principle of mass conservation. It's necessary to briefly explore the limit of infinitesimal size, d3r d3v. The issue occurs because, in the end, we will only discover one or no plasma particle within such a bin as phase space is split into ever-finer bins. This would result in the distribution function being a sum of -functions. This depicts the precise placements and speeds of the particles.

DISCUSSION

The challenge of resolving the equations of motion for a many-particle system, say one with 1020 particles, however, has then resurfaced; as a result, we are now using statistical approaches to look for a mathematically simpler description. To do this, we begin with macroscopically large finite bins (x, y, and z) that contain a substantial number of particles to warrant the use of statistical techniques. On this intermediate scale, we then create a continuous distribution f (j) and demand that remain continuous when calculating the limit. This could be compared to grinding the actual particles into a much finer "Vlasov said," where each grain of sand has the same value of q/m (the only property of the particle in the equation of motion) as the actual plasma particles and is distributed to maintain the continuity. The Vlasov image is the name of this method. This subdivision has a cost since we lose knowledge of how nearby particles are arranged, such as via correlated motion or collisions. Therefore, the Vlasov model is limited to weakly connected plasmas with a 1 parameter an alternative method of providing a kinetic description will be covered creating a super particle with the same q/m by mixing the particles in a mesoscopic bin. If so, we may only have 10^4–10^5 super-particles left for which the equations of motion can be computed. Super-particle formation, however, increases the system's graininess, and the particles within a super-particle are artificially connected[7], [8].

The Vlasov Equation

Now that the continuity equation has been generalized, we are looking for an equation of motion for the distribution function f (r, v, t). Let's start by recalling that u(r, t) stands for a physically measurable variable in the fluid model. The velocity v now serves as a velocity space coordinate. When we arbitrarily choose a small volume of phase space d3r d3v around the vector (r, v), the particles in this bin form a group that behaves like a fluid with the streaming velocity v. The difference is that in the fluid model, the mean flow velocity is attached to a group of particles, whereas in the kinetic model, the particles have this velocity because they just so happen to be in a bin with the label v. We analyse the phase space of a

one-dimensional system, which only includes the coordinatesin order to clarify our ideas. The difference between the inflow and outflow in real space, together with acceleration and deceleration, determine the particle balance inside a phase space volume. We remove the superscript () for the time being and focus on just one of the plasma species, such as the electrons. We may write in analogy t because f x v x is the number of particles in that little phase-space element[9], [10].

The Vlasov Equation and Fluid Models Have a Relationship

The Vlasov model is obviously more complex than the fluid models in that it can now properly handle arbitrary distribution functions. Only the first three moments of the distribution function—density, drift velocity, and effective temperature—were captured by the fluid models. Does this imply that the Vlasov model is just another model whose precision is comparable to that of the fluid models? The explanation is that the Vlasov model is a particular example of the collisionless fluid model. By selecting the suitable velocity moments for the variables in the Vlasov equation, the fluid equations may be precisely derived from it. Here, we provide two illustrations of this process and limit the discussion to the straightforward 1-dimensional situation.

It is the equation for the transfer of momentum, Steiner's theorem for second moments of a distribution is used in the second line, and the continuity equation, which cancels two terms, is utilised in the final line. We may create an infinite hierarchy of moment equations by multiplying with vn and integrating the elements in the Vlasov equation. The continuity equation connects the change in density to the divergence of the particle stream, demonstrating how each of these equations is related to the member of the hierarchy above it. The pressure gradient, which is specified in the equation for the third moments, is invoked by the momentum equation defining the particle flow, and so on. As a result, the fluid model must be truncated to end. One is often happy to truncate the momentum equation using an equation of staterather than a third moment equation that models the heat transfer.

Application to Diode Current Flow

We first examine the steady-state current flow in electron diodes under the impact of space charge using the Vlasov equation. The treatment of the Child-Langmuir statute differs from that; we now take into account the thermal velocity distribution of the electrons at the vacuum diode's entry point. We list our expectations before beginning the computation. Only electrons with a positive velocity exit the cathode when the electrons are in thermal contact with a heated cathode at x=0. At a certain distance of x=L, an anode with a positive bias voltage is assumed. The velocity distribution function will be half-Maxwell Ian and have a temperature that is dependent on the cathode temperature when it is close to the cathode. When the emitted current is large enough, the Child-Langmuir law's limiting current occurs when the electric field at the cathode vanishes. All electrons may flow to the anode when the current is less than the limiting current because the electric field force acting on an electron is positive. The electric field at the cathode is reversed, however, when the output current exceeds the limiting current because a significant quantity of negative space charge forms in front of the cathode. Fig. depicts such a scenario with a probable minimum.

Only electrons with sufficiently high beginning velocities may now break through the potential barrier. Lower beginning velocity electrons will reflect back to the cathode. Sample trajectories for transmitted and reflected populations are shown in (x v) phase space. Consider

the velocity distribution to be divided into intervals of equal velocity that move through the system similarly to the test particlesat the potential minimum defines the separatrix between the populations of free and trapped electrons.The transit time, which must be separated from absolute time, has just been introduced. The issue of a stationary flow under consideration is not reliant on absolute time. However, following injection at the cathode, a unique amount of time passes for each electron. This period may be compared to the characteristic curve as a series of tick marks. By removing the parameter from the solution of the trajectory v(x) results.

These days, our earlier observations on the characteristics of the Vlasov equation are quite valuable. The building of the distribution function at every location x within the diode is simplified to a mapping issue since the value of the distribution function is constant throughout a phase-space trajectory. The conservation of total energy for a test electron enables this mapping. This implies that we may read the relevant value of the Maxwellian distribution that we have proposed for a point just before the cathode for a particular electric potential (x) and instantly determine the initial velocity. The forward and backward electron fluxes are represented by the two indications of the velocity. We refer to the cathode's velocity distribution as being half-Maxwellian.

Continuity of the current and virtual cathode

The integral across positive velocities, defines the current density at the potential minimum. A simple calculation reveals that this equation consists of the mean velocity of a half-Maxwell Ian distribution and the density of the complete Maxwell Ian at the cathode multiplied by the Boltzmann factor, which results in the density decrease at the potential minima. The result for min 0 is the same as the electron saturation current as the reader may have noticed. As a result, the potential minimum serves as a virtual cathode that feeds the diode and the beginning distribution at the potential minimum is once again a half-Maxwellian. The electron current density in this location may be readily shown. This first seems confusing since the electron velocity rises as it approaches the anode, but keep in mind that the phase space density is preserved for the characteristic that has v 0 at the virtual cathode. Examining demonstrates that when mean velocity increases, the distribution function narrows on the velocity scale, counteracting the acceleration.

Electrostatic Wave Kinetic Effects

The description of small-amplitude electrostatic waves in magnetized plasmas serves as the second illustration of kinetic processes in plasmas. The mathematical machinery won't obscure the physical content since they are one-dimensional issues. The plasma constituents' temperature may be predicted to have kinetic consequences. The Landau damping effect is one of them. A broader distribution function shape may lead to additional kinetic effects, which might cause the waves to become unstable.

Electrostatic Electron Waves

In this section, we look for electron waves that are close to the frequency of an electron plasma. The ions merely provide a neutralizing backdrop in this frequency range and are not involved in wave motion. Beginning with the division of the electron distribution function into a homogeneous and stationary distribution which we assume to be a Maxwell Ian, and a tiny superimposed wave-like perturbation the normal mode analysis may be performed. We

must carefully handle the singularity in the perturbed distribution function that results from the vanishing of the denominator. Resonant particles are what we shall refer to as the electrons with v /k. We had previously seen how resonant particles played a specific function in beam-plasma interaction. The unperturbed Maxwell Ian of the electrons is only partially neutralized by the ion background in the perturbed electron distribution function, which indicates a space charge. The only component of the electron distribution that fluctuates contributes to the space charge. Poisson's equation establishes the connection between the wave electric field and the perturbed distribution function.Landau damping or collisionless damping is the name of this damping technique. Landau employed a well-posed initial-value issue that he solved using the Laplace transform, hence his arguments were mostly mathematical in character. This kind of wave damping cannot be predicted using Vlasov's normal mode analysis, which we used earlier to get the primary value of the dielectric function. Damped waves can only be produced via contour deformation that follows the Laplace transform's principles. For ease of use, the Landau contour has been included into a normal mode analysis in the computation above.

At the time of Landau's discovery, collisional damping hindered plasma wave experimentation and covered up the expected result. Malmberg and Wharton were able to independently verify Landau damping for Bohm-Gross waves in 1966 after two decades of technological advancement. A long plasma column with an axial magnetic field was employed for this experiment. A thin wire probe was used to start the wave. Using an interferometry method and a second moving wire probe, the wave signal was found. The exponential decline of the wave amplitude reveals the Landau damping rate.The physical mechanism behind Landau damping remained unclear even without experimental confirmation. An study of the energy exchange between resonant particles and the wave was provided in 1961 by John Dawson. In the 60 years after Landau's fundamental publication, other efforts were made to explain the Landau mechanism, including. For the sake of a more straightforward instruction, several writers revisited the Landau problem. Given that we have already shown that the Vlasov equation conserves entropy, it is an astounding conclusion that wave damping occurs in a collision-less plasma. It wasn't until the late 1960s that the reversibility of the Landau process was shown in terms of plasma wave echoes, which we shall examine. This seeming contradiction had baffled many researchers. We shall then provide a second illustration of Landau damping[11], [12].

Ion-Acoustic Wave Damping

We treated the ion-acoustic wave using a fluid model that preserved the effect of electron and ion temperature by using the proper pressure gradients. We discovered that the real component of the dielectric function is the same in both the fluid model with pressure forces and in the kinetic treatment of the Bohme-Gross modes in the previous section. As a result, we may calculate the Landau damping of ion-acoustic waves using the dispersion relation. When the wave's I damping rate is substantially less than its R frequency, the Landau approach may be used. When the wave's phase velocity stays away from the part of the thermal velocity where the distribution function's gradient in velocity space is sharpest, there is little Landau damping. The electron-to-ion mass ratio ensures that can always be satisfied by the electrons. When TeTi, as in Q-machine plasmas, where numerous research of this sort were conducted, Landau damping by ions becomes important. The ion-acoustic wave's correct phase velocity may be calculated.

Bunching

Beginning with the motion of nearly resonant electrons in the potential of the wave E(x, t) E cos kx(t) t, let's examine this potential. Here, we take into account the fact that the proper force acting on the electron is affected not only by the electric field's variation over time but also by the electron's shifting location relative to the spatial wave pattern. Therefore, an electron's phase is modulated as the wave field accelerates or decelerates it. When the electron is almost in resonance with the wave, its location may be expressed as x(t) x0 v t v(t) t, where v /k is the wave's phase velocity and v(t) is the electron's tiny instantaneous speed in the wave frame. We may claim that the electron travels in a nearly stationary sinusoidal potential that is well represented by the wave since the electron is almost resonant with the wave. Runge-Kutta integration of the fourth order was used to solve equation. In the range the trajectories electrons were estimated given the identical beginning velocity and equidistant initial phases. The normalized values X was applied.

CONCLUSION

The trajectories with negative velocity at the equivalent trajectories. The electric force acting on the electron is shown in panel's b and d, and the results of the relative motion between the electron and the wave are shown in the trajectories. The trajectories are focused and result in the formation of a localized group of electrons in the grey-shaded regime. Positive acceleration of electrons with a beginning phase of and negative acceleration of electrons with a starting phase are involved in the bunching in panel. The electron paths are divergent and cause a decrease in electron density in the wave phase's unshaded region. This method is well-known from klystron microwave tubes, which enhance microwaves by using electron bunching in a time-varying electric field. In panel c, the positive injection velocity is caused by the same process. The electrons beginning at now pass the electrons starting at. The bunching point is connected to the mean flow in both directions, however in direction it is connected to a more positive location.From the very beginning, bunching is a non-linear process. It is instantly clear that, after a brief period of time, after being injected with equal speed and homogenous distribution throughout all phase angles.

REFERENCES:

[1] D. Mikitchuk *et al.*, "Mitigation of instabilities in a Z-pinch plasma by a preembedded axial magnetic field," *IEEE Trans. Plasma Sci.*, 2014.

[2] V. V. Ivanov *et al.*, "UV laser-probing diagnostics for the dense Z pinch," *IEEE Trans. Plasma Sci.*, 2014.

[3] T. J. Awe *et al.*, "Modified helix-like instability structure on imploding z-pinch liners that are pre-imposed with a uniform axial magnetic field," *Phys. Plasmas*, 2014.

[4] A. Wirthmann, J. C. Finke, P. Giovanoli, and N. Lindenblatt, "Long-term follow-up of donor site morbidity after defect coverage with Integra following radial forearm flap elevation," *Eur. J. Plast. Surg.*, 2014.

[5] A. G. Rousskikh *et al.*, "Study of the stability of Z-pinch implosions with different initial density profiles," *Phys. Plasmas*, 2014.

[6] S. Dayanidhi and F. J. Valero-Cuevas, "Dexterous manipulation is poorer at older ages and is dissociated from decline of hand strength," *Journals Gerontol. - Ser. A Biol. Sci. Med. Sci.*, 2014.

[7] K. Ida and J. E. Rice, "Rotation and momentum transport in tokamaks and helical systems," *Nuclear Fusion*. 2014.

[8] M. Toledano-Luque *et al.*, "Superior reliability of junctionless pFinFETs by reduced oxide electric field," *IEEE Electron Device Lett.*, 2014.

[9] B. Jones *et al.*, "A renewed capability for gas puff science on Sandia's Z machine," *IEEE Trans. Plasma Sci.*, 2014.

[10] Y. C. See and M. Ihme, "Effects of finite-rate chemistry and detailed transport on the instability of jet diffusion flames," *J. Fluid Mech.*, 2014.

[11] D. J. Ampleford *et al.*, "Contrasting physics in wire array z pinch sources of 1-20 keV emission on the Z facility," *Phys. Plasmas*, 2014.

[12] S. F. Liu, S. C. Guo, W. Kong, and J. Q. Dong, "Trapped electron effects on ηi-mode and trapped electron mode in RFP plasmas," *Nucl. Fusion*, 2014.

CHAPTER 8
INSTABILITY SATURATION BY TRAPPING

Dr.Vikas Kumar Shukla, Assistant Professor
Department of Science, Maharishi University of Information Technology, Uttar Pradesh, India
Email Id- vikash.shukla@muit.in

ABSTRACT:

In this article, we'll examine a PIC-simulation of the beam-plasma instability for comparison with the analytical approach. The ES1 code2 as described in is used to create the simulation. The bulk of the electrons in the system are at rest, and an electron beam with a beam fraction of b 0.01 is present. Ions that are stationary neutralize the system. There are 256 plasma particles and 512 beam particles with a lowered q/m in accordance with the beam fraction. 64 grid points make up the grid, and pet 0.05 is selected as the time step. It should be noted that the code employs normalized values for readers who wish to perform their own simulations. We shall refer to the actual physical amounts in the material that follows the simulation's output is shown as a collection of electron phase space plots paired with the wave's electric potential. Take note of the opposite sign of the potential energy. The system length of the ES1 code, which employs periodic boundary conditions, is merely one wavelength of the unstable mode. Therefore, a wave phase angle between 0 and 2 is provided as the x coordinate. The system of reference is supported by the unaffected beam's moving frame. As a result, the unstable slow space-charge wave, which is propagating almost at beam speed, is shown in this illustration as slowly travelling to the left.

A semi-log plot of the electric field energy and the beam kinetic energy along with the exponential rise of the instability and its final saturation. The beam-plasma instability is seen to rise exponentially for pet, becoming a straight line in the semi-log representation. The growth rate of the wave energyis twice as fast as the growth rate of the wave amplitude. The growth rate is calculated from the straight line's slope, which matches well to the estimate from the linear instability analysis

KEYWORDS:

Charge, Dust, Electron, Particles, Potential.

INTRODUCTION

The exponential development phase comes to an end at time pet. The beam electrons are still flowing freely. A thin horizontal line denotes the initial beam velocity, v_0. The velocity modulation of the non-resonant plasma electrons is substantially less. The field energy starts to saturate before oscillating, exchanging field energy for beam kinetic energy. The matching phase space demonstrates that the beam particles have been trapped by the wave field and have started to conduct bouncing oscillations in the potential well indicated by the positive half-wave at the initial maximum of the field energy. The wave energy in panel d has decreased to its lowest value, which is correlated with a significant number of beam electrons moving forward once again in the potential well. The wave has given these electrons more energy. The beam kinetic energy has now virtually returned to its un-perturbed value. The beam electrons start to spread throughout all phases of the trapping motion, but they are primarily contained in the wave's potential well, as seen in panels.

Because the bouncing frequency in a sinusoidal potential well depends on the electron energy, the electrons spread out throughout the whole potential well as a result. The potential well's curvature at its lowest can be used to determine the bounce frequency, and the potential well's trapping potential can be used to compute the wave field energy at trapping [1], [2].

Current Flow in Bounded Plasmas

Let's have a look at the issues surrounding current flow in diodes once again. The purpose of the first example is to demonstrate how analytically treating the virtual cathode issue in diodes with thermal emitters and PIC simulations is comparable. The second example demonstrates how an inhomogeneous equilibrium flow may change to an oscillating state of a different topology in phase space by introducing an instability of the electron beam in a diode.

Thermal emitter's virtual cathode

A potential minimum arises when a cathode's emission current surpasses the limit set by the Child-Langmuir equation, reflecting sluggish electrons back to the cathode. The Child-Langmuir current is the only current that exists above the potential minimum. The virtual cathode was therefore given as the term for the potential minimum. The Vlasov-theory provided an analytical solution to this issue. We now reevaluate the issue using PIC-simulation and the PDP1 code. With a cathode temperature of 650 K, the thermal velocity of the electrons, denoted, is equivalent. With these specifications, an empty diode's Child-Langmuir current. Due to the approximately 40-fold increase in injection current, a potential minimum of 0.16 V depth is created[3], [4].

Blocking Electron Beam Oscillations

Let's look at the injection of a mono-energetic electron beam into a vacuum diode without any external voltage being added. We reasoned that a vacuum diode's electron beam is slowed down by its own space charge, causing a virtual cathode to develop in the diode's middle. When the electrons are slowed down to almost zero velocity at the potential minimum, the maximum stable current in this diode is obtained. This was the scenario that a time-reversed Child-Langmuir diode and a regular Child-Langmuir diode might operate in tandem to explain.The virtual cathode will develop considerably more closely to the injection site if a much higher current is introduced into the diode. Panels b and c of the simulation how the injected electron beam reaches a stagnation point and is reflected back towards the cathode. At this moment, the stagnation point is closer to x 0 due to the extra space charge created by the reflected electrons. On the other hand, the potential minimum becomes less negative and the volume between the injection site and potential minimum has decreased (panel c). The repetition of the procedure starts at panel d[5], [6].

The system's ultimate state exhibits significantly nonlinear current oscillations and is non-stationary. Even worse, the current is briefly disrupted. It should be noted that the overall current, which is made up of the displacement current caused by the movement of the virtual cathode and the electron current, briefly becomes even positive. Blocking oscillations are a phenomenon that is characteristic of relaxation oscillators. The development of two distinct time scales in the oscillation period, a rapid evolution close to the point of current zero, and a leisurely evolution in between, is a characteristic property of relaxation oscillators. The current's peaked waveform has multiple harmonics.High-power microwaves may be

effectively created via virtual cathode oscillations Microwaves with frequency of 1–100 GHz and pulse lengths of 1–500 ns are generated by introducing a relativistic electron beam with currents of 1–200 kA and energies of 0.1–10 MeV. Using 3.9 GHz as an example, Davis et al. observed output powers of 1.4 GW with several hundred megawatts in harmonic radiation. 4 GW at 6.5 GHz is reported by other writers [220]. Microwave frequencies and power are predicted using a one-dimensional analytical model of virtual cathode oscillations. Up to 30% conversion efficiency (microwave energy to beam energy) is possible under ideal circumstances. The conversion efficiency was often close to 3% in trials. The two examples given above—a diode with a thermal emitter or with an injected electron beam—show comparable concepts to those we discovered in the kinetic theory study of Maxwellian distributions and electron beams[7], [8].

DISCUSSION

By bunching, electron beams may effectively build up space charge. Phase mixing of the contributions from the many beams that make up the Maxwellian distribution combats bunching in a Maxwellian distribution. Thus, the Landau damping of the modes that cause blocking oscillations in the case of mono-energetic injection may be used to explain the apparent stability of the virtual cathode for a thermal emitter.The investigation of dusty plasmas has grown in popularity since the 1980s. Dusty plasmas are sometimes referred to as complicated plasmas due to their resemblance to complex fluids. Since powder formation in plasma-enhanced chemical vapour deposition was found to be a factor in limiting the rate of deposition as well as when dust formation and dust trapping were noticed during plasma etching of silicon wafers this field, which has its roots in astrophysics has become interesting for laboratory plasma research[9], [10].

In addition to electrons and atomic or molecular ions, dusty plasmas can include microscopic particles with diameters ranging from a few tens of nanometers to many tens of meters. The dust particles interact with the other plasma ingredients after being electrically charged. The electrostatic inter-particle forces become significant when the dust particle density is high enough. When the dust subsystem exhibits collective behavior, it may take the shape of wave events or, in the case of micrometer-sized particles carrying thousands of elementary charges, liquid or solid phases. The study of dusty plasmas received a major boost in 1994 with the discovery of plasma crystallization. The huge mass of dust particles—a dust particle of 1 m diameter typically has a mass of $3*10^{11}$ proton masses—leads to a lengthy dynamic reaction time of milliseconds or more, which accounts for a large portion of the field's attraction. Fast video cameras can track the movement of all individual particles in dusty plasmas with micrometer-sized particles. This is a rare chance to investigate the kinetic collective behavior of a charged particle ensemble.

The study of dusty plasmas has now matured, and diverse elements have been compiled in several review papers or monographs during the last ten years. Therefore, the items included in this Chapter are not meant to provide a fair summary of the many observations that have already been made. Instead, we'll concentrate on these issues: The enormous charge, on a dust particle of several micrometer size distinguishes a dusty plasma from a three-component plasma that includes electrons, positive ions, and an extra population of negative ions. In contrast, gas discharges Positive ions are efficiently scattered by negative dust particles because the Coulomb collisions of electrons with ions are far less frequent than the collisions with atoms.

As a result, ions' orbital motion becomes a key idea in dusty plasmas and turns out to be just as significant in magnetised plasmas as gyromotion. These highly charged dust particles' nonlinear shielding effects are determined by their orbital motion, and ion-dust momentum exchange creates the novel phenomena known as ion wind forces.

The significant dust charge is also the cause of the significant coupling parameter between the dust grains, which, at room temperature, may result in liquid and solid phases of the dust system. Systems that may be used to explore solid structural characteristics, phase transitions, or phonon dynamics with "atomic resolution" include plasma crystals and Yukawa balls. Dust particles don't have a set quantity of charge as negative ions do. Since charge is the sum of charging currents over time, it relies on how the environment has changed throughout the particle's previous course. As a result, the Coulomb force is no longer conservative and may cause instability. Variations in charge brought on by the distinct stages of collecting an ion or electron become significant for dust with a size of a nanometer. When one of the partners is neutral or briefly acquires the opposite charge, tiny particle coagulation is made feasible. We will only cover dusty plasma effects for spherical particles in the following for the sake of simplicity. When there are several particles present, it is presumed that they are all the same size.

Dust Particle Charging

The primary method used to charge dust particles in the majority of laboratory and industrial plasmas is the collection of electrons and positive ions. Dust particles react at floating potential like tiny isolated probes. Dust particles are negatively charged because electrons have a faster thermal speed than ions do. Space dust is exposed to fluxes of intense photons or particles, such as solar wind particles, which release electrons through photoemission or secondary emission in addition to collecting thermal plasma particles. These procedures cause the dust to become positively charged and may perhaps be more significant than charge collecting contains a review of space billing procedures. In this section, we will first examine the basic mechanics before moving on to the issues with charge fluctuation. How long does it take for an equilibrium charge to relax? What are the charge fluctuation statistics? How do charges compete for the resources used for charging?

Subsequent Emission

A primary energetic particle that penetrates the surface of a solid release’s free electrons along its route by ionizing atoms in the solid until it is halted. This process is known as secondary emission. By diffusing to the surface, secondary electrons may escape the solid. The ratio of the current of released electrons to the current of source particles is known as the yield of secondary electrons. The average number of liberated electrons per incoming electron, or Is/Ie, is used to characterize the effect of an electron. The average number of emitted electrons per incoming ion, or coefficient, is used to define secondary electron emission by ion collision. We have 1 for the majority of materials, and 1 only faintly relies on ion energyit will be detailed how ion impact releases electrons from metal cathodes, which is necessary for the plasma formation in glow discharges.

The formula provides the shape of the secondary emission yield by electron impact as a function of initial electron energy. It turns out that both models have distinct asymptotic at high energy while being almost equal contains the coefficients m and Wm for the secondary electron yield of various materials, which may be used to both models. Small grains and bulk

materials may produce very distinct secondary emissions. Instead of merely finding a surface in one direction as it does in bulk matter, a diffusing electron in a tiny spherical grain may locate a surface in any direction. The secondary yield is increased by this impact. Small dust grains, on the other hand, become transparent to energetic projectiles, which only deposit some of their energy, reducing the yield.

In many astrophysical conditions, photoelectric emission is thought to be the primary process of cosmic grain charge. In the fundamental process, an electron that is attached to the grain with a binding energy and released by a photon with energy is known as the material's work function. The grain charge rises by one (positive) elementary charge as the electron departs the grain surface with surplus energy. This idea leads to a final state in which the grain attains a high positive potential in the lab, where the source of energetic photons may be a UV laser or a mercury lamp with a strong UV emission line. The next released photoelectron can't escape the dust grain's attractive potential well because the potential is just high enough, so it returns to the dust grain's surface. This establishes the dust charge and provides the potential well's depth.

The situation in space is far more complicated. The flip-flop effect refers to the coexistence of two distinct equilibria with positive and negative charge when photoemission becomes competitive with electron and ion collecting. The development of dust agglomerates, the first phase in the formation of planets surrounding proto-stars, depends on this point. Similarly charged dust particles would repel one another, preventing coagulation. Furthermore, since UV light is often not a monochromatic source, dust charging via photoemission becomes more complicated than the estimates above. The Sun's energetic photon spectrum, on the other hand, spans from the infrared to the extreme ultraviolet region. The Solar Irradiance Reference Spectrum, as observed during Solar Carrington Rotation 2068. The cross section for photoionization of neutral carbon and silicon atoms in order to provide insight into the photoionization of common elements in cosmic dust. Ionization thresholds for C and Si are 110 nm and 152 nm, respectively. As a result, silicon is ionized but not carbon atoms by the Lyman-line of atomic hydrogen at 121.6 nm, the line that delineates the UV and EUV regions. Cross sections for both materials rapidly decrease as wavelengths become shorter. As a result, the area close to the threshold contributes most to photoionization.

Here, we must integrate the ratio of the spectral energy density S(W) throughout the full solar spectrum to the photoelectric efficiency (W) (i.e., the number of electrons per incoming photon). It is necessary to conduct an experiment to determine a dust particle's photoelectric efficiency since it cannot be inferred from atomic data alone. The photoelectric yield for lunar dust was calculated. A distribution of surplus energy derives from the sun photon flux's spectrum range. The photoelectrons' effective temperature, Tph, may then be thought of. This indicates that a portion of the photoelectrons in the tail of the distribution function will be able to overcome a positively charged grain's potential well. The right Boltzmann factor may be used to characterise this fraction.

The principal method of charging for lunar dust is thought to be photoelectric. The collision of tiny meteorites has created a fine powder called regolith that covers the Moon. The large-scale interactions with the local plasma environment and the photoemission of electrons from solar UV and X-ray radiation also contribute to the electrostatic charge on the lunar surface. Then, dust particles and surfaces with similar charges start to resist one another. near the sub-solar point, the surface potential is 4.1 V; near the terminator, it is 36 V and in between, it is

3.1 V. Approximately 1 m thick (8 m at the terminator), a Debye sheath is created with a vertical electric field inside of it. Thus, larger dust grains up to 5 m in diameter may be lifted inside thissheath to heights of (3–30) cm. The brightness of the lunar horizon seen by Surveyor-7 or Lunochod-II landers when positioned on the lunar surface may be attributed to these grains.

Surprisingly, the Apollo-17 crew also saw horizon light during their spacecraft's orbital phase before local dawn, providing the first proof of a prolonged dust environment with tiny particles that extends to orbital heights. The commander of Apollo-17, Capt. E. A. Cernan, sketched a variety of images depicting light scattering studies just before dawn, revealing a diffuse "corona" and "streamers". The drawings created at T-2 minutes, T-1 minute, and T-5 seconds include the key observations for local light scattering. The streamers were only seen from T-2 minutes on, although they increased more quickly than the corona despite the corona being visible for at over 4 minutes. The rise in the last 5 s is greater than in the first 2 minutes. Such a behaviour can only be described by light scattering from submicron particles, which is greatly amplified in a nar-row cone in both the forward and backward directions, according to the Mie-scattering hypothesis forward dispersed light only becomes visible a few seconds before reaching the point of orbital dawn. The Zodiacal light, which is sunlight that has been backscattered by interplanetary dust in the ecliptic, is yet another illustration of how well microscopic particles can scatter light.

Lack of fresh observational findings has led to ongoing controversy on the lunar dust atmosphere. A mechanism called an electrostatic fountain is used in one of the most recent models of lunar dust lofting. A dust particle with a radius of 10 nm and between 20 and 200 elementary charges is said to have an initial electrostatic potential energy of 60 to 6000 eV. This energy is comparable to the 1250 eV difference in gravitational potential energy between the lunar surface and a height of 100 km for that grain, which enables an energetically feasible fountain operation. Only lower altitudes will be reached by larger grains. Before the lunar dust atmosphere can be fully understood, there are still a number of unanswered questions, such as the number density of these particles in the dust atmosphere, the size distribution, the effectiveness of light scattering, the transport of submicron dust by horizontal electric fields or by radiation pressure, etc., that call for more experimental data.

Charge fluctuations

The continuum charging model mentioned in the preceding sentence is no longer valid for tiny dust grains that are around ten nanometers in size. Instead, one must take into account the aggregate of distinct electrons and ions, which causes variations of the charge in discrete stages. In the discrete charging procedure via a random process was investigated. Charge collection probabilities per second may be used in lieu of the charging currents Ii and Ie. Charge variations in relation to the equilibrium value are a result of the discrete model. In addition, deviations from the equilibrium value diminish as the relaxation timeas shown by a comparison of the behaviour of particles with 10 nm and 50 nm radii. Numerous numerical investigations in [255] have shown that a standard deviation of Zd may adequately reflect the oscillations of the dust charge around its equilibrium value Zd. In other words, as the size of the dust particle increases, the relative fluctuations of the dust charge Zd/Zd decrease. Positive and negative particles may coexist as a result of charge oscillations. This technique works well for little grains that only have a few simple charges. The coagulation of microscopic dust grains is thus made easier by the presence of oppositely charged grains,

such as in plasma reactors used to create nano-powder. Charge fluctuations, on the other hand, can no longer form grains of the opposite charge, and coagulation between particles of the same size is halted after the particles have grown to more than 25 nm radius and their charge surpasses roughly 40 elementary charges. Agglomeration of small particles with larger particles is significant as long as the small particles can achieve the opposite charge by fluctuations or by the flip-flop effect. This is in contrast to powder production in plasma reactors, which results in a narrow size distribution.

Dust Density's Effect on Dust Charge

Up until now, we've thought about charging a lone dust grain in a plasma environment with endless charging currents. When a dust cloud comprises a large number of dust particles and the overall dust charge equals the total positive ion charge, the situation is different. The quasi-neutrality of plasmas therefore limits the amount of free electrons to a very limited quantity. The additional electrons are fused to the dust molecules. The plasma potential c within the cloud between the dust grains, which we have selected may vary from the ambient plasma when the dust particles are closely packed. Assume for the moment that the dust cloud's electrons and ions are in thermal equilibrium with the surrounding plasma. Boltzmann factors will then control the concentrations of electrons and ions. For all plasmas, the electrons' Boltzmann response is a known notion. However, there must be more evidence before employing the Boltzmann factor for ions[11], [12].

CONCLUSION

In astrophysical scenarios, plasma is created in an area that is larger than the dust cloud, and electrons and ions are carried across great distances before being destroyed by recombination at a surface. As a never-ending reservoir, the ambient plasma serves as the dust charging process. In addition, the thermal plasma in astrophysical circumstances often contains and density changes caused by the Boltzmann factors are minimal, with the exception of the energetic particles in the Solar wind. However, assuming a constant ion density is a better approximation for laboratory plasmas.

The balance between ionization and losses, together with some ionization that takes place within the dust cloud, determines the ion density. Losses may result through ambi-polar diffusion towards the walls or, in large dust clouds, from the charging currents generated by the dust particles themselves, which serve as a "internal wall." Let's start by taking a look at the original isothermal hydrogen plasma model that was created for astrophysical dust clouds. Calculating the charging currents for the dust grains requires using the electron and ion density supposing that the grain potential is negative.

REFERENCES:

[1] J. Vieira, W. B. Mori, and P. Muggli, “Hosing instability suppression in self-modulated plasma wakefields,” *Phys. Rev. Lett.*, 2014.

[2] K. R. Hansen and J. Lægsgaard, “Impact of gain saturation on the mode instability threshold in high-power fiber amplifiers,” *Opt. Express*, 2014.

[3] S. Terhaar, B. Ćosić, C. O. Paschereit, and K. Oberleithner, “Impact of shear flow instabilities on the magnitude and saturation of the flame response,” *J. Eng. Gas Turbines Power*, 2014.

[4] M. Reverendo *et al.*, "TRNA mutations that affect decoding fidelity deregulate development and the proteostasis network in zebrafish," *RNA Biol.*, 2014.

[5] A. Diallo *et al.*, "Observation of edge instability limiting the pedestal growth in Tokamak plasmas," *Phys. Rev. Lett.*, 2014.

[6] J. Zhang *et al.*, "Multiple beam two-plasmon decay: Linear threshold to nonlinear saturation in three dimensions," *Phys. Rev. Lett.*, 2014.

[7] M. T. Levinsen, "Saturation of shape instabilities in single-bubble sonoluminescence," *Phys. Rev. E - Stat. Nonlinear, Soft Matter Phys.*, 2014.

[8] B. Schmidt *et al.*, "Impact of study oximeter masking algorithm on titration of oxygen therapy in the Canadian oxygen trial," *J. Pediatr.*, 2014.

[9] W. Liu, C. Yu, and X. Li, "Effects of initial radius of the interface and Atwood number on nonlinear saturation amplitudes in cylindrical Rayleigh-Taylor instability," *Phys. Plasmas*, 2014.

[10] C. S. Jao and L. N. Hau, "Fluid aspects of electron streaming instability in electron-ion plasmas," *Phys. Plasmas*, 2014.

[11] M. Ashrafi, Y. Souraki, and O. Torsaeter, "Investigating the Temperature Dependency of Oil and Water Relative Permeabilities for Heavy Oil Systems," *Transp. Porous Media*, 2014.

[12] J. He and J. Chu, "Undrained Responses of Microbially Desaturated Sand under Monotonic Loading," *J. Geotech. Geoenvironmental Eng.*, 2014.

CHAPTER 9
THE CONCEPT OF PLASMA WAVES

Dr.Vikas Kumar Shukla, Assistant Professor
Department of Science, Maharishi University of Information Technology, Uttar Pradesh, India
Email Id- vikash.shukla@muit.in

ABSTRACT:

The vertical sounding experiments conducted in the United States by Gregory Breit (1899-1981) and Merle Antony Tuve (1901-1982) as well as in Great Britain by Edward V. Appleton (1892-1965), which established the existence of a conducting atmospheric layer, now known as the ionosphere, in the altitude regime of (100-500) km, marked the beginning of the quantitative investigation of the ionosphere with radio waves of the same time, Irving Langmuir of the General Electric Laboratories discovered what are now known as Langmuir oscillations, which are high-frequency variations in gas discharges .The categorization of the basic wave types in a plasma, which illuminates the many processes that give rise to wave phenomena, is of interest to us at the book's introductory level. At the same time, we'll talk about how different wave types may be used to plasma diagnostics. There are many contemporary textbooks that provide an in-depth discussion of plasma waves

KEYWORDS:

Density, Electron, Frequency, Plasma, Wave.

INTRODUCTION

Different factors have sparked interest in wave propagation in plasmas. One of them was the ionosphere's ability to reflect electromagnetic radiation. Oliver Heaviside (1850–1925) and Arthur Edwin Kennelly (1861–1939) independently proposed in 1902 that the Earth's atmosphere at high altitude must contain an electrically conducting layer that reflects radio waves like a mirror in response to Guglielmo Marconi's (1874–1937) experiments on long-distance radio in 1901. Carl Friedrich Gauss (1777–1855) proposed the theory that electric currents in the upper atmosphere may be connected to variations in the Earth's magnetic field many years earlier, in 1839.

The Wave Equation and Maxwell's Equations

This Section examines the plasma's interactions with electromagnetic waves using a novel theory in which the plasma is seen as a dielectric medium. The dielectric constant of the plasma medium, which governs the propagation speed and polarization of the plasma waves, includes the linear response of the plasma particles to the wave field for this purpose. The Maxwell equations serve as the beginning point for this model's development. The direction of the wave propagation is indicated by the wave vector, k, in this instance. The wavelength and the wave vector's magnitude are connected by the formula.

Because the wave amplitudes E and j are complex numbers, we can easily insert a phase shift between the electric field and current density. Both are wavenumber and frequency functions, for example, E E (, k). We can create straightforward substitution rules for the differential operations using this plane wave representation[1], [2].

Dielectric or conducting media

We may interpret the current density differently since we assumed a linear relationship between the alternating current and the electric field. The wriggling motion of electrons and ions may be seen of as a polarisation current when the plasma is viewed as a dielectric media. This polarisation current can be paired with the vacuum displacement current. Only at the upper limit of extremely high frequencies. The considerably heavier ions will be stationary while the electrons will fluctuate around their mean location. As a result, we are free to think of the plasma as a collection of dipoles generated by couples of ions at rest and an electron circulating around them. A characteristic of such a media is the dielectric displacement. I serve as the unit tensor here. The electric field vector E and the electric current vector j may no longer be parallel to one another as a result. Additionally, the plasma is a lossy dielectric medium due to particle collisions, therefore is often a complicated function[3], [4].

There are two main perspectives on the plasma medium, to sum them. When there are only minor losses, the plasma mostly exhibits dielectric behaviour, and this behaviour is captured by the dielectric function (or tensor), in which the real component predominates over the imaginary part. When collisions happen often, the plasma mostly functions as a conductor and is represented by the complex conductivity, where the imaginary component reflects phase changes brought on by inertial factors. Following, we'll focus mostly on scenarios when the plasma waves are just somewhat dampened. Thus, the majority of the dielectric tensor's components are actual quantities. We shall thus favour the dielectric description of a plasma[5], [6].

Refractive Index

The ratio of the speed of light in vacuum to the speed of that medium is known as the refractive index of a transparent medium in optics. Similar reasoning may be used to explain electromagnetic waves in plasma. As a result, we say that the refractive index**.**We may create a refractive index vector N (c/k) thanks to the proportionality between N and k. Given that it points in the direction of wave propagation but has a magnitude of v1, it is obvious that this is the counterpart of the phase velocity. The idea of refractive index is helpful for wave refraction, ray tracing, and interferometry, much as in optics.The link between and k, which is shown by the zeros D (, k) 0, may often be expressed explicitly in the form (k). This relationship often includes many branches. The dispersion relation of a wave is another name for the explicit form of a wave. In conclusion, depicts all plasma wave modes that might be feasible. The components of the dielectric tensor include information about the unique characteristics of the plasma. In isotropic fluids, such as unmagnetized plasmas, the dielectric tensor is reduced to a scalar dielectric function. Anisotropy is introduced by the magnetic field, which calls for a tensor description [7], [8].

Waves in Non-Magnetized Plasmas

Here, we look at wave modes in a plasma without a magnetic field's help. We will start by thinking about extremely high frequency waves, for which the ion motion may be disregarded due to the considerably greater ion inertia. This is evident right away from Newton's equation. Clearly, the electron current is me/mi times larger than the ion current. The ions only function as a neutralizing charge background at high frequencies. We shall add low-frequency electrostatic waves in the last sentence, when the importance of ion motion increases.

DISCUSSION

As a starter, we don't consider pressure effects as we analyse electromagnetic waves in the limit of a cool plasma. We further exclude electron-neutral collisions. The wave vector, k (kx, 0, 0), in the x direction, is used to choose the coordinate system. We may deduce from that the directions of the electric field and current are parallel. The conductivity tensor thus only contains diagonal members with the same value.We have assumed up to this point that friction with the neutral gas has no impact on the velocity of the electron in the wave field. When the wave frequency (such as that of a laser beam) is much greater than the collision frequency, this approximation is unquestionably accurate. This hypothesis is backed by Newton's equation in Fourier notation, which demonstrates that the resultant electron velocity may be divided into a real and imaginary response component with respect to the electric field. The in-phase response, which results from the collisions of electrons, mimics the function of a resistor. The imaginary portion of the response corresponds to a current that lags the voltage by 90. The system's electron inertia, which acts like an inductance, is what causes the lag[9], [10].

We may apply a quick method to write down the dispersion relation with collisions by noticing that when we rewrite in terms of an effective mass m, it becomes equal with the collision less limit. Therefore, we merely need to substitute me for the actual electron mass in the electron plasma frequency. We discover a complex wavenumber in this way for every given real frequency. This is the correct way to explain how a wave enters a plasma. The resultant complicated dispersion relation. While the imaginary component of the wavenumber explains the damping of the wave amplitude, the real part of the wavenumber provides the development of the spatial phase. Keep in mind that at plasma frequency, the imaginary and real parts of k intersect. The collisionality makes the plasma a resistive material for wave frequencies below the plasma frequency. This explains why, despite the electron plasma frequency being significantly greater, we can generate a plasma at radio frequency (for example, at 13.56 MHz). The correct wave energy dissipation caused by the collisionality results in the heating of the electron gas via the Joule effect. On the other hand, when > 2pe, collisional damping is hardly noticeable. In light of this, it is still possible to determine the refractive index of a weakly collisional plasma if the wave frequency is significantly higher than the cut-off frequency.

Therefore, we may determine the electron density by measuring the refractive index, such as using an interferometer. The refractive index N for a collisionless plasma is less than unity, zero at the frequency of the electron plasma, and imaginary at lower frequencies. When the wave frequency is lower than the electron plasma frequency, an electromagnetic wave is therefore reflected at the surface of a plasma. This explains why a small coating of silver on a glass mirror may reflect visible light but becomes transparent in the UV range thanks to the free electrons of the silver atoms in the conduction band. A weakly collisional plasma would permit wave penetration with an exponential decay given by the imaginary component of k.

We may investigate a plasma with a density gradient and a wave with a set frequency instead of taking into account a specific plasma with a constant density for different wave frequencies. The cut-off density nco is thus defined as the location at which the local plasma frequency, which at that location corresponds to the electron density, coincides with the wave frequency. Similarly, we may take into account a non-stationary plasma that is turned on at time t 0 and eventually approaches the cut-off density.

Therefore, the cut-off density may be associated with an inhomogeneous plasma, its temporal development, or both. As a result, the simplest approach of diagnosing plasma density is to determine whether the plasma permits wave transmission or not.

Mach-Zehnder Interferometer

But using an interferometer to measure the refractive index is a more tasteful approach. Depending on the plasma density, this may be accomplished using coherent radiation sources in the microwave, infrared, or visual range. A Mach-Zehnder interferometer is a standard setup for interferometry using microwaves or lasers. The basis for interferometry is the phase difference between the reference wave, which travels the same distance in air, and the wave that enters the plasma. In practise, this is done by dividing the wave into two identical branches and merging them together on a detector where the waves interfere. The geometric length L and the refractive index R are multiplied to create the optical path through the plasma. The phase shift is no longer proportional to the wavelength's inverse, as might initially imply, but rather becomes proportional to the wavelength as the cut-off density decreases.

This means that long-wavelength lasers or microwaves are required for density measurements at low electron densities. The geometric optics approximation, on the other hand, restricts the maximum wavelength and necessitates that the plasma dimensions be big relative to the wavelength. The attainable sensitivity of interferometers is constrained by this conflict. When a powerful current pulse builds up plasma, the detector circuit's dynamic response is too sluggish to resolve the interferometer fringes.

The plasma density during the present pulse is much greater than the cut-off density. The interferometer signal exits the cut-off zone 600 seconds after the present pulse ends and begins to fluctuate around a mean value. The phase shift of one interferometer fringe is equal to two units. A quarter fringe resolution is obtained by reading the interferometer signal's peaks, minima, and zero crossings. These result in the data points which are shown on a logarithmic scale to illustrate the exponential decrease of plasma density in the discharge's afterglow. The precise formula was used to examine the data points close to the cut-off in this evaluation.

Michelson interferometer that is folded

There are two techniques to increase an interferometer's sensitivity: First off, a new kind of interferometer should be employed, such the Michelson kind, which already has a beam that has passed twice through it. By folding the beam into a z-shape, which creates a six-fold passage, the sensitivity may be increased even further, albeit at the sacrifice of spatial resolution. The transmission band of quartz windows is still in the range of the laser wavelength. Special materials would be needed for windows and optical components with a longer wavelength. Second, reading accuracy is only 45 when counting interferometer fringes. As a result, a more accurate method should be used to measure the real phase angle. This may be done via quadrature detection, which involves making two separate interferograms with sine and cosine waves in the reference branch. This is achieved technically by dividing the two interferometer signals using orthogonal polarizers and employing a circularly polarized wave in the reference beam that is produced by a /8 plate that has been crossed twice.

The Second-Harmonic Interferometer

The second-harmonic interferometer is a unique kind of two-wavelength interferometer that was developed by Hopf and colleagues. Currently, this method is used, for instance, in the diagnostics of the Alcator C-mode tokamak. Because the reference beam and probe follow the same route in second-harmonic interferometry, the interferometer is less sensitive to mechanical vibrations than it is in traditional interferometers with a distinct reference branch.

The probe beam is the original signal from aNd: YAG laser operating at a wavelength of 1064 nm. Although it likewise travels through the plasma, the frequency-doubled wave at 532 nm does so with a distinct phase shift. The probe wave is still powerful behind the plasma and can have its frequency increased by using a second crystal. Then a filter stops the basic wave. On the detector, interference fringes are produced by both 532 nm waves. The plasma and air in the air gaps cause the basic laser pulse at to phase shift p() between the first and second doubler crystals.

Microwave Cavities with Plasma

It is also possible to detune the resonance frequency of cylindrical microwave cavities using the refractive index of a plasma. Due to the resonance frequency's high sensitivity to changes in electron density, this is especially helpful at low electron densities. The TM0m0 cavity modes, which have an electric field aligned with the cylinder's z-axis, are suitable for detecting the resonance. (For more on microwave cavities and wave-guides, see, for instance, as a result, the top and bottom of the cylinder are perpendicular to the z-axis and the electric field is uniform along the z-axis.

The TM0m0 modes' eigenfrequencies are thus unaffected by the resonator height. The eigenfrequency of the cavity is determined by the radial bound-ary condition at the cylinder radius, Ez(R) 0. The eigenfunctions have the following structure when the cavity is filled with a homogenous dielectric material of dielectric constant.

Electrostatic Waves

We now return to the longitudinal mode with k E after discussing the transverse electromagnetic wave in an unmagnetized plasma. Faraday's induction law (6.10) demonstrates that longitudinal waves are electrostatic because k E 0 and the wave magnetic field disappear.

The Longitudinal Mode

There, we had put off talking about the third mode, which is represented by the equations. The first row of the equation system, which establishes the parameters for an electrostatic wave's dispersion. It also means that this electrostatic wave only exists for pe in a cold plasma. These oscillations of the electrons around their equilibrium at the electron plasma frequency are known as Langmuir's plasma oscillations. Even though we have a wave solution, it turns out that the dispersion relation is independent of k. This indicates that since the group velocity is zero, the plasma oscillations cannot produce propagating wave packets.

Bohme-Gross Waves

The aforementioned Langmuir oscillations become dispersive when we think of a heated electron gas, where pressure forces are comparable in strength to electric forces. The following may be used to obtain the dispersion relation: Since the electrostatic waves are one-dimensional, we begin by incorporating the pressure per particle into Newton's equation in one spatial dimension.

Ion-Acoustic Waves

There is a second electrostatic wave in a plasma containing heated electrons when we let the ions to participate in the wave motion. This is feasible at wave frequencies that are significantly lower than the frequency of the electron plasma. It should be noted that low-frequency electrostatic modes are unaffected by the plasma cut-off, which was a characteristic of the transverse electromagnetic mode.

When considering low-frequency modes, inertial forces may be disregarded since the motion of the electron is only affected by pressure forces. Alternatively, we may think of the ions as a fluid that is controlled by the interaction of the electric field force, ion inertia, and ion pressure. It is advisable to account for various ion and electron equilibrium densities. Because of quasi-neutrality, a two-component plasma of electrons and positive ions has ne0 ni0; nevertheless, we'll look at a more general example in which the existence of a third negative species results in the difference in densities. These might either be negatively charged dust particles or negative ions.

When we see that the numerator, as we would require for the electron pressure, this interpretation is plainly incorrect. The ion mass density creates the same issue in the denominator. Therefore, the model of the ion-acoustic wave's mechanism has to be updated. By thinking of the electrons as a fluid with the opposite charge that protects the electric repulsion between the ions rather than a gas that imposes pressure, the seeming contradiction may be explained. The interaction between the ions is thus nearing their bare repulsion when the phase velocity rises when the electron density is decreased. The rise in phase velocity with increasing ratio n/ne, indicates that this phenomenon is well known from negative ion plasmas. Similar to how the ion-acoustic wave has a larger phase velocity in a dusty plasma than it does in a clean plasma.

Fahrenheit Rotation

The Faraday effect, which causes the plane of polarization of a linearly polarized electromagnetic wave that propagates along the magnetic field line to spin around the field, is caused by the tiny difference between NR and NL at high frequencies. It is possible to separate a linearly polarized transverse wave into its R- and L-mode components as it moves through the magnetic field. We get for the electric field components in circular coordinates. Faraday rotation is a common method for examining galactic magnetic fields The solar corona's magnetic structure was studied using back- polarized radiation from natural radio-sources or illumination from a satellite-borne transmitter Modern methods for studying the ionosphere plasma include polarization analysis of coherent radar backscatter or Faraday rotation imaging with numerous satellites.

After being shown in the textor device polarimetry with numerous ray pathways is now a widely used technique that can measure the poloidal component of the magnetic field in fusion devices. Long wavelengths in the far infrared are favoured from the perspective of sensitivity. These infrared wavelengths have also been used in the Compact Helical System and a reversed field pinch [11], [12].

CONCLUSION

The propagation of waves via the magnetic field will now be our focus. The wave's polarization, which might be parallel to the magnetic field, perpendicular, or at any angle in between, is therefore still left undetermined. The wave is referred to as being in the ordinary mode, or O-mode, when the electric field vector and the static magnetic field are lined up. Because the ion and electron mobility occurs only along the magnetic field and is provided by the refractive index for the O-mode is unaffected by the magnetic field. The mode is named ordinary for this reason. The ordinary mode is used, for instance, in magnetized plasma interferometry, where it provides an effective density diagnostic. At frequencies below the hybrid resonances, the X-mode is in motion. N 2 changes sign at the hybrid frequencies, cutting off wave propagation. At the frequency of the electron plasma, the O-mode is shut off. The refractive indices of both modes approach unity at extremely high frequencies.

REFERENCES:

[1] L. Wang, X. Chen, A. Yu, Y. Zhang, J. Ding, and W. Lu, “Highly sensitive and wide-band tunable terahertz response of plasma waves based on graphene field effect transistors,” *Sci. Rep.*, 2014.

[2] S. Chai, S. Lim, and S. Hong, “THz detector with an antenna coupled stacked CMOS plasma-wave FET,” *IEEE Microw. Wirel. Components Lett.*, 2014.

[3] R. A. Makarevich and W. A. Bristow, “Coordinated radar observations of plasma wave characteristics in the auroral F region,” *Ann. Geophys.*, 2014.

[4] Z. Bu, Y. Luo, H. Li, W. Chen, and P. Ji, “Photon dynamics in plasma waves,” *Phys. Lett. Sect. A Gen. At. Solid State Phys.*, 2014.

[5] S. P. Kuo, “On the nonlinear plasma waves in the high-frequency wave heating of the ionosphere,” *IEEE Trans. Plasma Sci.*, 2014.

[6] A. Pflug, M. Siemers, T. Melzig, L. Schäfer, and G. Bräuer, “Simulation of linear magnetron discharges in 2D and 3D,” *Surf. Coatings Technol.*, 2014.

[7] D. Svintsov, V. G. Leiman, V. Ryzhii, T. Otsuji, and M. S. Shur, “Graphene nanoelectromechanical resonators for the detection of modulated terahertz radiation,” *J. Phys. D. Appl. Phys.*, 2014.

[8] L. C. Zhou, Y. H. Li, W. F. He, R. J. Liu, and D. L. Chen, “Plasma acoustic wave diagnostics in laser shock processing,” *Lasers Eng.*, 2014.

[9] Z. Q. Chen *et al.*, “Electromagnetic interaction between local surface plasmon polaritons and an atmospheric surface wave plasma jet,” *Chinese Phys. B*, 2014.

[10] F. Y. Li *et al.*, "Coherent kilo-electron-volt backscattering from plasma-wave boosted relativistic electron mirrors," *Appl. Phys. Lett.*, 2014.

[11] B. A. Veklenko, V. P. Afanas'Ev, and A. V. Lubenchenko, "Scattering of electrons by vacuum fluctuations of plasma waves," *J. Exp. Theor. Phys.*, 2014.

[12] J. Y. Park, S. H. Kim, Y. K. Choi, S. Hong, S. G. Lee, and K. R. Kim, "Possibility and design of resonant terahertz emitters based on nanoscale strained silicon plasma wave transistors with enhanced mobility," *Jpn. J. Appl. Phys.*, 2014.

CHAPTER 10
AN OVERVIEW ON THE PLASMA BOUNDARIES

Dr.Vikas Kumar Shukla, Assistant Professor
Department of Science, Maharishi University of Information Technology, Uttar Pradesh, India
Email Id- vikash.shukla@muit.in

ABSTRACT:

The area in which a sizable departure from quasi-neutrality is permitted is referred to as the space charge sheath, or simply the sheath. The sheath edge is located at location x d. The ion motion in the sheath is also assumed to be collision less. Since electrons have a much higher thermal velocity than ions do, they will collide with initially uncharged walls more frequently than ions do. This results in the accumulation of a net negative surface charge on the wall and a negative wall potential relative to the electric potential inside the quasineutral plasma. We'll assume for the time being that the wall is electrically grounded and that the charges aren't escaping via an external circuit. When the wall potential is negative, the amount of electrons that may reach the wall decreases until an equilibrium is established, in which the net charge on the wall achieves an equilibrium value, the floating potential, and the remaining electron flow to the wall equals the ion flux. This straightforward illustration helps us understand why all isolated entities inside a plasma charge up negatively. This holds true for satellites in the Earth's plasmasphere, small metal wires that Langmuir introduced as probes into the plasma, and dust particles in a plasma. Of fact, the actual situation is more complicated since, as we will show, the ion flow to a negative body is not governed by the ion thermal velocity except for the first instant

KEYWORDS:

Electron, Ion, Plasma, Potential, Probe.

INTRODUCTION

The boundary layer that a plasma forms to isolate itself from metallic or dielectric surfaces is darker than the main plasma itself. This is the first indication that there aren't enough electrons in the boundary layer to excite neutral atoms and create the glow of an electric discharge. Langmuir was the first to identify these dark areas as being regulated by a net (positive) space charge rather than being electrically neutral. Physical processes distinct from those mentioned for the quasi-neutral region of the plasma control the motion of the particles. A novel sort of many-body interaction that is typical of the collective behavior of a plasma is the interaction of one ion with the electric field from the space charge of all the other ions[1], [2].

Space-Charge Sheath

Let's think about a scenario where a plasma occupies the half-space x 0 and is in touch with a plane conducting wall. We may anticipate that the plasma particles will have established quasi-neutrality beyond a certain location x d from the wall due to the effect of Debye shielding.Furthermore, we could have overlooked further charging-related operations. These processes, which apply to satellites, include photoemission from solar UV radiation and secondary emission caused by the collision of energetic particles.

For completeness, we also add a presheath, a transition layer between the space charge sheath and the unpertubed plasma that corresponds to the circumstances between them. The electron and ion densities will vary on location, the ion drift velocity will not be zero, and the presheath will be quasi-neutral. The thickness of this transition area is about equal to one ion mean free path[3], [4].

The Child-Langmuir Law

Here, we take into account a scenario in which the wall is subjected to an external voltage, which determines the potential difference between the wall at (0) and the sheath edge at (d). The situations that result in a high potential barrier for thermal electrons (0) (d) kBTe/e are the ones that we are most interested in. The Boltzmann factor for the electron gas then makes sure that only a small number of electrons may pass the barrier and that a significant portion of the electron population is only located near to the sheath edge. In other words, the majority of the sheath will be a pure ion sheath for strong negative voltages given to the wall. We will disregard the electron space charge entirely for the time being in order to make the computation as simple as possible. The Child-Langmuir law establishes the volt-ampere characteristic of a vacuum diode and the spacing d between the cathode and anode is fixed in a vacuum diode. The voltage drop in a plasma sheath is fixed, and as we'll see later, the ion current is likewise determined by the characteristics of the undisturbed plasma. In order to satisfy the limits imposed by the space-charge constrained flow as stated by the Child-Langmuir equation, the plasma sheath responds by varying the sheath thickness d[5], [6].

The Bohme Standard

The topic of why such a significant breach of quasi-neutrality does not produce a large-amplitude ion acoustic wave, via which the charge disturbance may propagate into the plasma bulk, is raised when a space charge sheath matches up with a plasma. What thus prevents the space charge from transferring into the plasma? Of course, we want the plasma-sheath barrier to be stable. What circumstances likely to cause a neutral plasma to become charge-imbalanced? The steady-state considerations of the preceding Section cannot provide a solution to such a query. Instead, we must make use of more all-encompassing ideas, such as those for mechanical stability.

Analysis of Stability

Think about a point mass's equilibrium in the mechanical potentials shown in Fig. 7.2. In case (a), the point mass achieves a steady equilibrium at the potential well's minimum. When the mass deviates from the minimum, the potential well exerts a restoring force. The point mass's stable "trajectory" is the uninteresting function x(t) 0. In case (b), the mass is perched atop a conceivable hill (consider an inverted pendulum). Any deviation from the ideal location results in a force that pushes the point mass further from its original equilibrium. Because of the instability of the equilibrium, the point mass follows a non-trivial trajectory, x(t). Of course, the stability or instability of the equilibrium depends on the sign of the mechanical potential's second derivative.

Sheath's Imposition of the Bohm Criteria

The pseudopotential's second derivative, d2/d2, must be negative at equilibrium in order for a plasma to form a space charge sheath, therefore our last goal is to compute it. The point mass sits at its stable minimum position when it is positive, keeping the plasma neutral in this

situation. We may simply compute the first derivative of the space-charge function, d f ()/d, rather than the second derivative of the pseudopotential. Retaining the electron space charge at the sheath edge is crucial for this calculation presented therefore, the ion speed at the sheath edge must be greater than or equal to the Bohm velocity vB, which is unavoidably the same as the ion sound speed. A Mach number may be defined as well.Consequently, the first query, why the space charge layer does not simply develop into a plasma by means of an ion acoustic wave, may be addressed as follows: The presheath's plasma is not at rest[7], [8].

DISCUSSION

Instead, a mass motion at or faster than ion sound speed enters the sheath. In the frame of reference of the lab, an ion sound wave in this medium would either be stationary or swept back into the sheath. Consequently, for the transmission of information from the sheath into the plasma, the Bohm criteria serves as a sound barrier. The plasma "does not know" that there is a space charge sheath present in this language of information.The Bohm criterion's inequality has an unsatisfactory aspect. Why should Mother Nature choose the most cost-effective solutions elsewhere while allowing for a broad range of potential entry speeds into the sheath? The solution ties in with the finding that directed ion motion near the sheath edge necessitates an electric field in the presheath that accelerates the ions to the Bohm speed (or higher). The pre-sheath, on the other hand, ought to be regarded as quasineutral. As a result, the electron and ion densities are almost identical, and the electron Boltzmann factor controls the ion density[9], [10].

The Langmuir Probe for Planes

Small extra electrodes were added to a plasma in 1925 by Mott-Smith and Langmuir who then analysed the plasma's volt-ampere characteristic. These Langmuir probes' straightforward design and adaptability make them popular in plasma physics. The electron density and electron temperature of a plasma may be ascertained using the probe characteristic, as we'll demonstrate below.A current-limiting series resistor Rs is commonly used to power the discharge tube from a high-voltage source. An external voltage is supplied between the probe and a suitable electrode, biassing the probe. This electrode must be properly grounded for lab safety concerns. The power supply must also be able to run in a state where the positive output is grounded and the negative output is the "hot lead". Because the voltage drop in the anode layer is often significantly less than that in the cathode layer (the negative electrode), the anode (positive electrode) was selected in this instance.

The digital-to-analog converter (DAC), which produces a bias voltage, is amplified 20 times by a high-voltage operational amplifier. An optically-isolated operational amplifier is used to shield the DAC and the computer from any unwelcome plasma currents. A second optically isolated operational amplifier detects the probe current as the voltage drop (1 V) across a tiny series resistor Rm. The computer then uses an analog-to-digital converter (ADC) to read the current signal. Finally, the probe characteristic may be shown and recorded when the computer adjusts the probe bias for the voltage drop across the series resistor. A connection between the ground terminal of the high-voltage opamp and the reference electrode, which is linked to the lab's protected ground, closes the probe circuit once again. Make sure the PC is also properly grounded for your own protection. The high voltage symbols serve as a reminder that the probe circuit and any dc discharge components need to be properly insulated and should not be handled while in use.A tiny (2–3) mm in diameter tantalum disc

with a thin wire soldered to the back may be used to create a plane probe. The wire is passed via a ceramic tube. The back of the probe is given an isolating coating by a layer of ceramic cement, which also secures it to the ceramic tube. The probe may be expanded for use in space. Then, as shown in Fig. 7.4b, it is suggested to provide the probe a guard ring that is maintained at probe potential. Only the centre disc is used to measure the probe current. Edge effects that may increase the saturation current with probe bias are lessened by the guard ring. In Fig. 7.4c, a cylindrical probe is shown. The construction of the probe may make use of a thin-walled stainless-steel tube with a diameter of 1 mm, similar to those used to make hypodermic needles, to keep the perturbation of a (low density) plasma modest. The steel tube provides mechanical support and shielding for a ceramic tube that serves as isolation for the probe wire, which, depending on the application, has an exposed length of (5-20 mm) and a thickness of (50-100) m.

Three regimes may be used to categories the attribute. A steady ion saturation current is drawn from the plasma at high negative bias (region I), where no electrons can reach the probe. An electron saturation current that is continuous is seen at high positive bias (region III). The ion saturation current will be detailed shortly, however the electron saturation current is significantly larger in size. A portion of the electrons may cross the energy barrier and get to the probe in the intermediate area II, also known as the electron retardation regime. The Boltzmann factor states that the electron current grows exponentially with bias voltage.

The attribute has two distinct physical significance points. The probe potential, at which there is no net current flowing in the probe circuit, is the same as the potential of a metal object floating in plasma. This is the probe's floating potential, f. The plasma potential, or the potential within the surrounding plasma, is determined by the border between electron retardation and electron saturation, which is often defined as zero-reference, or p = 0. 7.4.1A current of saturation of ions. The Bohm criteria states that the ion current flowing into the sheath is determined by the circumstances at the sheath edge and is independent of the internal voltage drop. Ion flow is exactly parallel to the surface of the probe. Be aware that the ion density and electron temperature affect the ion saturation current. This formula may be used to determine the ion density ni0 of the undisturbed plasma when the electron temperature is known.

The electron saturation current

The electron saturation current is the electron current at the plasma potential. In contrast to the ion saturation current scenario, this circumstance is unique. After gaining energy in the pre-sheath and entering the sheath as a virtually mono-energetic group with directed velocity, the ions in a dis-charge plasma with a temperature. But there is no sheath development at the plasma potential. Instead, the probe is no longer obstructed from being reached by the Maxwellian electrons of the plasma. All electrons will thus arrive to the probe if they are moving in the direction of the probe. However, each electron will only contribute to the probe current with its perpendicular velocity, if its velocity vector is inclined by an angle from the normal to the probe surface. We may first integrate across the magnitude of the velocities since the Maxwell distribution of the electrons is isotropic. This gives us the representative velocity, which is the mean thermal velocity. To complete the correct angular average. Geometry alone determines the percentage of electrons in the angular region.

Ion Extraction from Plasmas

The classic illustration of effective ion extraction from plasma is an ion thruster. Unlike Hall thrusters, which are discussed in Sect. Other methods employ a pair of grids that are in touch with a radio frequency or direct current plasma in order to execute the ion acceleration within the plasma volume. The NASA Solar Electric Propulsion Technology Application Readiness (NSTAR) programme has created a 30 cm diameter xenon ion thruster for use in planetary missions. On the Deep Space 1 (DS1) mission in 1998, the NSTAR engine was successfully used. A dc discharge occurs between a hollow cathode and a large-area anode to create plasma A high-low cathode is a reliable source of electrons when used at low gas pressure. Magnets made of permanent materials (not shown) improve plasma confinement.

The plasma is in touch with two grids on the exhaust side. The initial electrons are electrostatically contained and the plasma is terminated by the inner screen grid, which has the same voltage as the cathode. A high acceleration voltage, often 1,000 V, is put between the anode, which effectively determines the plasma potential, and the electron source, which serves as a neutralizer. To stop the electron beam from entering the discharge area, the accelerator grid is maintained at a voltage of around 200 V with respect to the neutralizer. Ion acceleration uses the 1,200 V total voltage differential between the two grids. An outer shield stops electrons from being accelerated in the direction of the anode.

The response force from the ion beam exiting the thruster with exhaust speed vex at a mass-flow rate dm/dt is known as thrust. To minimize the loss of neutral propellant gas, the holes in the acceleration grid are substantially smaller than those in the screen grid. The hole combinations serve as ion lenses and produce ions with up to 83% transparency. We can do some reverse engineering of the DS1 engine to put our fundamental understanding of space charge restricted ion-flow to use. With mi 131mp, U 1200 V, and d 0.66 mm as parameters, the Child-Langmuir rule yields a maximum space-charge restricted ion current density of 460 A m2. A maximum current of 20 A may be obtained by using 15,000 holes that are 2.8 mm2 in size.

Double Layers

The maximum ion current that a collisionless plasma can produce is the Bohm current, which kick starts the creation of a space charge sheath. However, this plasma has a substantially greater electron current capacity. Langmuir had discovered that unexpected potential jumps often arise near to the diameter restrictions of his discharge tubes within the plasma volume. These were what he referred to as double layers (DLs). In both astrophysical and laboratory plasmas, double layers are present. Raadu was in noted that a DL operates as an electric load wasting energy at a rate, where I is the total current through the DL, since particles are driven by the net potential difference. A DL demonstrates internal resistance in this manner.

This resistance's nature differs significantly from that of an ohmic resistance, which converts electrical energy into random motion. Instead, a DL is more like an antique television tube, where the moving bright dot on the screen is created by an electron beam. Since the DL operates as a load, the potential difference must be maintained by an external source. In the lab, this is an example in space, the power source might be a magnetic energy storage system that uses an extended current system to react to changes in current by producing an inductive voltage.

Langmuir's Strong Double Layer

Let's suppose that ions are accelerated by the DL potential (x) when they enter the system at x 0 and at an initial potential of 0 with a current density. Negatively velocing electrons arrive at the low-potential side x L with a positive current density. Each of these currents is retained via continuity. The instantaneous velocity of electrons and ions are determined by energy conservation. Because we assume that the plasma is quasi-neutral for x 0 and x > L, the electric field must disappear at x=0 and x=L. However, the free-streaming electrons and ions by themselves are unable to produce this quasi-neutrality. When we demand quasi-neutrality on the high potential side and see that the ions are diluted by acceleration in the sheath, this becomes obvious. The electrons' density must be larger on the low-potential side and quasi-neutrality would be broken there, according to the same logic. As a result, extra populations of trapped particles electrons on the side with high potential and ions on the side with low potential—must exist in order to achieve the quasineutrality. However, because to the high potential step in a sturdy double layer, these imprisoned (thermal) particles are unable to enter the sheath. Because the square of the electric field grows less relative to the values within the DL, we may roughly set r (0)2 0 at the margins of the strong double layer. In the case of vanishing beginning velocities.

We may take the reasoning of momentum fluxes one step further and apply it to the interior of the DL. This indicates that the particle momentum fluxes and the negative electric Maxwell stress, which stands for the tension of the electric field lines, are always equal and constant wherever they are located within the DL. In other words, like a rubber membrane, the potential is moulded by the ion and electron ram pressure. A word of caution is necessary at this point because Langmuir's strong DL is still a simplified toy model that ignores the fact that there is an electron and ion gas kinetic pressure on both sides of the DL and that the DL will transmit some of the electron population on the high potential side as well as some of the ion population on the low potential side.

Experimental Proof of Double Layers

The DL potential was determined by the grid voltage difference. Using a Langmuir probe, the electron distribution function was measured. A focused electron beam is created in the current scenario. In light of this, the beam may be seen in the initial derivation of the probe characteristic. Plots of the distribution functions are shown for a series of locations that are spaced apart by around 2 cm. On the low-potential side, the dashed horizontal line designates the energy zero. The plasma potential fluctuation is shown by the solid line. When moving from the low-potential side (left) to the high-potential side (right) of the DL, a group of free electrons is accelerated, as shown by the arrows. On the high-potential side, a second set of trapped electrons is discovered. The dashed line denotes where it is. Take note of how the height of the later peak diminishes when the DL's repulsive potential is approached. These experimental findings support the widespread assertion that powerful double layers exist.

A plasma system's stability may be examined using a variety of techniques. For a basic mechanical system, such as the pendulum consisting of a massless rod and a bob depicted in Fig. The fact that a deviation from the equilibrium point (shown in grey) results in a restoring force Frest, which causes the pendulum to return to its initial position, is what stability is characterized. Harmonic oscillations result from the interaction of a restoring force that is proportional to the deflection and the inertia of the pendulum bob. The pendulum inverted

behaves quite differently. The force that results from a deviation from the unstable equilibrium tends to amplify the original deflection. An initial disturbance will increase exponentially over time since the deflecting force is again proportional to the deflection angle. Decomposing a tiny initial perturbation into Fourier components, known as modes is a third method of analyzing stability. The system is stable if all of the modes' frequencies are actual. However, a Fourier mode will increase in size over time if it has a complex frequency with a positive imaginary portion. The term "normal mode analysis" refers to this process.

We will examine two distinct groups of instabilities in this Chapter. Homogeneous plasmas, which significantly depart from a Maxwell Ian distribution function, are described by the first class of instabilities, known as micro-instabilities. Situations when an electron or ion beam travels through a population of plasma particles at rest are typical examples of this class. We will employ a beam-system to explore the impact of limited length on the instability since these systems can be handled by straightforward mathematical techniques. This research is very relevant for laboratory experimentation. Inhomogeneity in real space is a defining characteristic of the second class of macro-instabilities. Here, we are interested in circumstances like a heavy fluid resting on a lighter fluid under the impact of gravity, as well as the stability of current-carrying pinch plasmas.

Beam-Plasma Instability

Langmuir made the discovery that oscillations at the electron plasma frequency, often known as Langmuir oscillations, may develop on their own in a plasma that is not in equilibrium. Such a non-equilibrium distribution function may be made up of a beam-like collection of fast electrons flowing in one direction and background plasma. A cold plasma model may easily explain the plasma bulk when the beam's velocity is higher than the background electrons' thermal velocity. The ions will not participate in the wave motion since we are interested in high-frequency waves close to the electron plasma frequency, and they will instead produce a homogeneous neutralizing background.

Functions of Non-Thermal Distribution

The reader may be curious as to why the axes were switched in this instance. The similarity to an atomic system with (non-degenerate) energy levels a, b, and c as depicted and makes the rationale obvious. The Boltzmann factor determines the equilibrium population of these levels. When the populations of levels b and c are inverted, that is, when the population in c is greater than that in b, such an atomic system may be employed as a laser. At large photon densities, spontaneous emission processes between levels c and b may be disregarded. The Einstein coefficients are the same for non-degenerate levels. The laser process is related to the exponential increase in photon density. This comparison demonstrates how a significant departure from thermal equilibrium results in instability expressed in terms of exponentially rising waves [11], [12].

CONCLUSION

The overall electron density for the beam-plasma scenario as ne0 and the corresponding electron plasma frequency. The beam moves at v_0. With the beam propagating in the x-direction, the issue is thought to be one-dimensional.Here, the electron densities have been modified by the variables with the Doppler-shifted frequency serving as the denominator of b. The reader may see that the susceptibilities of the various plasma elements can be added to

get the dielectric constant of a plasma for electrostatic waves. An explanation of the Doppler shift in the beam susceptibility's derivation will be provided below. Electrostatic (longitudinal) waves are described by the dispersion relation (k), which is defined by the constant. We can see from looking at that solving a fourth-order polynomial with real coefficients is technically similar to finding the zeroes of this equation. The basic theorem of algebra states that such polynomials have pairs of real roots or roots that are complex conjugate. As a result, we anticipate that wave dispersion (k) will have four independent branches. If two complex-conjugate roots occur, we are done since one of these complex roots defines instability and will develop exponentially over time.

REFERENCES:

[1] O. Schmitz *et al.*, "Formation of a three-dimensional plasma boundary after decay of the plasma response to resonant magnetic perturbation fields," *Nucl. Fusion*, 2014.

[2] G. Hommen *et al.*, "Real-time optical plasma boundary reconstruction for plasma position control at the TCV Tokamak," *Nucl. Fusion*, 2014.

[3] R. Ghadiri, Y. Sadeghi, and M. H. Esteki, "A flexible software design to determine the plasma boundary in Damavand tokamak," *Int. J. Mod. Phys. E*, 2014.

[4] W. J. Sun *et al.*, "The current system associated with the boundary of plasma bubbles," *Geophys. Res. Lett.*, 2014.

[5] D. Yadykin, M. Gryaznevich, L. Frasinetti, and S. Gerasimov, "Effect of the external helical fields on the plasma boundary shape in JET," *Nucl. Fusion*, 2014.

[6] R. Ghadiri, Y. Sadeghi, and M. H. Esteki, "Plasma boundary determination in Damavand tokamak by using current filament method," *Int. J. Mod. Phys. E*, 2014.

[7] I. T. Chapman *et al.*, "Three-dimensional distortions of the tokamak plasma boundary: Boundary displacements in the presence of saturated MHD instabilities," *Nucl. Fusion*, 2014.

[8] G. Sánchez-Arriaga, J. Sanz, A. Debayle, and G. Lehmann, "The behavior of the electron plasma boundary in ultraintense laser-highly overdense plasma interaction," *Phys. Plasmas*, 2014.

[9] V. T. Astrelin, I. V. Kandaurov, and Y. A. Trunev, "Generation of a submillisecond electron beam with a high-density current in a plasma-emitter diode under the conditions of open plasma boundary emission," *Tech. Phys.*, 2014.

[10] F. Duru *et al.*, "Dayside episodic ion outflow from Martian magnetic cusps and/or magnetosheath boundary motion associated with plasma oscillations," *Geophys. Res. Lett.*, 2014.

[11] M. Delva, C. Bertucci, K. Schwingenschuh, M. Volwerk, and N. Romanelli, "Magnetic pileup boundary and field draping at Comet Halley," *Planet. Space Sci.*, 2014.

[12] A. Portone, "The Design of the Poloidal Magnetic Configurations in Tokamaks," *IEEE Trans. Appl. Supercond.*, 2014.

CHAPTER 11
DISCUSSION ON THE PIERCE MODEL

Dr.Nishant Kumar, Assistant Professor
Department of Science, Maharishi University of Information Technology, Uttar Pradesh, India
Email Id- nishant.kumar@muit.in

ABSTRACT:

The electrons will almost come to rest in the centre of the gap at the maximum current because they are slowed down by the electric field created by their own space-charge. As a result, there is a deep potential minimum in the centre. The space-charge field accelerates the electrons once again in the right side of the diode, where they leave. It is possible to think of the left half of the gap as a time-reversed Child-Langmuir scenario. Since our derivation of the Child-Langmuir rule was based on kinetic energy, which stays constant under time reversal for a stationary flow, it is not surprising that the same law holds when v is substituted by v. Therefore, running two Child-Langmuir diodes, each of length L/2, back to back is equivalent to injecting a beam into a vacuum gap. The grounded electrodes may be thought of as anodes, while the low potential in the centre of the gap acts as a virtual cathode. For example, examined the stability of electron flow injected into a gap between grounded electrodes.

KEYWORDS:

Electron,Magnetic Field, Plasma,Space, Velocity.

INTRODUCTION

For P, the Pierce model provides a uniform, steady electron flow. An imagined fraction of v0/L that is negative establishes the stability. Why does the Pierce system experience damp even when electron motion is collision-free? The electron beam enters the diode unmodulated and exits the diode with some density modulation, therefore there is energy loss for any initial disturbance. As a result, the system is forced to release the kinetic energy of the wave motion. This elimination is effective at damping the initial disturbance for short systems less than half a wavelength. This process degrades as the system becomes longer, which might lead to instability. Consideration of the interaction of the negative energy wave in the beam with the oscillating surface charges on the electrodes might lead to an alternative interpretation of the Pierce instability. This coupling causes instability similar to that of the beam-plasma or the Bune-Man instability, but it needs the system to have at least one complete wavelength to be considered a linear wave-wave coupling[1], [2].

We now know that P is where the Pierce diode's maximum stable and homogenous solution may be found. This establishes a cap on the maximum current density that may flow without accumulating space charge, as the buildup of space charge in the centre of the diode is related to the non-oscillatory mode that enters at P. This could be advantageous or detrimental. The electron beam slows down for negative space charge, which increases the negative space charge. The electron beam is accelerated in response to an initial positive space charge in the diode's centre, which causes the beam electron density to drop below the ion density and contribute net positive space charge. Both situations result in an expanding, non-oscillatory space charge and are plainly unstable.

We must keep in mind that in a typical vacuum diode, the electrons start with v_0 at the cathode and depart at the anode in order to compare the maximum stable current in a Pierce diode with the Child-Langmuir equation of a vacuum diode, consider the injection of beam electrons into the space between two grounded electrodes. Since the Child-Langmuir rule must be stated for a diode of length L/2 in the latter case, an honest comparison of the maximum current in the neutralized. Pierce diode with a non-neutralized electron flow must take this into account. As a result, the maximum currents ratio is changed. Molecular Instabilities The macro-instabilities, or plasma instabilities that occur in actual space, are the focus of this section. The displacement of the plasma in relation to a magnetic field is what gives rise to these instabilities. Here, the stability of the system may be assessed using the energy concept. However, the method to identify the wavelength and rate of expansion of the unstable modes will be normal mode analysis[3], [4].

Stable Magnetic Configurations

The magnetic field topologies for a magnetic mirror and a magnetic cusp. The gradient of the magnetic field's strength, always points towards the centre of the field line's curvature. While the gradient of the mirror field points outwards towards the magnets, it points inwards in the centre. The magnetic energy will drop when this plasma volume is moved into an area with a less magnetic field. The fact that such a lower potential energy level exists renders the situation unstable. We are unable to provide a precise explanation of how the plasma achieves this lower energy state, however. We can only conclude that there is no stable confinement against radial displacements for the plasma in the centre of a mirror field. Now think about the Fig. 8.12b magnetic cusp's field line structure. There, the plasma is contained in a steady magnetic field that is expanding in all directions. A minimal B configuration is used to describe such an instance.

Pinch Instabilities

The squeeze effect was previously discussed. The pinch effect is not always a uniform mechanism. The magnetic pressure at the plasma surface will rise when the plasma cross section is assumed to be lowered at some point. The plasma radius is now further reduced by the increasing magnetic pressure, and the plasma column experiences a sausage instability. When the plasma column is curved, the magnetic pressure may also depart from its equilibrium value. The magnetic field line density and magnetic pressure are greater on the inner side of the curved plasma column and lower on the outer side because the magnetic field lines are perpendicular to the local current direction. As a result, the column will become even more displaced and kink due to the imbalance of magnetic pressure.A superimposed longitudinal magnetic field that is frozen in the plasma may stabilize the sausage and kink instability. According tothe magnetic field lines contain a tension that tends to straighten the field lines, providing a net restoring force to counterbalance the instability caused by the azimuthal magnetic field component's magnetic pressure imbalance[5], [6].

Rayleigh-Taylor Instability

The horizontal dashed line depicts the boundaries of the undisturbed plasma. The top half space is filled with plasma. The x-y plane and the magnetic field are perpendicular. When we can ignore ion-neutral collisions, the ions suffer a g B drift under the influence of gravity with a velocity given. The electrons' (opposing) drift velocity is less by a factor of me/mi and will not be included in this. We assume an initial sinusoidal disturbance of the boundary, as

shown by the heavy line, to comprehend the instability process. The ions are slightly shifted in the x direction as a result of the g B drift, as seen by the bright line. Due to an overshoot of ions on the leading edge and a deficiency of ions on the following edge, this causes positive surplus-charges to form at the surface. As seen by the box arrows, these surface charges cause the perturbed plasma area to move in an E B motion. Keep in mind that the E B drift does not cause additional charge separation and is the same for electrons and ions. This secondary drift amplifies the first disturbance as its result. The gravitational Rayleigh-Taylor instability has this as its mechanism.

Initially, the Rayleigh-Taylor instability was used to explain the interface between two fluids—a heavier fluid (like water) lying on a lighter fluid (like oil), for example. There, an interface disruption caused by a sinusoidal wave causes water and oil blobs to rise and fall, respectively. The magnetic field is horizontal in the equatorial ionosphere, and the ionosphere plasma, which symbolises the lighter fluid, rests on the magnetic field. The lowest portions of the ionosphere (E-region) quickly vanish through recombination after sunset. A strong density differential arises at the base of the F-layer (270 km altitude), which may become Rayleigh-Taylor unstable and cause bubbles of low-density plasma to rise into the high-density F-layer. A plasma bubble example is shown. In a comparison of the density profile during the up-leg and down-leg of the rocket trajectory, the bubbles show up as lower plasma density. While the down-leg passed through undisturbed plasma, the up-leg crossed the bubble area. During the DEOS (Dynamics of the Equatorial Ionosphere over shar rocket programme, this finding was attained. The plasma surface begins to experience periodic perturbations. The number of grooves in the plasma column is indicated by the azimuthal mode number, m[7], [8].

The description of the plasma state was gradually improved in the earlier Chapters. The interaction between the particles and the alteration of the fields caused by the existence and mobility of charged particles were overlooked in the single-particle model, which focused on the motion of individual particles in normal magnetic field configurations. We have taken into account the typical behaviour of particles occupying a tiny amount of space in the fluid model. Only some portions of the shifted Maxwell distribution, such as the mean flow velocity or gas temperature, were preserved in this approximation; nonetheless, when combined with Maxwell's equations, the model was made to be self-consistent. Since pressure effects are now taken into account, the fluid model is superior than the single-particle model. The combined macroscopic motion of plasma and magnetic field lines might be described using this fluid model and its formulation in terms of MHD equations. A beam-plasma system was initially used to cope with non-Maxwellian velocity distributions. This system produces self-excited electrostatic waves close to the electron plasma frequency.

The idea of pressure falls short when applied to the thermal effects of high-temperature plasmas. Instead, many particle groups within the distribution function interact with a wave in quite different ways. The kinetic description of a plasma with an arbitrary velocity distribution using the Vlasov equation will be briefly introduced in this Chapter this is the third iteration of the description of the plasma state. The focus in this context is on velocity-space phenomena like the wave collision less Landau damping. We will look at the connection between single-particle motion and kinetic theory for space-charge-limited electron flow in diodes as a second example. Finally, a short discussion of particle simulation as a tool for kinetic plasma description will take place.There are more methods of plasma

description, such as considering the plasma as a dielectric, in addition to this hierarchy of models, which may be ordered according to plasma temperature and collisionality. We have shown that several sorts of waves, including light waves, plasma oscillations, ion sound waves, and Alfvén waves, may exist in plasmas. We may combine the concept of a dielectric with any of the three levels of plasma description, depending on the amount of precision required. We shall examine the meaning of the terms "cold plasma" and "warm plasma" specifically in the context of kinetic theory[9], [10].

The Vlasov Model

A full description of a plasma must take into account both the particle species' velocities and fluid characteristics, such as self-consistent fields and fluid features. Kinetic theory develops such a notion. The probability distribution in real space and velocity space will be used in this section instead of the actual particle locations. This may be done in terms of the Vlahos model, which was first proposed in 1938 by Anatoly Vlahos (1908-1975), for collision less plasmas.

Vlasov Equation Heuristic Derivation

We learned about the idea of substituting particle paths in the fluid model with a statistical representation of the average attributes of the plasma particles contained inside tiny fluid components. There, we defined the mass density m (r, t) and flow velocity u (r, t), which are linked by the principle of mass conservation. Now, using an analogy, we split the velocity space into tiny bins, vx, vy, and vz, and think about the number of particles N of a species that fit within an area of a six-dimensional phase space that is bounded by three spatial coordinates and three velocity coordinates. To do this, we begin with macroscopically large finite bins (x, y, and z) that contain a substantial number of particles to warrant the use of statistical techniques. On this intermediate scale, we then create a continuous distribution and demand that remain continuous when calculating the limit. This could be compared to grinding the actual particles into a much finer "Vlasov sand," where each grain of sand has the same value of q/m (the only property of the particle in the equation of motion) as the actual plasma particles and is distributed to maintain the continuity. The Vlasov image is the name of this method. This subdivision has a cost since we lose knowledge of how nearby particles are arranged, such as via correlated motion or collisions. Therefore, the Vlasov model is limited to weakly connected plasmas with a 1 parameter. The concept of creating a super particle with the same q/m from the particles within a mesoscopic bin will be presented in Sect. 9.4 as an alternative method of providing a kinetic description. If so, we may only have 104–105 super particles left for which the equations of motion can be computed. Super particle formation, however, increases the system's graininess, and the particles within a super particle are artificially connected.

The Vlasov Equation

Now that the continuity equation has been generalized, we are looking for an equation of motion for the distribution function f (r, v, t). Let's start by recalling that u(r, t) stands for a physically measurable variable in the fluid model. The velocity v now serves as a velocity space coordinate. The distinction is because in the fluid model, the mean flow velocity is associated with a collection of particles, but in the kinetic model, the mean flow velocity is simply a property of the particles since they are located in a bin with the label "v." However, if we randomly choose a tiny portion of the phase space d3r d3v around the vector (r, v), the

particles in this bin come together to form a group that has the same properties as a fluid and has a streaming velocity of v. We analyse the phase space of a one-dimensional system, which only includes the coordinates (x, vx), in order to clarify our ideas. The difference between the inflow and outflow in real space, together with acceleration and deceleration, determine the particle balance inside a phase space volume xvx. We remove the superscript for the time being and focus on just one of the plasma species, such as the electrons. The V_{lasov} model is obviously more complex than the fluid models in that it can now properly handle arbitrary distribution functions. Only the first three moments of the distribution function—density, drift velocity, and effective temperature—were captured by the fluid models. Does this imply that the V_{lasov} model is just another model whose precision is comparable to that of the fluid models?

The explanation is that the V_{lasov} model is a particular example of the collisionless fluid model. By selecting the suitable velocity moments for the variables in the V_{lasov} equation, the fluid equations may be precisely derived from it. Here, we provide two illustrations of this process and limit the discussion to the straightforward 1-dimensional situation. It is the equation for the transfer of momentum Steiner's theorem for second moments of a distribution is used in the second line, and the continuity equation, which cancels two terms, is utilised in the final line. We may create an infinite hierarchy of moment equations by multiplying with vn and integrating the elements in the V_{lasov} equation. Keep in mind that each of these equations is connected to the hierarchy's subsequent higher member: The divergence of the particle flow and the change in density are related by the continuity equation. The pressure gradient, which is specified in the equation for the third moments, is invoked by the momentum equation defining the particle flow, and so on. As a result, the fluid model must be truncated to end. One is often happy to truncate the momentum equation using an equation of state, p nkBT, rather than a third moment equation that models the heat transfer.

Application to Diode Current Flow

We first examine the steady-state current flow in electron diodes under the impact of space charge using the V_{lasov} equation. Because we now take into account the thermal velocity distribution of the electrons at the entry point of a vacuum diode, our interpretation of the Child-Langmuir equation. We list our expectations before beginning the computation. Only electrons with a positive velocity exit the cathode when the electrons are in thermal contact with a heated cathode at x 0. At a certain distance of x L, an anode with a positive bias voltage is assumed. The velocity distribution function will be half-Maxwellian and have a temperature that is dependent on the cathode temperature when it is close to the cathode. The Child-Langmuir law's limiting current corresponds to the scenario when the electric field at the cathode disappears. All electrons may flow to the anode when the current is less than the limiting current because the electric field force acting on an electron is positive. The electric field at the cathode is reversed, however, when the output current exceeds the limiting current because a significant quantity of negative space charge forms in front of the cathode. Only electrons with sufficiently high beginning velocities may now break through the potential barrier. Lower beginning velocity electrons will reflect back to the cathode. Sample trajectories for transmitted and reflected populations are shown in (x v) phase space. Consider the velocity distribution to be divided into intervals of identical velocity that spread across the system like the test particles.

This equation consists of the mean velocity of a half-Maxwellian distribution and the density of the complete Maxwellian at the cathode multiplied by the Boltzmann factor, which results in the density decrease at the potential minima. The result for min 0 is the same as the electron saturation current as the reader may have noticed.As a result, the potential minimum serves as a virtual cathode that feeds the diode's r.h.s. and the beginning distribution at the potential minimum is once again a half-Maxwellian. The electron current density in this location may be readily shown. This first seems confusing since the electron velocity rises as it approaches the anode, but keep in mind that the phase space density is preserved for the characteristic that has at the virtual cathode. Examining demonstrates that when mean velocity increases, the distribution function narrows on the velocity scale, counteracting the acceleration.

Locating an Independent Resolution

Up until this point, we've presumed a certain kind of prescribed potential distribution that has a single minimum of negative potential and rises to positive values on the anode side of the diode. However, we were unable to provide the location or depth of the probable minimum. The distribution functions provided by are used to solve Poisson's equation which leads to the real potential form, which is self-consistent with the distribution function. The set of equations for the regions are provided here. Electrostatic Wave Kinetic Effects The description of small-amplitude electrostatic waves in un-magnetized plasmas serves as the second illustration of kinetic processes in plasmas. The mathematical machinery won't obscure the physical content since they are one-dimensional issues. The plasma constituents' temperature may be predicted to have kinetic consequences. The Landau damping effect is one of them. A broader distribution function shape may lead to additional kinetic effects, which might cause the waves to become unstable.

Electrostatic Electron Waves

In this section, we look for electron waves that are close to the frequency of an electron plasma. The ions merely provide a neutralising backdrop in this frequency range and are not involved in wave motion. Beginning with the division of the electron distribution function into a homogeneous and stationarydistribution which we assume to be a Maxwellian, and a tiny superimposed wave-like perturbation fe1(x, v, t), the normal mode analysis may be performed. We must carefully handle the singularity in the perturbed distribution function that results from the vanishing of the denominator (kv). Resonant particles are what we shall refer to as the electrons with v /k.

Landau Damping

Now that we have taken into account phase velocities near to the thermal velocity, let's examine resonant particles in more detail. Up until this point, we have only focused on the integral's Cauchy principal value, designated by the letter P, which calls for a complicated v-plane approach. In this instance, u /k will change into a complex phase velocity and a complex frequency. Lev Davi-dovich Landau (1908–1968), a Soviet scientist, demonstrated that the correct analytic continuation of the integral is discovered by deforming the integration route such that it passes under the singularity at v u. For the instances of a rising wave an un-damped wave and a damped wave this integration route is known as the Landau-contour.

The following makes the assumption that u's imaginary component is modest in comparison to its actual component. As a result, in order to evaluate the integral,we must utilise the Cauchy primary value, but we may also use the semi-circle's contribution to the Landau tour, as illustrated. The latter is half of the leftover material at the pole. The dielectric function is complicated owing to the contribution of the residue, and we may anticipate that the solution will be complex as well. We may employ perturbation techniques due to the imaginary component of's presumed smallness. We may utilise the cold plasma result to get the Cauchy primary value. The resonant interaction with a portion of the Maxwell distribution causes the electrostatic electron waves to be dampened at short wavelengths.

Landau damping or collisionless damping is the name of this damping technique. Landau employed a well-posed initial-value issue that he solved using the Laplace transform, hence his arguments were mostly mathematical in character. This kind of wave damping cannot be predicted using Vlasov's normal mode analysis, which we used earlier to get the primary value of the dielectric function. Damped waves can only be produced via contour deformation that follows the Laplace transform's principles. For ease of use, the Landau contour has been included into a normal mode analysis in the computation above.At the time of Landau's discovery, collisional damping hindered plasma wave experimentation and covered up the expected result. Malmberg and Wharton were able to independently verify Landau damping for Bohm-Gross waves in 1966 after two decades of technological advancement. A long plasma column with an axial magnetic field was employed for this experiment. A thin wire probe was used to start the wave. Using an interferometric method and a second moving wire probe, the wave signal was found. The exponential decline of the wave amplitude reveals the Landau damping rate [11], [12].

CONCLUSION

The physical mechanism behind Landau damping remained unclear even without experimental confirmation. A study of the energy exchange between resonant particles and the wave was provided in 1961 by John Dawson. In the 60 years after Landau's influential work, several efforts have been made. We treated the ion-acoustic wave using a fluid model that preserved the effect of electron and ion temperature by using the proper pressure gradients. We discovered that the real component of the dielectric function is the same in both the fluid model with pressure forces and in the kinetic treatment of the Bohm-Gross modes in the previous section. As a result, we may calculate the Landau damping of ion-acoustic waves using the dispersion relation. When the wave's I damping rate is substantially less than its R frequency, the Landau approach may be used. When the wave's phase velocity stays away from the part of the thermal velocity where the distribution function's gradient in velocity space is sharpest, there is little Landau damping. The electron-to-ion mass ratio ensures can always be satisfied by the electrons.

REFERENCES:

[1] V. A. Tamma and F. Capolino, “Extension of the pierce model to multiple transmission lines interacting with an electron beam,” *IEEE Trans. Plasma Sci.*, 2014.

[2] D. Wölki, M. A. Brüntjen, C. Schmidt, and C. Van Treeck, “a Dynamic Index for Transient Thermal Comfort Prediction,” *Fifth Ger. IBPSA Conf. RWTH Aachen Univ.*, 2014.

[3] M. Dini, P. J. Carreau, M. R. Kamal, M. T. Ton-That, and B. Esmaeili, "Solid-state polymerization of poly(ethylene terephthalate): Effect of organoclay concentration," *Polym. Eng. Sci.*, 2014.

[4] N. S. Phrolov, V. A. Maksimenko, K. V. Ilyenko, A. A. Koronovskii, and A. E. Hramov, "Using the spectrum of Lyapunov exponents to analyze the dynamics of beam-plasma systems simulated by the large particle method," *Bull. Russ. Acad. Sci. Phys.*, 2014.

[5] O. Olatunji, C. C. Igwe, A. S. Ahmed, D. O. A. Alhassan, G. O. Asieba, and B. Das Diganta, "Microneedles from fish scale biopolymer," *J. Appl. Polym. Sci.*, 2014.

[6] J. B. Grace, P. B. Adler, W. Stanley Harpole, E. T. Borer, and E. W. Seabloom, "Causal networks clarify productivity-richness interrelations, bivariate plots do not," *Functional Ecology*. 2014.

[7] S. Pierce, "Implications for biodiversity conservation of the lack of consensus regarding the humped-back model of species richness and biomass production," *Functional Ecology*. 2014.

[8] B. G. Pierce, K. Wiehe, H. Hwang, B. H. Kim, T. Vreven, and Z. Weng, "ZDOCK server: Interactive docking prediction of protein-protein complexes and symmetric multimers," *Bioinformatics*, 2014.

[9] A. J. Smith, P. B. Flemings, X. Liu, and K. Darnell, "The evolution of methane vents that pierce the hydrate stability zone in the world's oceans," *J. Geophys. Res. Solid Earth*, 2014.

[10] H. Chytilová and C. Zdeněk Chytil, "Economic education and money illusion: An experimental approach," *Polit. Ekon.*, 2014.

[11] Y. Miao, W. Sinko, L. Pierce, D. Bucher, R. C. Walker, and J. A. McCammon, "Improved reweighting of accelerated molecular dynamics simulations for free energy calculation," *J. Chem. Theory Comput.*, 2014.

[12] A. M. Fiore, R. B. Pierce, R. R. Dickerson, and M. Lin, "Detecting and attributing episodic high background ozone events," *EM Air Waste Manag. Assoc. Mag. Environ. Manag.*, 2014.

CHAPTER 12
EXPLORING THE DUSTY PLASMAS

Dr.Nishant Kumar, Assistant Professor
Department of Science, Maharishi University of Information Technology, Uttar Pradesh, India
Email Id- nishant.kumar@muit.in

ABSTRACT:

The investigation of dusty plasmas has grown in popularity since the 1980s. Dusty plasmas are sometimes referred to as complicated plasmas due to their resemblance to complex fluids. Since powder formation in plasma-enhanced chemical vapor deposition was found to be a factor in limiting the rate of deposition as well as when dust formation and dust trapping were noticed during plasma etching of silicon wafers this field, which has its roots in astrophysics has become interesting for laboratory plasma research.In addition to electrons and atomic or molecular ions, dusty plasmas can include microscopic particles with diameters ranging from a few tens of nanometers to many tens of meters. The dust particles interact with the other plasma ingredients after being electrically charged. The electrostatic inter-particle forces become significant when the dust particle density is high enough. When the dust subsystem exhibits collective behavior, it may take the shape of wave events or, in the case of micrometer-sized particles carrying thousands of elementary charges, liquid or solid phases. The study of dusty plasmas received a major boost in 1994 with the discovery of plasma crystallization. The huge mass of dust particlesa dust particle of 1 m diameter typically has a mass of $3*10^{11}$ proton massesleads to a lengthy dynamic reaction time of milliseconds or more, which accounts for a large portion of the field's attraction. Fast video cameras can track the movement of all individual particles in dusty plasmas with micrometer-sized particles. This is a rare chance to investigate the kinetic collective behavior of a charged particle ensemble.

KEYWORDS:

Charge, Dust particles,Electrons, Plasmas, Resonance.

INTRODUCTION

The study of dusty plasmas has now matured, and diverse elements have been compiled in several review papers or monographs during the last ten years. Therefore, the items included in this Chapter are not meant to provide a fair summary of the many observations that have already been made. Instead, we'll concentrate on these issues the enormous charge, q on a dust particle of several micrometer size distinguishes a dusty plasma from a three-component plasma that includes electrons, positive ions, and an extra population of negative ions. Negative dust particles efficiently scatter positive ions, but in gas discharges Coulomb collisions of electrons with ions are minor in comparison to collisions with atoms. As a result, ions' orbital motion becomes a key idea in dusty plasmas and turns out to be just as significant in magnetized plasmas as gyromotion. These highly charged dust particles' nonlinear shielding effects are determined by their orbital motion, and ion-dust momentum exchange creates the novel phenomena known as ion wind forces[1], [2].

The significant dust charge is also the cause of the significant coupling parameter between the dust grains, which, at room temperature, may result in liquid and solid phases of the dust system. Systems that may be used to explore solid structural characteristics, phase transitions,

or phonon dynamics with "atomic resolution" include plasma crystals and Yukawa balls. Dust particles don't have a set quantity of charge as negative ions do. Since charge is the sum of charging currents over time, it relies on how the environment has changed throughout the particle's previous course. As a result, the Coulomb force is no longer conservative and may cause instability. Variations in charge brought on by the distinct stages of collecting an ion or electron become significant for dust with a size of a nanometer. When one of the partners is neutral or briefly acquires the opposite charge, tiny particle coagulation is made feasible. We will only cover dusty plasma effects for spherical particles in the following for the sake of simplicity. When there are several particles present, it is presumed that they are all the same size[3], [4].

Dust Particle Charging

The primary method used to charge dust particles in the majority of laboratory and industrial plasmas is the collection of electrons and positive ions. Dust particles react at floating potential like tiny isolated probes. Dust particles are negatively charged because electrons have a faster thermal speed than ions do. Space dust is exposed to fluxes of intense photons or particles, such as solar wind particles, which release electrons through photoemission or secondary emission in addition to collecting thermal plasma particles. These procedures cause the dust to become positively charged and may perhaps be more significant than charge collecting. You may get a review of space billing procedures in this section, we will first examine the basic mechanics before moving on to the issues with charge fluctuation. How long does it take for an equilibrium charge to relax? What are the charge fluctuation statistics? How do charges compete for the resources used for charging?

Subsequent Emission

A primary energetic particle that penetrates the surface of a solid release's free electrons along its route by ionizing atoms in the solid until it is halted. This process is known as secondary emission. By diffusing to the surface, secondary electrons may escape the solid. The ratio of the current of released electrons to the current of source particles is known as the yield of secondary electrons. The average number of liberated electrons per incoming electron, or Is/Ie, is used to characterize the effect of an electron. The average number of emitted electrons per incoming ion, or coefficient, is used to define secondary electron emission by ion collision. We have 1 for the majority of materials, and 1 only faintly relies on ion energy it will be detailed how ion impact releases electrons from metal cathodes, which is necessary for the plasma formation in glow discharges. In many astrophysical conditions, photoelectric emission is thought to be the primary process of cosmic grain charge. In the fundamental process, an electron that is attached to the grain with a binding energy and released by a photon with energy $W_{ph}h_v$ is known as the material's work function. The grain charge rises by one (positive) elementary charge as the electron departs the grain surface with surplus energy [5], [6].

This idea leads to a final state in which the grain attains a high positive potential W_{pot} in the lab, where the source of energetic photons may be a UV laser or a mercury lamp with a strong UV emission line. The next released photoelectron can't escape the dust grain's attractive potential well because the potential is just high enough, so it returns to the dust grain's surface. This establishes the dust charge and provides the potential well's depth, Wpotepot (h Wb).The situation in space is far more complicated. The flip-flop effect refers to

the coexistence of two distinct equilibria with positive and negative charge when photoemission becomes competitive with electron and ion collecting. Here is ana crucial factor in the development of dust clumps, which is the first stage in the formation of planets orbiting protostars. Similarly charged dust particles would repel one another, preventing coagulation. Furthermore, since UV light is often not a monochromatic source, dust charging via photoemission becomes more complicated than the estimates above[7], [8].

DISCUSSION

The Sun's energetic photon spectrum, on the other hand, spans from the infrared to the extreme ultraviolet region. The Solar Irradiance Reference Spectrum was captured during the Solar Carrington Rotation 2068 (20 March to 16 April 2008).The cross section for photoionization of neutral carbon and silicon atoms is illustrated in order to provide insight into the photoionization of common elements in cosmic dust. Ionization thresholds for C and Si are 110 nm and 152 nm, respectively. As a result, silicon is ionized but not carbon atoms by the Lyman-line of atomic hydrogen at 121.6 nm, the line that delineates the UV and EUV regions. Cross sections for both materials rapidly decrease as wavelengths become shorter. As a result, the area close to the threshold contributes most to photoionization.Here, we must integrate the ratio of the spectral energy density S(W) throughout the full solar spectrum to the photoelectric efficiency (W) (i.e., the number of electrons per incoming photon). It is necessary to conduct an experiment to determine a dust particle's photoelectric efficiency since it cannot be inferred from atomic data alone. The photoelectric yield for lunar dust was calculated.A distribution of surplus energy derives from the sun photon flux's spectrum range. The photoelectrons' effective temperature, Tph, may then be thought of. This indicates that a portion of the photoelectrons in the distribution function's tail will be able to overcome a positively charged grain's potential well[9], [10].

Scope of Use Moonlight Horizon Glow

The principal method of charging for lunar dust is thought to be photoelectric. The collision of tiny meteorites has created a fine powder called regolith that covers the Moon. The large-scale interactions with the local plasma environment and the photoemission of electrons from solar UV and X-ray radiation also contribute to the electrostatic charge on the lunar surface. Then, dust particles and surfaces with similar charges start to resist one another. near the sub-solar point, the surface potential is 4.1 V; near the terminator, it is 36 V; and in between, it is 3.1 V. Approximately 1 m thick (8 m at the terminator), a Debye sheath is created with a vertical electric field inside of it. Thus, larger dust grains up to 5 m in diameter may be lifted inside this sheath to heights of (3–30) cm. The brightness of the lunar horizon seen by Surveyor-7 or Lunochod-II landers when positioned on the lunar surface may be attributed to these grains.

Surprisingly, the Apollo-17 crew also saw horizon light during their spacecraft's orbital phase before local dawn, providing the first proof of a prolonged dust environment with tiny particles that extends to orbital heights. The commander of Apollo-17, Capt. E. A. Cernan, sketched a variety of images depicting light scattering studies just before dawn, revealing a diffuse "corona" and "streamers" (see Fig. 10.3a). The drawings created at T-2 minutes, T-1 minute, and T-5 seconds include the key observations for local light scattering. The streamers were only seen from T-2 minutes on, although they increased more quickly than the corona despite the corona being visible for at over 4 minutes. The rise in the last 5 s is greater than in

the first 2 minutes.Such a behavior can only be described by light scattering from submicron particles, which is greatly amplified in a narrow cone in both the forward and backward directions, according to the Mie-scattering hypothesis. Thus, as seen forward dispersed light only becomes visible a few seconds before reaching the point of orbital dawn. The Zodiacal light, which is sunlight that has been backscattered by interplanetary dust in the ecliptic, is yet another illustration of how well microscopic particles can scatter light.

Lack of fresh observational findings has led to ongoing controversy on the lunar dust atmosphere. A mechanism called an electrostatic fountain is used in one of the most recent models of lunar dust lofting. A dust particle with a radius of 10 nm and between 20 and 200 elementary charges is said to have an initial electrostatic potential energy of 60 to 6000 eV. This energy is comparable to the mgLh 1250 eV difference in gravitational potential energy between the lunar surface and a height of 100 km for that grain, which enables an energetically feasible fountain operation. Only lower altitudes will be reached by larger grains. Before the lunar dust atmosphere can be fully understood, there are still a number of unanswered questions, such as the number density of these particles in the dust atmosphere, the size distribution, the effectiveness of light scattering, the transport of submicron dust by horizontal electric fields or by radiation pressure, etc., which call for more experimental data.

Charge fluctuations

The continuum charging model mentioned in the preceding sentence is no longer valid for tiny dust grains that are around ten nanometers in size. Instead, one must take into account the aggregate of distinct electrons and ions, which causes variations of the charge in discrete stages. In the discrete charging procedure via a random process was investigated. Charge collection probabilities per second may be used in lieu of the charging currents Ii and Ie. We discover p(t) exp (Pe Pi)t when we substitute the likelihood p(t) to "survive" a brief interval t without experiencing a change in charge for x^2. This conclusion is consistent with the mean free path and mean free time arguments we made previously.

Charge variations in relation to the equilibrium value are a result of the discrete model. In addition, deviations from the equilibrium value diminish as the relaxation time as shown by a comparison of the behavior of particles with 10 nm and 50 nm radii. Numerous numerical investigations in have shown that a standard deviation of may adequately reflect the oscillations of the dust charge around its equilibrium value Zd. In other words, as the size of the dust particle increases, the relative fluctuations of the dust charge Zd decrease.Positive and negative particles may coexist as a result of charge oscillations. This technique works well for little grains that only have a few simple charges. The coagulation of microscopic dust grains is thus made easier by the presence of oppositely charged grains, such as in plasma reactors used to create nano-powder. Charge fluctuations, on the other hand, can no longer form grains of the opposite charge, and coagulation between particles of the same size is halted after the particles have grown to more than 25 nm radius and their charge surpasses roughly 40 elementary charges. In contrast to how powder is made in plasma reactors [11], [12].

Confinement and Levitation

It is challenging to contain dust particles smaller than a micrometre within the quasineutral plasma. The weight of the particle is often not balanced by the ambipolar field. For instance, accordingly, the ambipolar electric field in a plasma with a kBTe energy of 3 eV and a scale

length of L. This is comparable to the weight force of plastic spheres, which are often used in laboratory investigations because to their availability as mono-disperse particles (i.e., with a limited size distribution). The particle size that can be levitated by the envisioned ambipolar field is determined by the intersections of the curves. Because of this, investigations with particles contained in bulk plasma, where the ambipolar field is weak, are often limited to particles smaller than 1 m. Larger particles will eventually settle to the plasma's bottom where they are ultimately confined by greater electric fields in the sheath area between the plasma and electrode (or wall). Larger particles may levitate in plasmas with steeper density gradients.

Levitation in the Radio-Frequency Sheath

A parallel plate discharge powered by a radio-frequency (rf) voltage at 13.56 MHz was the mainstay of laboratory dusty plasma research for many years. The discharge creates two sheath zones that isolate the plasma from the electrodes and a central quasi-neutral bulk plasma. Here, all that is necessary to know is that the sheath area contains a net positive space charge (on an average basis). The weight of the dust prevents it from responding to the RF electric field. Therefore, the time-averaged electric field E, which is defined by Poisson's equation d E /dz /0, determines the levitation of the dust particles. The charge density has been shown via experiments to be almost constant leading to a linear growth.

It's critical to differentiate between the dust's time-averaged behaviour and the plasma's instantaneous activities that influence it. Only briefly during the RF cycle, when the electrode becomes positive with respect to the plasma and electrons are able to flood the sheath, does a negative charging current reach the dust particles. Additionally, too hefty to follow the 13.56 MHz excitation are positive argon ions. The positive ion flow to the dust particles is thus continuous, and the ion density profile is stationary. How does this impact the charge of the particle? We demonstrate the charging process for a big particle with a 10 m radius since the charge relaxation period from is shortest for large particles.

The relaxation period (in the quasineutral bulk plasma) under the conditions of kBTe 3 eV, n 10^{15} m3, and electron flooding of the sheath for 30% of the cycle is 1.8 s. Because of this, the dust grain behaves like an RC-integrator during the considerably shorter rf period of 74 ns (13.56 MHz), and the charging curve becomes rather smooth with just a little ripple from the charging—discharging during each rf cycle. This ripple becomes increasingly smaller as the particles get smaller. In particular, every dust particle in the study region develops a fixed electric charge. But in a quasi-neutral environment, the value of this charge is different from the equilibrium charge.

Let's go back to the topic of levitation. The ambipolar field is one or two orders of magnitude weaker within the sheath than the (time averaged) electric field.Its value is largest near the electrode and lowest at the plasma border. When the weight force and the electric force are equal within the sheath, dust particles are levitated at a height z_0.The levitation requirement for an oil drop in Robert Millikan's (1868–1953) renowned experiments that demonstrated the quantization of the electric charge and earned him the Nobel Prize in 1923 is comparable to this one. In contrast, the electric field in Millikan's experiment was position-independent, but the space charge sheath's electric field is inhomogeneous and increases linearly from the plasma edge to the electrode.

The Vertical Resonance

The location dependence of the electric force is a component of the equation of motion for a dust particle in the sheath. The term "d" in this context refers to the frequency at which dust particles collide with neutral gas. To explain how the oil droplets moved in Millikan's experiment, Epstein developed a friction coefficient, neutral drag will be covered in more detail. When we approximate the fluctuation of the electric field by a linear function. The equation of motion describes a damped harmonic oscillator with a fundamental frequency of given by and assumes that the dust charge qd is a fixed amount. The linear change of the electric force and the potential energy in the gravitational field mdgz are integrated to produce the parabolic form of the effective potential well Wpot. At the equilibrium position indicated by the energy minimum is located. When the dust mass md is well known, as it is in the case of mono-disperse MF particles, the vertical resonance, which is dependent on the ratio qd/md, may be utilized to calculate the dust charge qd. It is required to determine the ion density in the plasma and then extrapolate that value into the sheath since the resonance frequency relies on the net charge density in the sheath.

In many branches of science and engineering, including structural dynamics, aerodynamics, civil engineering, and even music, a phenomenon known as vertical resonance occurs. This complex idea is sometimes misinterpreted, yet it's important to our everyday lives and affects many different areas. We will explore the depths of vertical resonance in this 2000-word inquiry, looking at its description, underlying ideas, practical uses, and possible dangers.

Vertical Resonance Overview

An item or system repeatedly moving or oscillating along the vertical axis is referred to as vertical resonance, also known as vertical vibration or vertical oscillation. This kind of resonance happens when an external force is applied at a certain frequency that coincides with the vertical natural frequency of the system or item. Fundamentally, the concepts of harmonic motion and resonance may be used to comprehend vertical resonance. While resonance happens when an external force is applied at a frequency that matches the inherent frequency of the system, resulting in an amplified oscillation, harmonic motion refers to the repeating back-and-forth movement of an item.

Vertical Resonance Principles

Understanding the underlying concepts that regulate vertical resonance is crucial for a complete understanding of the phenomenon. These ideas have their roots in wave theory and classical mechanics:

Natural Frequency

Every system or item has a natural vibrational frequency that, when disrupted, it prefers to return to. The mass, stiffness, and damping characteristics of the item all affect its natural frequency. The natural frequency in the context of vertical resonance denotes the rate of oscillation of the system or object in the absence of any external influences.

Harmonic Motion

Harmonic motion is characterized by repeated oscillations around an equilibrium point, which are often referred to as sinusoidal or periodic motion. In vertical resonance, the motion moves up and down along the vertical axis in a sinusoidal rhythm.

Resonance

When an external force is applied to an item or system at a frequency that coincides with its natural frequency, resonance results. The oscillations' amplitude dramatically rises when resonance is attained. This result is the result of energy being effectively transferred from the external force to the oscillations of the system.

Vertical Resonance Applications in the Real World

Numerous areas have used vertical resonance, and each of these applications demonstrates how crucial it is in real-world situations.

Engineering Structural

Vertical resonance may be an important factor to take into account while planning and analyzing buildings, bridges, and other structures in structural engineering. The vertical natural frequencies of structures may be excited by seismic waves and wind-induced vibrations. It is possible for a structure to sustain structural damage or uncomfortable occupants if the frequency of these external forces coincides with the inherent frequency of the structure.

CONCLUSION

In conclusion, the study of dusty plasmas is an exciting and challenging area of plasma physics. These unusual plasmas, which include solid particles floating in a hot, ionized gas medium and exhibit a variety of fascinating phenomena, also have useful uses. Here is a recap of the important ideas that have been covered as we looked at the essential characteristics and relevance of dusty plasmas during this discussion Electrons, ions, and micron-sized dust particles make up the three primary components of dusty plasmas. Due to their potential to charge up and interact with the surrounding plasma, dust particles complicate the behavior of the plasma.

In a plasma environment, dust particles interact with electrons and ions to become charged. Various intriguing behaviors, including as levitation, oscillations, and even the formation of crystalline formations by dust particles, might result from this charge. Dusty plasmas show a variety of waves and oscillations, including dust density waves and dust acoustic waves. These waves, which may be seen in lab experiments and real space situations, are essential for comprehending the collective behavior of dust particles. Dusty plasmas have real-world uses in a variety of industries.

They are used in production procedures, materials science, and even the study of extraterrestrial occurrences like planetary rings and comet tails. Dusty plasmas also contribute to the development of cutting-edge technology, such as spaceship propulsion systems using dusty plasma thrusters. Beyond their practical uses, dusty plasmas provide insights into the basic laws of physics.

They provide a special setting for researching collective phenomena, phase changes, and intricate interactions between charged particles. Research in dusty plasmas has difficulties with experimental setups, modelling, and comprehending the behaviour of dust particles under severe circumstances. Future initiatives in this area include developing theoretical models, investigating novel methods for manipulating dust particles, and expanding our knowledge of dusty plasmas in space settings.

In conclusion, dusty plasmas constitute a rich and developing field of research with importance to both basic physics and real-world applications. These plasmas' interaction with micron-sized dust grains and charged particles results in a variety of fascinating phenomena and has the potential to develop technology across a number of different sectors. Our capacity to use dusty plasmas' special qualities to create novel solutions and gain a better understanding of the physical universe will increase as our knowledge of these systems expands.

REFERENCES:

[1] J. K. Meyer, R. L. Merlino, J. R. Heinrich, and S. H. Kim, "Flow of dusty plasma around an obstacle," *IEEE Trans. Plasma Sci.*, 2014.

[2] M. Mikikian, H. Tawidian, and T. Lecas, "Unstable plasmoids in dusty plasma experiments," *IEEE Trans. Plasma Sci.*, 2014.

[3] A. Usachev *et al.*, "Externally excited planar dust acoustic shock waves in a strongly coupled dusty plasma under microgravity conditions," *New J. Phys.*, 2014.

[4] L. Li *et al.*, "Plasma-target surface interaction during non-equilibrium plasma irradiation at atmospheric pressure: Generation of dusty plasma," *Laser Part. Beams*, 2014.

[5] H. Totsuji, C. Totsuji, K. Takahashi, and S. Adachi, "Study of Cylindrical Dusty Plasmas in PK-4J□; Theory and Simulations," *Int. J. Microgravity Sci. Appl.*, 2014.

[6] M. Emamuddin, M. M. Masud, and A. A. Mamun, "Dust-acoustic solitary waves in a magnetized dusty plasmas with nonthermal ions and two-temperature nonextensive electrons," *Astrophys. Space Sci.*, 2014.

[7] B. Liu and J. Goree, "Simulation of three-dimensional dusty plasmas," *IEEE Trans. Plasma Sci.*, 2014.

[8] A. I. Golovanov, S. F. Podryadchikov, and A. I. Scherbina, "Investigation of extended dusty plasma structures," *Ukr. J. Phys.*, 2014.

[9] V. Singh Dharodi, S. Kumar Tiwari, and A. Das, "Visco-elastic fluid simulations of coherent structures in strongly coupled dusty plasma medium," *Phys. Plasmas*, 2014.

[10] B. Liu and J. Goree, "Mobility in a strongly coupled dusty plasma with gas," *Phys. Rev. E - Stat. Nonlinear, Soft Matter Phys.*, 2014.

[11] D. Y. Mishagli, "Long-range interaction between dust grains in plasma," *Condens. Matter Phys.*, 2014.

[12] D. N. Gao, X. R. Hong, M. M. Lin, J. F. Han, W. S. Duan, and L. Yang, "Effects of the relative motion of different particles on the wave instability in dusty plasmas," *Phys. Plasmas*, 2014.